Thermodynamic Properties and Debye-Waller Factor of fcc Materials

by

Nouri Mokhtar Elmiladi, B.Sc.

A Thesis
submitted to the Department of Physics
in partial fulfilment of the requirements for
the degree of Master of Science

May 1991
Brock University
St.Catharines, Ontario

TABLE OF CONTENTS

Abstract i

Acknowledgements v

List of Tables vi

List of Figures. vii

1. Introduction 1

2. High Temperature-Limit Expressions 10
   - 2.1. The Helmholtz Free Energy. 10
   - 2.2. Debye-Waller Factor 13

3. Thermodynamic Properties of fcc Materials. 15
   - 3.1. Nearest-Neighbour Distance. 17
   - 3.2. Thermodynamic Relations 21
   - 3.3. Interatomic Potentials 25
   - 3.4. Results and Discussion 30
     - 3.4.1. Thermodynamic Properties of Rare-Gas Solids 30
     - 3.4.2. Thermodynamic Properties of Gold. 47

4. Calculation of Debye-Waller Factor. 62
   - 4.1. Mössbauer Recoilless Fraction for Kr and Xe 64
     - 4.1.1. Results and Discussion 65
   - 4.2. DWF Results for fcc Metals 71

5. Phonon Dispersion Curves. 77
5.1. Quasiharmonic phonon Frequency 77
5.2. Renormalized Phonon Frequency 77
5.2.1 The Green's Function Method 78
5.3. Results and Discussion 83

6. Grüneisen Parameter 105
6.1. Theory. 105
6.2. Results and Discussion 108

7. Summary. 113

References 115

Abstract

We have calculated the equation of state and the various thermodynamic properties of monatomic fcc crystals by minimizing the Helmholtz free energy derived in the high temperature limit for the quasiharmonic theory, QH, and the lowest-order (cubic and quartic), λ^2, anharmonic terms of the perturbation theory, PT. The total energy in each case is obtained by adding the static energy. The calculation of the thermal properties was carried out for a nearest-neighbour central-force model of the fcc lattice by means of the appropriate thermodynamic relations. We have calculated the lattice constant, the thermal expansion, the coefficient of volume expansion, the specific heat at constant volume and at constant pressure, the isothermal and adiabatic bulk moduli, and the Grüneisen parameter, for the rare-gas solids Kr and Xe, and gold. Morse potential and modified Morse potential were each used to represent the atomic interaction for the three fcc materials.

For most of the calculated thermodynamic properties from the QH theory, the results for Kr and Xe with the modified Morse potential show an improvement over the results for the Morse potential when compared with the experimental data. However, the results of the λ^2 equation of state with the modified Morse potential are in good agreement with experiment only in the case of the specific heat at constant volume and at constant pressure. For Au we have calculated the lattice contribution from the QH and λ^2 PT and the electronic contribution to the thermal properties. The electronic contribution was taken into account by using the

free electron model. The results of the thermodynamic properties calculated with the modified Morse potential were similar to those obtained with the Morse potential.

Using the minimized equation of state we also calculated the Mössbauer recoilless fraction for Kr and Xe and the Debye-Waller factor (DWF) for Pb, Al, Cu, Ag, and Au. The Mössbauer recoilless fraction was obtained for the above two potentials and Lennard-Jones potential. The L-J potential gives the best agreement with experiment for Kr. No experimental data exists for Xe. At low temperature the calculated DWF results for Pb, Al, and Cu show a good agreement with experimental values, but at high temperature the experimental DWF results increase very rapidly. For Ag the computed values were below the expected results at all temperatures. The DWF results of the modified Morse potential for Pb, Al, Cu and Ag were slightly better than those of the Morse potential. In the case of Au the calculated values were in poor agreement with experimental results.

We have calculated the quasiharmonic phonon dispersion curves for Kr, Xe, Cu, Ag, and Au. The calculated and experimental results of the frequencies agree quite well for all the materials except for Au where the longitudinal modes show serious discrepancies with the experimental results. In addition, the two lowest-order anharmonic contributions to the phonon frequency were derived using the Green's function method. The λ^2 phonon dispersion curves have been calculated only for Cu, and the results were similar to those of the QH dispersion curves.

Finally, an expression for the Grüneisen parameter γ has been derived from the anharmonic frequencies, and calculated for these materials. The γ results are comparable with those obtained from the thermodynamic definition.

In the Name of Allah Most Gracious, Most Merciful.

To My Dear Mother

Acknowledgements

I would like to thank Dr. R. C. Shukla for suggesting this research project, and his assistance and helpful suggestions throughout the period of this research.

I also would like to thank my country Libya for sponsoring me during the period of my education. And last but not least, I want to express my deep appreciation to my family (especially my kind mother) and my friends for their continuous support.

List of Tables

Table 3.1 Coefficients of the Least-Squares Fit of the Functions $f(a_1)$, etc. 18

Table 3.2 Potential Parameters and The Debye Temperatures For Kr and Xe. 28

Table 3.3 Experimental Data Required in The Calculation of The Potential Parameters 29

Table 3.4 Potential Perameters For The fcc Metals 29

Table 4.1 Coefficients of The Least-Squares Fit of The Functions S_{QH}, etc 63

Table 4.2 Perameters of Lennard-Jones For Kr and Xe. 66

Table 6.1 Grüneisen Parameter For Kr and Xe With Morse Potential 110

Table 6.2 Grüneisen Parameter For Kr and Xe With Modified Morse Potential 110

Table 6.3 Grüneisen Parameter For Cu, Ag, and Au With Morse Potential 111

Table 6.4 Grüneisen Parameter For Cu, Ag, and Au With Modified Morse Potential 112

List of Figures

Figure 3.1 Lattice Constant of Kr With Morse and Modified Morse Potentials 32

Figure 3.2 Lattice Constant of Xe With Morse and Modified Morse Potentials 33

Figure 3.3 Coefficient of Volume Expansion of Kr With Morse and Modified Morse Potentials 34

Figure 3.4 Coefficient of Volume Expansion of Xe With Morse and Modified Morse Potentials 35

Figure 3.5 Specific Heat at Constant Volume of Kr With Morse and Modified Morse Potentials 36

Figure 3.6 Specific Heat at Constant Volume of Xe With Morse and Modified Morse Potentials 37

Figure 3.7 Specific Heat at Constant Pressure of Kr With Morse and Modified Morse Potentials 38

Figure 3.8 Specific Heat at Constant Pressure of Xe With Morse and Modified Morse Potentials 39

Figure 3.9 Isothermal Bulk Modulus of Kr With Morse and Modified Morse Potentials 40

Figure 3.10 Isothermal Bulk Modulus of Xe With Morse and

Modified Morse Potentials 41

Figure 3.11 Adiabatic Bulk Modulus of Kr With Morse and Modified Morse Potentials 42

Figure 3.12 Adiabatic Bulk Modulus of Xe With Morse and Modified Morse Potentials 43

Figure 3.13 Grüneisen Parameter of Kr With Morse and Modified Morse Potentials 44

Figure 3.14 Grüneisen Parameter of Xe With Morse and Modified Morse Potentials 45

Figure 3.15 Thermal Expansion of Au With Morse and Modified Morse Potentials 50

Figure 3.16 Coefficient of Linear Expansion of Au With Morse and Modified Morse Potentials 51

Figure 3.17 Specific Heat at Constant Volume of Au With Morse Potential. 52

Figure 3.18 Specific Heat at Constant Volume of Au With Modified Morse Potentials 53

Figure 3.19 Specific Heat at Constant Pressure of Au With Morse Potential. 54

Figure 3.20 Specific Heat at Constant Pressure of Au With Modified Morse Potentials 55

Figure 3.21 Isothermal Bulk Modulus of Au With Morse Potential 56

Figure 3.22 Isothermal Bulk Modulus of Au With Modified Morse Potential 57

Figure 3.23 Adiabatic Bulk Modulus of Au With Morse Potential 58

Figure 3.24 Adiabatic Bulk Modulus of Au With Modified Morse Potential 59

Figure 3.25 Grüneisen Parameter of Au With Morse Potential 60

Figure 3.26 Grüneisen Parameter of Au With Modified Morse Potential 61

Figure 4.1 Mössbauer Recoilless Fraction of Kr With Morse and Modified Morse Potentials 67

Figure 4.2 Mössbauer Recoilless Fraction of Kr With Morse and Lennard-Jones Potentials. 68

Figure 4.3 Mössbauer Recoilless Fraction of Xe With Morse and Modified Morse Potentials. 69

Figure 4.4 Mössbauer Recoilless Fraction of Xe With Morse and Lennard-Jones Potentials. 70

Figure 4.5 Debye-Waller Factor of Pb With Morse and Modified Morse Potentials 72

Figure 4.6 Debye-Waller Factor of Al With Morse and Modified Morse Potentials 73

Figure 4.7 Debye-Waller Factor of Cu With Morse and Modified Morse Potentials 74

Figure 4.8 Debye-Waller Factor of Ag With Morse and Modified Morse Potentials 75

Figure 4.9 Debye-Waller Factor of Au With Morse and Modified Morse Potentials 76

Figure 5.1 QH Phonon Dispersion Curves for Kr Along the [1 0 0] Direction With Morse and Modified Morse Potentials . 85

Figure 5.2 QH Phonon Dispersion Curves for Kr Along the [1 1 0] Direction With Morse Potential 86

Figure 5.3 QH Phonon Dispersion Curves for Kr Along the [1 1 0] Direction With Modified Morse Potential. 87

Figure 5.4 QH Phonon Dispersion Curves for Kr Along the [1 1 1] Direction With Morse and Modified Morse Potentials . 88

Figure 5.5 QH Phonon Dispersion Curves for Xe Along the [1 0 0] Direction With Morse and Modified Morse Potentials . 89

Figure 5.6 QH Phonon Dispersion Curves for Xe Along the [1 1 0]

Direction With Morse Potential. 90

Figure 5.7 QH Phonon Dispersion Curves for Xe Along the [1 1 0] Direction With Modified Morse Potential. 91

Figure 5.8 QH Phonon Dispersion Curves for Xe Along the [1 1 1] Direction With Morse and Modified Morse Potentials . 92

Figure 5.9 QH and λ^2 Phonon Dispersion Curves for Cu Along the [1 0 0] Direction With Morse Potential 93

Figure 5.10 QH Phonon Dispersion Curves for Cu Along the [1 1 0] Direction With Morse Potential 94

Figure 5.11 λ^2 Phonon Dispersion Curves for Cu Along the [1 1 0] Direction With Morse Potential 95

Figure 5.12 QH and λ^2 Phonon Dispersion Curves for Cu Along the [1 1 1] Direction With Morse Potential 96

Figure 5.13 QH Phonon Dispersion Curves for Ag Along the [1 0 0] Direction With Morse and Modified Morse Potentials . 97

Figure 5.14 QH Phonon Dispersion Curves for Ag Along the [1 1 0] Direction With Morse Potential 98

Figure 5.15 QH Phonon Dispersion Curves for Ag Along the [1 1 0] Direction With Modified Morse Potential 99

Figure 5.16 QH Phonon Dispersion Curves for Ag Along the [1 1 1] Direction With Morse and Modified Morse Potentials . 100

Figure 5.17 QH Phonon Dispersion Curves for Au Along the [1 0 0] Direction With Morse and Modified Morse Potentials. 101

Figure 5.18 QH Phonon Dispersion Curves for Au Along the [1 1 0] Direction With Morse Potential 102

Figure 5.19 QH Phonon Dispersion Curves for Au Along the [1 1 0] Direction With Modified Morse Potential. 103

Figure 5.20 QH Phonon Dispersion Curves for Au Along the [1 1 1] Direction With Morse and Modified Morse Potentials 104

1. Introduction

At low temperatures crystal lattice vibrations are studied by means of the harmonic approximation where the displacement of atoms from equilibrium sites are small. This approximation is introduced when the Taylor's expansion of the crystal potential energy is truncated after the quadratic term. At higher temperatures there are some important physical properties that can not be accounted for in a purely harmonic theory. However, if the neglected higher-order (anharmonic) terms in the Taylor's expansion of a crystal potential energy are taken into consideration in the theory, the above discrepancies can be accounted for. The harmonic approximation is inadequate in explaining thermal expansion, thermal conductivity, and the deviation of the specific heat from the classical Dulong-Petit law (3R limit) at higher temperature. The presence of anharmonic terms in the interaction energy in some cases provides a consistent explanation of some of these properties.

The anharmonic contributions to these physical properties can be calculated by several methods such as perturbation theory (PT), where the anharmonic contributions are evaluated from the harmonic eigenfunctions and eigenvalues and the derivatives of the potential function. There are other methods, purely numerical in nature, such as the Monte Carlo (MC) and Molecular Dynamics (MD) which can be used for the calculation of the anharmonic contributions to physical properties without expanding the crystal potential energy. These methods give all harmonic and anharmonic contributions to the physical property. Because both of these methods are limited to classical systems, they are valid only in the

high temperature limit, i.e. temperatures greater than the Debye temperature θ_D.

The perturbation theory approach to the evaluation of anharmonic contributions to quantities such as the Helmholtz free energy (F) or the atomic mean square displacement (MSD) leads to an infinite series of F or MSD in terms of the perturbing potential. However, this perturbing potential itself is an infinite series of terms in the Taylor's expansion of the potential function. Thus, some kind of scheme is required to group terms of the same order of magnitude arising in the Taylor's expansion of the potential function. One such scheme is given by the Van Hove (1961) ordering parameter λ, where λ is defined as the ratio of the root mean square displacement and the nearest neighbour distance. Terms of the same order in λ have to be collected for the calculation of the physical properties of the crystal.

The next terms beyond the harmonic approximation are the cubic and quartic terms. They contribute to the lowest-order of PT, which is of order λ^2. The contribution to a physical property from the quartic term is as important as the contribution from the cubic term, because both terms have the same order of magnitude. We should also mention that these two terms have opposite signs. For example, the inclusion of these two terms in the calculation of the phonon frequency, ω, will cause the harmonic frequency to be shifted from its mean value. These anharmonic frequency shifts are known as the cubic shift and the quartic shift. The characteristics of these two shifts are that they have the same order of magnitude, but they carry opposite signs. Therefore, the cubic and quartic

terms in the Taylor's expansion of the potential energy must be both retained in the calculation of any physical property to the λ^2 order in PT.

Anharmonic effects have been investigated in insulators, rare-gas solids, alkali halides, and metals for almost thirty years. The early period of the last thirty years contained mostly results for rare-gas solids only in terms of rough estimates or in order of magnitude estimates of anharmonic contributions to specific heat at constant volume. The first complete calculation of the thermodynamic properties of a face centred cubic (fcc) lattice was carried out by Klien et. al. (1969) employing the λ^2 anharmonic PT. They have obtained numerical results for the rare-gas solids Ar, Kr, and Xe by employing a nearest-neighbour central force (NNCF) model using the 6-12 Lennard-Jones (12-6 L-J) potential. For the case of alkali halides Cowley (1971) has calculated the λ^2 anharmonic contributions to the thermodynamic properties of sodium chloride.

The calculation of all the thermodynamic properties for metals has been carried out by several authors. Cowley and Shukla (1974) have calculated the thermodynamic properties of an anharmonic crystal for a simple model of copper. They have carried out these calculations by several methods in the lowest order of PT. Shukla and MacDonald (1980) have presented a method for an exact calculation, to $O(\lambda^2)$ in PT, of the thermal expansion (ε) of cubic crystals in the high temperature limit. This calculation was carried out for NNCF model of a monatomic fcc crystal by minimizing the sum of the static energy, U, and the vibrational parts of the Helmholtz free energy of the crystal as a function of temperature and volume. Numerical results for a number of materials (Pb, Al, Ag, Ni, Cu, Ca, and Sr) were obtained using the three parameter Morse potential.

MacDonald and MacDonald (1981) have modified this Morse potential by introducing a fourth parameter b. With this modified Morse potential they have carried out a consistent calculation of the thermodynamic properties of monatomic fcc crystals at high temperatures. These properties were obtained from the Helmholtz free energy of the crystal F(V,T) by means of the appropriate thermodynamic relations.

In the case of body centred cubic (bcc) crystals the thermodynamic properties of monatomic crystal were carried out at high temperatures from F(V,T) for a second-neighbour central-force of the bcc lattice. MacDonald, Shukla, and Kahaner (1983) have calculated the thermodynamic properties for the alkali metals Li, Na, K, Rb, and Cs. MacDonald and Shukla (1985) have applied the second-neighbour central-force model of a bcc crystal on the transition metals V, Nb, Ta, Mo, and W.

The knowledge of the atomic mean-square displacement is important in determining the Debye-Waller factor (DWF) which enters in the calculation of the intensity of X-ray and neutron scattering and the Mössbauer fraction. It is also important in the theory of melting based on the Lindemann approach and in the determination of the ordering parameter λ. The first lowest-order anharmonic calculation of DWF was carried out by Maradudin and Flinn (1963). Their calculation was done in the leading-term approximation for NNCF model of a fcc lattice. This approximation requires the retention of the highest ordered radial derivatives of the interatomic potential. However, it has since been shown by Shukla and Wilk (1974) that this approximation overestimates the cubic and the quartic contributions by 1% and 40%, respectively.

The anharmonic contributions to MSD were calculated for all the bcc alkali metals by Shukla and Mountain (1982) and Shukla and Heiser (1986) for a long-range sixth neighbour interaction potential. Their calculation was performed without making the leading-term approximation. A comparison of the lowest-order (λ^2) perturbation theory and MD method results for the same potential function shows the adequacy of the λ^2 PT for the alkali metals.

The calculation of MSD has been carried out by Heiser, Shukla, and Cowley (1986) (HSC) for short-range interaction, such as the 12-6 L-J potential, for the NNCF model of the fcc crystal using the λ^2 PT, MD, and the MC methods. To investigate the adequacy of the λ^2 PT they have compared the numerical results of the λ^2 PT and those of the MD and MC methods. The agreement between the λ^2 PT and MC results was quite good at low temperatures, in fact up to 3/4 of the melting temperature (T_m). Because the λ^2 PT contribution to MSD was inadequate at higher temperature, they concluded that to obtain good agreement of the results with MC the next order of PT of $O(\lambda^4)$ would be required.

Recently, Shukla and Hübschle (1989) proposed a Green's function method to calculate the MSD of a crystal. This method sums a class of all anharmonic contributions to the MSD. It has been shown that the MC results for MSD can be sufficiently represented up to $T \approx T_m$ for the 12-6 L-J NNCF model of the fcc crystal. Even though discrepancy exists for $T \approx T_m$ between the Green's function method and the MC results, the total MSD calculation to $O(\lambda^2)$ is more accurately given in their work than in HSC.

The most recent work done on MSD was carried out by Shukla and Plint (1989). They have developed an algebraic method for an exact calculation of the quasiharmonic and two lowest-order (cubic and quartic) anharmonic contributions to DWF of an anharmonic crystal in the high temperature limit. Although this method is applicable to any monatomic cubic crystal, Shukla and Plint (1989) have presented algebraic equations only for a NNCF model of a fcc crystal for any two-body potential $\phi(r)$. In particular, they have calculated DWF for Al from a Morse potential.

In this thesis we want to calculate the various thermodynamic properties of the rare-gas solids Kr and Xe for a Morse potential and a modified Morse potential. Also, we fill the gap in the existing series of calculations on copper, silver, and gold by calculating the thermodynamic properties of gold. MacDonald and MacDonald (1981) have carried out calculations of the thermal properties of Pb, Al, Cu, Ag, Ni, Ca, and Sr at high temperatures for a modified Morse potential in the NNCF approximation. Calculation of the thermodynamic properties of Kr, Xe and Au requires determining the paramters of the modified Morse potential.

Once the potential parameters are determined, and the free energy is minimized, the crystal lattice-spacing is calculated at any temperature. With this lattice-spacing we will calculate the mean square displacement for the rare-gas solids Kr and Xe. From this calculated MSD the Mössbauer recoilless fraction of Kr and Xe can be determined for the Morse potential, the modified Morse potential, and the Lennard-Jones potential. In addition, we will carry out the calculation of the DWF for the

fcc metals Pb, Al, Cu, Ag, and Au. The method described by Shukla and Plint (1989) has been followed to calculate the MSD and the DWF.

The two basic ingredients in all the thermodynamic calculations are: the phonon frequencies, and the derivatives of a potential function $\phi(r)$. The measured phonon frequencies have in them both the harmonic and anharmonic effects. The first and second derivatives of $\phi(r)$ enter in the calculation of the harmonic frequencies, ω. On the other hand, the calculation of the anharmonic contributions to the phonon frequencies requires the knowledge of higher order derivatives of $\phi(r)$. For example, the third derivative along with the other two derivatives are needed in the evaluation of the cubic shift, and the calculation of the quartic shift requires the knowledge of the first four derivatives. One way to test the effect of a potential function in the calculation of thermodynamic properties of a crystal is to determine the phonon dispersion curves using different potential functions and compare them with experimental results. Previous calculations did not show this type of testing of the potential function.

In this thesis we want to calculate the quasiharmonic phonon dispersion curves for the three principal symmetry directions for the rare-gas solids, Xe and Kr, and for the fcc metals, Cu, Ag, and Au. The calculation is carried out for a NNCF model of a monatomic fcc crystal in the high temperature limit. The phonon frequencies are calculated with the Morse potential and modified Morse potential in order to investigate the effect of different potentials on the calculated results. We compare these curves with the experimental results which are measured by neutron scattering. In addition to the calculation of the quasiharmonic frequencies,

we will determine the cubic and the quartic frequency shifts using the Green's function approach (Shukla and Muller (1971). These shifts are calculated only for Cu. In order to see the effect of these anharmonic shifts we compare the total of the quasiharmonic and anharmonic frequencies with the quasiharmonic frequencies.

The Grüneisen parameter, γ, is a thermodynamic property which is usually obtained from the free energy of the crystal by means of the appropriate thermodynamic definition. The specific heat and bulk modulus enter directly in the calculation of γ through the thermodynamic definition. Also, the Grüneisen parameter can be calculated from the knowledge of the phonon frequency as a function of volume. In this thesis we will calculate the Grüneisen parameter from these two different approaches for the rare-gas solids, Kr and Xe ,and the fcc metals, Cu, Ag, and Au. This calculation is carried out in the high temperature limit to the lowest order in PT. In the case of the rare-gas solids we expect to get comparable results. However, in the case of metals we have to account for the electronic contribution to γ. This can be added in the thermodynamic definition through the specific heat and bulk modulus. Since the phonon frequency considered here does not account for the electron-electron interactions, we will not be able to estimate the electronic contribution to γ from the second approach.

The outline of the thesis is as follows. In chapter 2. we present the high temperature limit expressions for the $O(\lambda^2)$ Helmholtz free energy contributions and the Debye-Waller factor. The details of the calculation of the thermodynamic properties of the rare-gas solids Kr and Xe, and gold are presented in chapter 3, along with the results and

discussion. In chapter 4. we evaluate the Mossbuaer recoilless fraction for Kr and Xe. Also, the calculated DWF for Pb, Al, Cu, Ag, and Au is presented in this chapter. In order to test the potentials used in our calculations we determine the phonon dispersion curves in chapter 5. for Kr and Xe, and Cu, Ag, and Au. In chapter 6. the Grüneisen parameter is calculated, for the fcc materials studied here, using the renormalized phonon frequency, and compared with the values obtained from the thermodynamic definition. A summary of our results is presented in chapter 7.

2. High Temperature-Limit Expressions

2.1. The Helmholtz Free Energy:

In this section we present the formal expression of the Helmholtz free energy needed in the calculation of the thermodynamic properties of a crystal. The free energy (F) of a weak anharmonic crystal has been derived by several authors in the past. Ludwig (1985) and Maradudin et al. (1961) have derived F from straight forward perturbation expansion; whereas, Cowley (1963) has used diagramatic method for the derivation of F. The Helmholtz free energy can also be obtained by integrating the interaction energy over a coupling parameter. Shukla and Muller (1971) have used a Green's function approach to derive an explicit expression for the interaction energy.

Here, we present the full expression of the Helmholtz free energy at a finite temperature to the order λ^2 in PT. The quasiharmonic contribution to F is denoted by F_0, and the two lowest-order (cubic and quartic) anharmonic contributions by F_3 and F_4, respectively. These are given by

$$F = F_0 + F_3 + F_4 \tag{2.1}$$

$$F_0 = K_B T \sum_{\mathbf{q}j} \ln \left(2 \sinh \tfrac{1}{2}\beta\hbar\omega_{\mathbf{q}j}\right) \tag{2.2}$$

$$F_3 = \frac{\hbar^2}{96N} \sum_{q_1 j_1} \sum_{q_2 j_2} \sum_{q_3 j_3} \Delta(q_1+q_2+q_3) \frac{|\Phi(q_1 j_1, q_2 j_2, -q_3 j_3)|^2}{\omega_{q_1 j_1}\, \omega_{q_2 j_2}\, \omega_{q_3 j_3}} \times$$

$$\left\{ \frac{(N_{q_1 j_1} + N_{q_2 j_2})}{2} \left[- \frac{\coth \frac{1}{2}\beta\hbar\,(\omega_{q_1 j_1} + \omega_{q_2 j_2}) + \coth \frac{1}{2}\beta\hbar\omega_{q_3 j_3}}{\omega_{q_1 j_1} + \omega_{q_2 j_2} + \omega_{q_3 j_3}} + \right.\right.$$

$$\left.\left. + \frac{\coth \frac{1}{2}\beta\hbar\,(\omega_{q_1 j_1} + \omega_{q_2 j_2}) - \coth \frac{1}{2}\beta\hbar\omega_{q_3 j_3}}{\omega_{q_1 j_1} + \omega_{q_2 j_2} - \omega_{q_3 j_3}} \right] + \right.$$

$$+ \frac{(N_{q_2 j_2} - N_{q_1 j_1})}{2} \left[- \frac{\coth \frac{1}{2}\beta\hbar\omega_{q_3 j_3} + \coth \frac{1}{2}\beta\hbar\,(\omega_{q_1 j_1} - \omega_{q_2 j_2})}{\omega_{q_3 j_3} + \omega_{q_1 j_1} - \omega_{q_2 j_2}} + \right.$$

$$\left. \left. + \frac{\coth \frac{1}{2}\beta\hbar\omega_{q_3 j_3} - \coth \frac{1}{2}\beta\hbar\,(\omega_{q_1 j_1} - \omega_{q_2 j_2})}{\omega_{q_3 j_3} - \omega_{q_1 j_1} + \omega_{q_2 j_2}} \right] \right\} \quad (2.3)$$

$$F_4 = \frac{\hbar^2}{32N} \sum_{q_1 j_1} \sum_{q_2 j_2} \frac{\Phi(q_1 j_1, q_2 j_2, -q_1 j_1, -q_2 j_2)}{\omega_{q_1 j_1}\, \omega_{q_2 j_2}} N_{q_1 j_1}\, N_{q_2 j_2} \quad (2.4)$$

The various symbols in Eqs. (2.2)-(2.4) are defined as follows: K_B is Boltzmann constant, $\hbar^2$ is Plank's constant divided by 2π, $\beta=1/(K_B T)$, T is temperature, N represents the number of unit cells in the crystal, $N_{qj} = \coth(\frac{1}{2}\beta\hbar\omega_{qj})$. The delta function $\Delta(q_1+q_2+ \ldots +q_n)$ is unity if $(q_1+q_2+\ldots+q_n)$ is zero or vector of the reciprocal lattice (τ) and zero otherwise. The Φ functions appearing in Eqs. (2.3) and (2.4) are the Fourier transforms of the third- and fourth-order atomic force constant. In general, the Fourier transforms of the n^{th} - order atomic force constant $\phi_{\alpha\beta \ldots \mu}(l)$ is defined by the following:

$$\Phi(q_1 j_1, q_2 j_2, \ldots, q_n j_n) = \frac{1}{2M^{n/2}} \sum_{l}{}' \sum_{\alpha\beta \ldots \mu} \phi_{\alpha\beta \ldots \mu}(l) \times$$

$$\times\ e_{\alpha}(q_1 j_1) \ldots e_{\mu}(q_n j_n) \times (1 - e^{iq_1 \cdot r_l}) \ldots (1 - e^{iq_n \cdot r_l}) \quad (2.5)$$

where the prime over the direct lattice vector (l) summation in the previous equation indicates the omission of the origin point, and $\omega(qj)$ and $e(qj)$ are the eigenvalues and eigenvectors, respectively, for the wave vector $\mathbf{q}$ and branch index j. M is the atomic mass.

In our calculation we have used the high temperature approximation ($T > \theta_D$) where N_{qj} is approximated to $N_{qj} \approx 2/(\beta\hbar\omega_{qj})$. The harmonic and cubic and quartic anharmonic contributions to F are then given as:

$$F_0 = K_B T \sum_{qj} \ln(\beta\hbar\omega_{qj}) + \frac{\hbar^2}{K_B T} \sum_{qj} \omega_{qj}^2 \quad (2.6)$$

$$F_3 = -\frac{1}{12\beta^2 N} \sum_{q_1 j_1} \sum_{q_2 j_2} \sum_{q_3 j_3} \Delta(q_1+q_2+q_3) \frac{|\Phi(q_1 j_1, q_2 j_2, -q_3 j_3)|^2}{\omega_{q_1 j_1}^2 \omega_{q_2 j_2}^2 \omega_{q_3 j_3}^2} \quad (2.7)$$

$$F_4 = \frac{1}{8\beta^2 N} \sum_{q_1 j_1} \sum_{q_2 j_2} \frac{\Phi(q_1 j_1, q_2 j_2, -q_1 j_1, -q_2 j_2)}{\omega_{q_1 j_1}^2 \omega_{q_2 j_2}^2} +$$

$$+ \frac{\hbar^2}{48N} \sum_{q_1 j_1} \sum_{q_2 j_2} \frac{\Phi(q_1 j_1, q_2 j_2, -q_1 j_1, -q_2 j_2)}{\omega_{q_1 j_1} \omega_{q_2 j_2}} \quad (2.8)$$

Next, we have to express F_0, F_3, F_4 in computational forms. The calculation of F_3 and F_4 has been carried out for the NNCF model of the fcc crystal by Shukla (1980) and Shukla and Wilk (1974). These forms are presented in chapter 3.

2.2. The Debye-Waller Factor:

In this section the high temperature expressions for the harmonic and the two lowest-order (λ^2) anharmonic contributions to Debye-Waller factor (DWF) are presented. Maradudin and Flinn (1963) have derived the high temperature limit ($T > \theta_D$) expressions for the anharmonic contributions to DWF in the lowest order (λ^2) perturbation theory by retaining the cubic and quartic terms in the Hamiltonian . They found four anharmonic contributions: two of these were isotropic and proportional to $|\mathbf{q}|^2$ and the other two were nonisotropic and proportional to $|\mathbf{q}|^4$. Their calculation was done in the leading-term approximation .

In our calculation we use the appropriate expressions for DWF for cubic crystals that are summarized by Shukla and Mountain (1982). The quasiharmonic contribution to DWF is represented by $2M_{QH}(\mathbf{q})$, and cubic and quartic contributions to DWF by $2M_2(\mathbf{q})$ and $2M_1(\mathbf{q})$, respectively. These are given by

$$2M_{QH}(\mathbf{q}) = |\mathbf{q}|^2 \frac{K_B T}{3NM} \sum_{q_1 j_1} \frac{1}{\omega_{qj}^2} \tag{2.10}$$

$$2M_2(\mathbf{q}) = |\mathbf{q}|^2 \frac{(K_B T)^2}{6N^2 M} \sum_{q_1 j_1} \sum_{q_2 j_2} \sum_{q_3 j_3} \Delta(q_1+q_2+ \ldots +q_n) \times \times \frac{|\Phi(q_1 j_1, q_2 j_2, -q_3 j_3)|^2}{\omega_{q_1 j_1}^2 \, \omega_{q_2 j_2}^2 \, \omega_{q_3 j_3}^4} \tag{2.11}$$

$$2M_1(\mathbf{q}) = - |\mathbf{q}|^2 \frac{(K_B T)^2}{6N^2 M} \sum_{q_1 j_1} \sum_{q_2 j_2} \frac{\Phi(q_1 j_1, q_2 j_2, -q_1 j_1, -q_2 j_2)}{\omega_{q_1 j_1}^2 \, \omega_{q_2 j_2}^4} \tag{2.12}$$

The calculation of F or DWF requires a method to evaluate a certain number of dimensionless sums. The evaluation of these sums as described by Shukla and Wilk (1974) requires the knowledge of tensor-type functions involving single whole Brillouin zone (BZ) sums. The calculation of F or DWF is applied for a NNCF model of a fcc crystal for any two-body potential. Here, we consider only the final forms of these two quantities.

3. Thermodynamic Properties of fcc Materials

The total free energy equation of state for a crystal is expressed as the sum of the static lattice energy U, the harmonic F_0, and the $O(\lambda^2)$ anharmonic contributions $F(\lambda^2)$. This equation is written as

$$E(QH) = U + F_0 \tag{3.1}$$

$$E(\lambda^2) = E(QH) + F(\lambda^2) \tag{3.2}$$

The various contributions to the equation of state, obtained from Shukla and MacDonald (1980), are defined as follows:

$$F_0 = F_0^{(1)} + F_0^{(2)} \tag{3.3}$$

where

$$F_0^{(1)} = 3\,N\,K_B T\,[\,\ln\{\frac{\hbar}{K_B T}(\frac{8\,B}{M})^{1/2}\} + \{\frac{1}{2}f(a_1) - 0.4288\}\,] \tag{3.4}$$

$$F_0^{(2)} = 3\,N\frac{\hbar^2}{6MK_B T}B\,(1 + 3\,a_1) \tag{3.5}$$

$$F(\lambda^2) = F_4^{(1)} + F_4^{(2)} + F_3 \tag{3.6}$$

where

$$F_4^{(1)} = 3\,N\frac{\hbar^2}{24MB}[\,D\,S_{2A}(a_1) + \frac{2C}{r}S_{2B}(a_1) + \frac{4B}{r^2}S_{2C}(a_1)\,] \tag{3.7}$$

$$F_4^{(2)} = 3\,N\frac{(K_B T)^2}{192B^2}[\,D\,S_{4A}(a_1) + \frac{2C}{r}S_{4B}(a_1) + \frac{4B}{r^2}S_{4C}(a_1)\,] \tag{3.8}$$

$$F_3 = -3N\frac{(K_BT)^2}{9216B^3}\left[C^2 S_{3A}(a_1) + \frac{12BC}{r} S_{3B}(a_1) + \frac{4B^2}{r^2} S_{3C}(a_1)\right] \qquad (3.9)$$

$$U = \frac{N}{2} \sum_{i \neq j} \phi(r_{ij}) \qquad (3.10a)$$

For the NNCF model,

$$U = \frac{N}{2} 12\, \phi(r) = 6N\, \phi(r) \qquad (3.10b)$$

B, C, and D are combinations of derivatives of ϕ (r) defined as:

$$B(r) = \phi''(r) - \frac{1}{r}\phi'(r) \qquad (3.11)$$

$$C(r) = \phi'''(r) - \frac{3}{r}\phi''(r) + \frac{3}{r^2}\phi'(r) \qquad (3.12)$$

$$D(r) = \phi^{iv}(r) - \frac{6}{r}\phi'''(r) + \frac{15}{r^2}\phi''(r) - \frac{15}{r^3}\phi'(r) \qquad (3.13)$$

These combinations are evaluated at the nearest-neighbour distance corresponding to the temperature T. The functions $f(a_1)$, $S_{2A}(a_1)$, $S_{2B}(a_1)$, $S_{2C}(a_1)$; $S_{3A}(a_1)$, $S_{3B}(a_1)$, $S_{3C}(a_1)$; $S_{4A}(a_1)$, $S_{4B}(a_1)$, and $S_{4C}(a_1)$ are the various BZ sums which are evaluated at the same temperature for the ratio a_1:

$$a_1 = \frac{\phi'(r)/r}{\phi''(r) - \phi'(r)/r} \qquad (3.14)$$

The details of the calculation of the threse sums can obtained from Shukla (1980). Shukla and MacDonald (1980) have fitted these BZ sums to the following functional form:

$$f(a_1) = P(a_1)$$

where $$P(a_1) = \sum_{n=0}^{6} b_n (a_1)^n$$

and the other functions S_{2A}, etc., each fitted to the form $y = \exp [P(a_1)]$. In Table 3.1 the least-squares coefficients from which all the BZ sums can be calculated for values of a_1 in the range $-0.1 \leq a_1 \leq 0.1$ are presented. These fits reproduce the numerical values of the BZ sums to better than 1 part in 10^3.

3.1. Nearest-Neighbour Distance:

The $E(\lambda^2)$ equation of state was minimized with respect to r at constant temperature, and we obtain the nearest-neighbour separation r_T, by applying The Newton-Raphson method:

$$r_{i+1} = r_i - \frac{E'(\lambda^2)}{E''(\lambda^2)} \tag{3.15}$$

Where E' and E'' denote the first and the second derivatives of $E(\lambda^2)$ with respect to r. These derivatives were obtained analytically. The various components of $E'(\lambda^2)$ and $E''(\lambda^2)$ are given as follows:

$$[F_0^{(1)}]_1 = 3NK_BT \left[\frac{B'}{B} + \phi'(a_1)\, a_1' \right] \tag{3.16}$$

$$[F_0^{(1)}]_2 = 3NK_BT \left[\frac{B''}{B} - \frac{B'^2}{B^2} + \phi''(a_1)\, a_1'^2 + a_1''\, \phi'(a_1) \right] \tag{3.17}$$

$$[F_0^{(2)}]_1 = 3N \frac{\hbar^2}{6MK_BT} [\, B'(1 + 3a_1) + 3B\, a_1' \,] \tag{3.18}$$

$$[F_0^{(2)}]_2 = 3N \frac{\hbar^2}{6MK_BT} [\, B''(1 + 3a_1) + 6B'\, a_1' + 3B\, a_1'' \,] \tag{3.19}$$

Table 3.1: Coefficients of the least-squares fit of the functions $f(a_1)$, etc.

Function	b_0	b_1	b_2	b_3	b4	b_5	b_6
$f(a_1)$	0.0000	3.5892	-6.6768	16.8293	-48.9623	197.3788	-689.6764
$S_{2A}(a_1)$	0.0000	-3.5929	8.5369	-27.6926	108.6641	-1219.9278	7250.4428
$S_{2B}(a_1)$	1.6667	-3.7867	9.2900	-30.4436	120.0002	-1390.1624	8342.2428
$S_{2C}(a_1)$	1.5010	-4.1647	10.6480	-35.2060	138.9856	-1660.1682	10058.5591
$S_{4A}(a_1)$	2.4849	-7.1856	17.0777	-55.4237	216.2252	-2437.4300	14571.7692
$S_{4B}(a_1)$	4.2057	-7.5530	18.4681	-60.4178	237.8025	-2743.1526	16445.6889
$S_{4C}(a_1)$	4.1707	-8.3623	21.4617	-17.0621	280.8543	-3373.1748	20463.4373
$S_{3A}(a_1)$	5.1507	-10.9028	26.4829	-87.0026	343.6693	-3870.2265	23007.1720
$S_{3B}(a_1)$	4.5251	-10.6448	25.5145	-83.9222	322.2881	-3553.1758	20747.0075
$S_{3C}(a_1)$	6.6127	-10.8787	26.6242	-87.0519	343.0085	-4357.7099	26894.3897

$$[\,F_4^{(1)}\,]_1 = 3N\,\frac{\hbar^2}{24MB}\,[\,D\,S_{2A}\,A_1^{(1)} + \frac{2C}{r}\,S_{2B}\,A_2^{(1)} + \frac{4B}{r^2}\,S_{2C}\,A_3^{(1)}\,] \quad (3.20)$$

$$\begin{aligned}[\,F_4^{(1)}\,]_2 = 3N\,\frac{\hbar^2}{24MB}\,[\,D\,S_{2A}\,\{\,(A_1^{(1)})^2 + \left(\frac{B'}{B}\right)^2 - \frac{B''}{B} - \left(\frac{D'}{D}\right)^2 + \\ + \frac{D''}{D} + \frac{S_{2A}''}{S_{2A}}\,a_1'^2 + \frac{S_{2A}'}{S_{2A}}\,a_1'' - \left(\frac{S_{2A}'}{S_{2A}}\,a_1'\right)^2\,\} + \\ + \frac{2C}{r}\,S_{2B}\,\{\,(A_2^{(1)})^2 + \left(\frac{B'}{B}\right)^2 - \frac{B''}{B} - \left(\frac{C'}{C}\right)^2 + \\ + \frac{C''}{C} + \frac{1}{r^2} + \frac{S_{2B}''}{S_{2B}}\,a_1'^2 + \frac{S_{2B}'}{S_{2B}}\,a_1'' - \left(\frac{S_{2B}'}{S_{2B}}\,a_1'\right)^2\,\} + \\ + \frac{4B}{r^2}\,S_{2C}\,\{\,(A_3^{(1)})^2 + \frac{2}{r^2} + \frac{S_{2C}''}{S_{2C}}\,a_1'^2 + \frac{S_{2C}'}{S_{2C}}\,a_1'' - \\ - \left(\frac{S_{2C}'}{S_{2C}}\,a_1'\right)^2\,\}]\end{aligned} \quad (3.21)$$

where in Eqs. (3.20) and (3.21):

$$A_1^{(1)} = -\frac{B'}{B} + \frac{D'}{D} + a_1'\,\frac{S_{2A}'}{S_{2A}}\ , \quad (3.22)$$

$$A_2^{(1)} = -\frac{B'}{B} + \frac{C'}{C} - \frac{1}{r} + a_1'\,\frac{S_{2B}'}{S_{2B}}\ , \quad (3.23)$$

$$A_3^{(1)} = -\frac{2}{r} + a_1'\,\frac{S_{2C}'}{S_{2C}}\ . \quad (3.24)$$

$$[\,F_4^{(2)}\,]_1 = 3N\,\frac{(K_BT)^2}{192B^2}\,[\,D\,S_{4A}\,A_1^{(2)} + \frac{2C}{r}\,S_{4B}\,A_2^{(2)} + \frac{4B}{r^2}\,S_{4C}\,A_3^{(2)}\,] \quad (3.25)$$

$$\begin{aligned}[\,F_4^{(2)}\,]_2 = 3N\,\frac{(K_BT)^2}{192B^2}\,[\,D\,S_{4A}\,\{\,(A_1^{(2)})^2 + 2\left(\frac{B'}{B}\right)^2 - 2\,\frac{B''}{B} - \left(\frac{D'}{D}\right)^2 \\ + \frac{D''}{D} + \frac{S_{4A}''}{S_{4A}}\,a_1'^2 + \frac{S_{4A}'}{S_{4A}}\,a_1'' - \left(\frac{S_{4A}'}{S_{4A}}\,a_1'\right)^2\,\} +\end{aligned}$$

$$+\frac{2\,C}{r}S_{4B}\{(A2^{(2)})^2+2\left(\frac{B'}{B}\right)^2-2\frac{B''}{B}-\left(\frac{C'}{C}\right)^2+$$

$$+\frac{C''}{C}+\frac{1}{r^2}+\frac{S_{4B}''}{S_{4B}}a_1'^2+\frac{S_{4B}'}{S_{4B}}a_1''-\left(\frac{S_{4B}'}{S_{4B}}a_1'\right)^2\}+$$

$$+\frac{4\,B}{r^2}S_{4C}\{(A3^{(2)})^2+\left(\frac{B'}{B}\right)^2-\frac{B''}{B}+\frac{2}{r^2}+$$

$$+\frac{S_{4C}''}{S_{4C}}a_1'^2+\frac{S_{4C}'}{S_{4C}}a_1''-\left(\frac{S_{4C}'}{S_{4C}}a_1'\right)^2\}] \qquad (3.26)$$

where in Eqs. (3.25) and (3.26):

$$A1^{(2)}=-2\frac{B'}{B}+\frac{D'}{D}+a_1'\frac{S_{4A}'}{S_{4A}}\quad, \qquad (3.27)$$

$$A2^{(2)}=-2\frac{B'}{B}+\frac{C'}{C}-\frac{1}{r}+a_1'\frac{S_{4B}'}{S_{4B}}\quad, \qquad (3.28)$$

$$A3^{(2)}=-\frac{B'}{B}-\frac{2}{r}+a_1'\frac{S_{4C}'}{S_{4C}}\quad. \qquad (3.29)$$

$$[F3]_1=-3N\frac{(K_BT)^2}{9216B^3}\;[C^2S_{4A}A_1^{(3)}+\frac{12BC}{r}S_{3B}A_2^{(3)}+$$

$$+\frac{4B^2}{r^2}S_{3C}A_3^{(3)}] \qquad (3.30)$$

$$[F3]_2=-3N\frac{(K_BT)^2}{9216B^3}[C^2S_{3A}\{(A1^{(3)})^2+3\left(\frac{B'}{B}\right)^2-3\frac{B''}{B}-$$

$$-2\left(\frac{C'}{C}\right)^2+2\frac{C''}{C}+\frac{S_{3A}''}{S_{3A}}a_1'^2+$$

$$+\frac{S_{3A}'}{S_{3A}}a_1''-\left(\frac{S_{3A}'}{S_{3A}}a_1'\right)^2\}+$$

$$+\frac{12BC}{r}S_{3B}\{(A2^{(3)})^2+2\left(\frac{B'}{B}\right)^2-2\frac{B''}{B}-$$

$$+\left(\frac{C'}{C}\right)^2+\frac{C''}{C}+\frac{1}{r^2}+$$

$$+\frac{S_{3B}''}{S_{3B}}a_1'^2+\frac{S_{3B}'}{S_{3B}}a_1''-\left(\frac{S_{3B}'}{S_{3B}}a_1'\right)^2\}+$$

$$+\frac{4B^2}{r^2}S_{3C}\{(A3^{(3)})^2+\left(\frac{B'}{B}\right)^2-\frac{B''}{B}+\frac{2}{r^2}+$$

$$+\frac{S_{3C}''}{S_{3C}}a_1'^2+\frac{S_{3C}'}{S_{3C}}a_1''-\left(\frac{S_{3C}'}{S_{3C}}a_1'\right)^2\}] \qquad (3.31)$$

where in Eqs. (3.30) and (3.31):

$$A1^{(3)}=-3\frac{B'}{B}+2\frac{C'}{C}+a_1'\frac{S_{3A}'}{S_{3A}}\ , \qquad (3.32)$$

$$A2^{(3)}=-2\frac{B'}{B}+\frac{C'}{C}-\frac{1}{r}+a_1'\frac{S_{3B}'}{S_{3B}}\ , \qquad (3.33)$$

$$A3^{(3)}=-\frac{B'}{B}-\frac{2}{r}+a_1'\frac{S_{3C}'}{S_{3C}}\ . \qquad (3.34)$$

The single and double primes in Eqs. (3.16)-(3.34) denoted differentiations with respect to r except in the f and S functions where the differentiations are with respect to a_1.

3.2. Thermodynamic Relations:

The calculated r_T value is the zero pressure result since

$$P=-\left(\frac{\partial E(\lambda^2)}{\partial V}\right)_T \qquad (3.35)$$

and thus all the calculated thermodynamic properties will be at zero pressure. Once the zero pressure volume V(T) is known the other

thermodynamic properties can be calculated by taking the derivatives of $E(\lambda^2)$ with respect to V and T. Thus, we can calculate the following quantities:

Thermal expansion $\varepsilon(T)$:

$$\varepsilon(T) = \frac{r(T) - r_c}{r_c} \tag{3.36}$$

where r_c is the reference length.

For rare-gas solids, coefficient of volume expansion $\beta(T)$:

$$\beta(T) = \frac{1}{V(T)} \left(\frac{dV}{dT} \right)_p = \frac{1}{B_T} \left(\frac{\partial^2 E}{\partial V \partial T} \right)_p \tag{3.37}$$

For gold the experimental coefficient of linear expansion $\alpha(T)$:

$$\alpha(T) = \frac{1}{r(T_c)} \left(\frac{dr}{dT} \right)_p \tag{3.38}$$

where T_c is the reference temperature.

Specific heat at constant volume C_V:

$$C_V^{\,l} = - T \left(\frac{\partial^2 E}{\partial T^2} \right)_v \tag{3.39}$$

Isothermal bulk modulus B_T:

$$B_T^{\,l} = V(T) \left(\frac{\partial^2 E}{\partial V^2} \right)_T \tag{3.40}$$

Specific heat at constant pressure C_p:

$$C_p^{\,l} = C_V^{\,l} + 9\, \alpha^2(T)\, V(T)\, B_T^{\,l}\, T \tag{3.41}$$

Adiabatic bulk modulus B_S:

$$B_S^{\,l} = \frac{C_p^{\,l}}{C_V^{\,l}}\, B_T^{\,l} \tag{3.42}$$

The Grüneisen parameter γ:

$$\gamma^l = \frac{3\,\alpha\,V\,B_T^l}{C_V^l}$$

In the above relations l stands for lattice contribution.

In order to compare our calculated thermodynamic properties with the experimental values for gold, we must take into account the effect of the electrons. We will use the free electron theory (Slater (1939), and MacDonald and MacDonald (1981)) to make a rough estimate of the electronic contribution to the specific heat and the bulk modulus. The electronic free energy is defined as

$$F^{el} = \frac{3}{5}\, zNE_{00}\, [\, 1 - \frac{5}{12} (\frac{\pi K_B T}{E_{00}})^2\,] \tag{3.43}$$

where z is the number of free electrons per atom, E_{00} is the fermi energy at T = 0K and is written as

$$E_{00} = \frac{1}{2m^*} (\frac{3h^3N}{8\pi})^{2/3} (\frac{z}{V})^{2/3}, \tag{3.44}$$

m* is the effective mass of the electron. The electronic contributions to the isothermal bulk modulus and specific heat, respectively, are

$$B_T^{el} = \frac{2}{3} z \frac{N}{V} E_{00}\, [\, 1 + \frac{\pi^2}{12} (\frac{K_B T}{E_{00}})^2\,]\,, \tag{3.45}$$

since $(\frac{K_B T}{E_{00}}) << 1$ for the metals in this study, B_T^{el} can be approximated as

$$B_T^{el} = \frac{2}{3} z \frac{N}{V} E_{00}\,, \tag{3.46}$$

and

$$C_v^{el} = \frac{\pi^2}{2} z R \frac{K_B T}{E_{00}} = \sigma_0 T \tag{3.47}$$

where R is the gas constant, and σ_0 is the low-temperature coefficient of soecific heat.

Since the values of E_{00}, m*, and σ_0 are not consistent with the relations in Eqs. (3.44) and (3.47), we use the most reliable of these parameters, σ_0, to determine a particular combination of parameters. We have followed the procedure which was outlined by MacDonald and MacDonald (1981). The value of σ_0, 174.1 μcal / K^2 (g atom), for Au used in the calculations was taken from Martin (1964). We define

$$M' = (m^*/m_0) z^{1/3} = \frac{2c}{\pi^2 R K_B r_0^2 N^{2/3}} \tag{3.48}$$

where

$$c = (\frac{1}{2m_0}) (\frac{3\sqrt{2}\, h^3 N}{8\pi})^{2/3} \tag{3.49}$$

and m_0 is the free electron mass. The B_T^{el} can now be rewritten as

$$B_T^{el} = \frac{2\sqrt{2}\, c\, z^2}{3M' r_T^5 N^{2/3}} \tag{3.50}$$

Now the total of the electronic and lattice contributions for the specific heat, the bulk modului, and the Grüneisen parameter can be written as

$$C_v = C_v^{el} + C_v^{l} \tag{3.51}$$

$$B_T = B_T^{el} + B_T^{l} \tag{3.52}$$

$$C_p = C_V + 9\alpha^2(T)\, V(T)\, B_T\, T \tag{3.53}$$

$$B_S = \frac{C_p}{C_V} B_T \tag{3.54}$$

$$\gamma = \frac{3\ \alpha\ V\ B_T}{C_V} \tag{3.55}$$

3.3. Interatomic Potentials:

In order to calculate the total free energy equation of state for a crystal, a pair potential and its derivatives are required. The three parameter Morse potential was used in the calculation of the thermodynamic properties of the materials studied here. This potential is given by

$$\phi_M(r) = U_0\ \{\exp[-2\alpha(r - r_0)] - 2\exp[-\alpha(r - r_0)]\} \tag{3.56}$$

The parameters U_0, r_0, and α denote the well depth, the nearest-neighbour distance, and the steepness of the potential function, respectively. For rare-gas solids, Kr and Xe, these parameters were determined by Shukla and Shanes (1984) from the zero pressure volume at T = 0K. In their calculation they included the harmonic-zero point energy. The values of these parameters are listed in Table 3.2. Also, in this table the Debye temperatures for Kr and Xe (Urvrvas, Losee, and Simmons (1967)) are presented.

For the fcc metals we obtain these parameters with the neglect of the zero-point energy. U_0 and r_0 are determined from the expaerimental values of the sublimation energy, L, (Seitz (1940)) and the

lattice constant (a_0) at T = 0K (Varshni and Bloor (1963)), respectively. The α parameter is determined from the following relation:

$$K_B \theta_D = \hbar \left[\frac{8 \phi''(r_0)}{M} \right]^{1/2} = 4 \hbar \left(\frac{U_0}{M} \right)^{1/2} \alpha \qquad (3.57)$$

where θ_D is the Debye temperature. The value of θ_D for Au was obtained from Martin(1964), and for the other materials from Touloukian and Buyco (1970). Experimental data required in the calculation of the potential parameters are presented in Table 3.3. The potential parameters for the fcc metals: Pb, Al, Cu, Ag, and Au are listed in Table 3.4.

The calculated parameters of the Morse potential, in this work, for Al, Cu, and Ag were in excellent agreement with the parameters reported in Shukla and MacDonald (1980). However, the α parameter, the steepness of the potential function, for lead was higher than the value reported in Shukla and MacDonald (1980). This disagreement is due to the difference in experimental value chosen for θ_D at 0 K. However, the calculated thermodynamic properties with this corrected value were not very much different from those obtained by MacDonald and MacDonald (1981). Therefore, we will not present these corrected thermodynamic properties of Pb.

Shukla and MacDonald (1980) have noted that the slope of the calculated thermal expansion $\varepsilon(T)$ depends greatly on the second derivative of the potential and some adjustment of the potential function might give a better agreement between calculated and experimental $\varepsilon(T)$. Accordingly, MacDonald and MacDonald (1981) have modified the Morse potential function as follows:

$$\phi_{MM}(r) = \frac{U_0}{1 - 2b} \{\exp[-2\alpha(r - r_0)\sqrt{b}] - 2b \exp[-\alpha(r - r_0)/\sqrt{b}]\} \qquad (3.38)$$

where the values of the parameters U_0 and r_0 are not affected by this modification of the potential. The parameter b is determined by matching the computed $\varepsilon(T)$ to experimental values in the neighbourhood of the Debye temperature. The usual form of the Morse potential is obtained when b is set equal to one. Values of b for the metals: Al, Cu, and Ag were obtained from MacDonald and MacDonald (1981).We have determined the values of b for the metals: Pb and Au.

The calculated values of the parameter b for Kr and Xe do not quite satisfy the condition required for the determination of b because with these values the computed and the experimental $\varepsilon(T)$ are not exactly equal near θ_D. The procedure to determine this parameter was to change b until the computed $\varepsilon(T)$ matches very closely the experimental value at a temperature near θ_D. This gave a value of b=0.501. The restriction on the value of b is that it can not be exactly equal to 0.5, because that is a singular point for the potential function. Also, b can not be less than 0.5, since that would change the sign of the potential function. Therefore, the value of b must be greater than 0.5. The best agreement between computed and experimental $\varepsilon(T)$ was obtained with b in the neighbourhood of 0.5. However, this agreement is not very good. The values of b are presented in Tables 3.2 and 3.4.

Table 3.2: Potential parameters and the Debye temperatures for Kr and Xe. The units of r_0, α, and U_0 are (Å), ($Å^{-1}$), and (10^{-14} erg), respectively.

	r_0	α	U_0	b	θ_D (K)
Kr	3.969	1.556	3.254	0.501	71.7
Xe	4.321	1.375	4.576	0.501	64.0

Table 3.3: Experimental Data Required in The Calculation of The Potential Parameters.

Metals	r_0 (Å)	θ_D (K)	-L (10^{11}erg/mol)
Pb	3.4779	102	19.87
Al	2.8485	423	23.01
Cu	2.5471	342	33.97
Ag	2.8765	228	28.45
Au	2.8742	162.4	38.49

Table 3.4: Potential Parameters For The Metals Studied.

Metals	r_0 (Å)	α ($Å^{-1}$)	U_0 (10^{-12}erg)	b
Pb	3.4779	0.8350	0.5500	1.7
Al	2.8485	1.1611	0.6369	2.5
Cu	2.5471	1.1857	0.9403	2.265
Ag	2.8765	1.1255	0.7874	2.3
Au	2.8742	0.9313	1.0653	1.7

3.4. Results and Discussion:

We present here the equation of state results of our calculations in two sections. The first section contains our calculated thermodynamic properties of the rare-gas solids Kr and Xe, for the Morse potential and the modified Morse potential. In the second section, we will present our calculated thermodynamic properties for Au. The properties were calculated for each interatomic potential, from two different equation of state; i.e. , quasiharmonic, and quasiharmonic plus $O(\lambda^2)$ PT. These will be denoted by the abbreviations E(QH) and $E(\lambda^2)$, respectively. A comparison of our results obtained from the two different equations of state will be made with the experimental thermodynamic properties.

3.4.1. Thermodynamic Properties of Rare-Gas Solids:

The calculated thermodynamics properties are presented in Figures (3.1) through (3.14) together with the experimental values, Losee and Simmon (1968) for Kr, and Trifny and Serin (1969) for Xe. The properties calculated from the E(QH) equation of state seem to give the general shape of the thermodynamic properties. The results obtained from the modified Morse potential show a better agreement with experiment at low temperature. However, at high temperature both potentials do not give the correct magnitudes. This suggests that a correction is needed to bring the theory into agreement with the experimental values. The correction that was added to the E(QH) equation of state was the $O(\lambda^2)$ anharmonic.

The thermal properties obtained from the $E(\lambda^2)$ equation of state were calculated for the entire temperature range (θ_D through T_m).

The computed lattice constant for Kr and Xe are presented in Figures 3.1 and 3.2. The results for both elements are well below the experimental values. However, the results of Morse potential seem to be better than those of modified Morse potential. Similarly, the above description also applies to the computed volume expansion coefficient shown in Figure 3.3 and 3.4 for Kr and Xe respectively. The results obtained from Morse potential are slightly higher than those obtained by modified Morse for temperatures up to 5/6 T_m. At this temperature $E(\lambda^2)$ results of Morse potential starts to break down; whereas the $E(\lambda^2)$ results of modified Morse are still maintaining a positive slope.

The calculated specific heat at constant volume for Kr is shown in Figure 3.5, and the results of modified Morse potential are in good agreement with experiment for the temperature range $\theta_D<T<T_m$; whereas the C_V results for Xe are in fair agreement with experiment for the range $\theta_D<T<3/4T_m$ as shown in Figure 3.6. The C_p curves which are shown in Figure 3.7 and 3.8 for the temperature range $\theta_D<T<T_m$. The E(QH) curves, for both Kr and Xe, have shifted towards the experimental curve when the modified Morse potential was used.

The calculated isothermal and adiabatic bulk moduli are presented in Figures 3.9 through 3.12. The results for both Kr and Xe are in poor agreement with experiment.

Figure 3.1

Lattice Constant of Kr

With Morse (M) and Modified Morse (MM) Potentials.

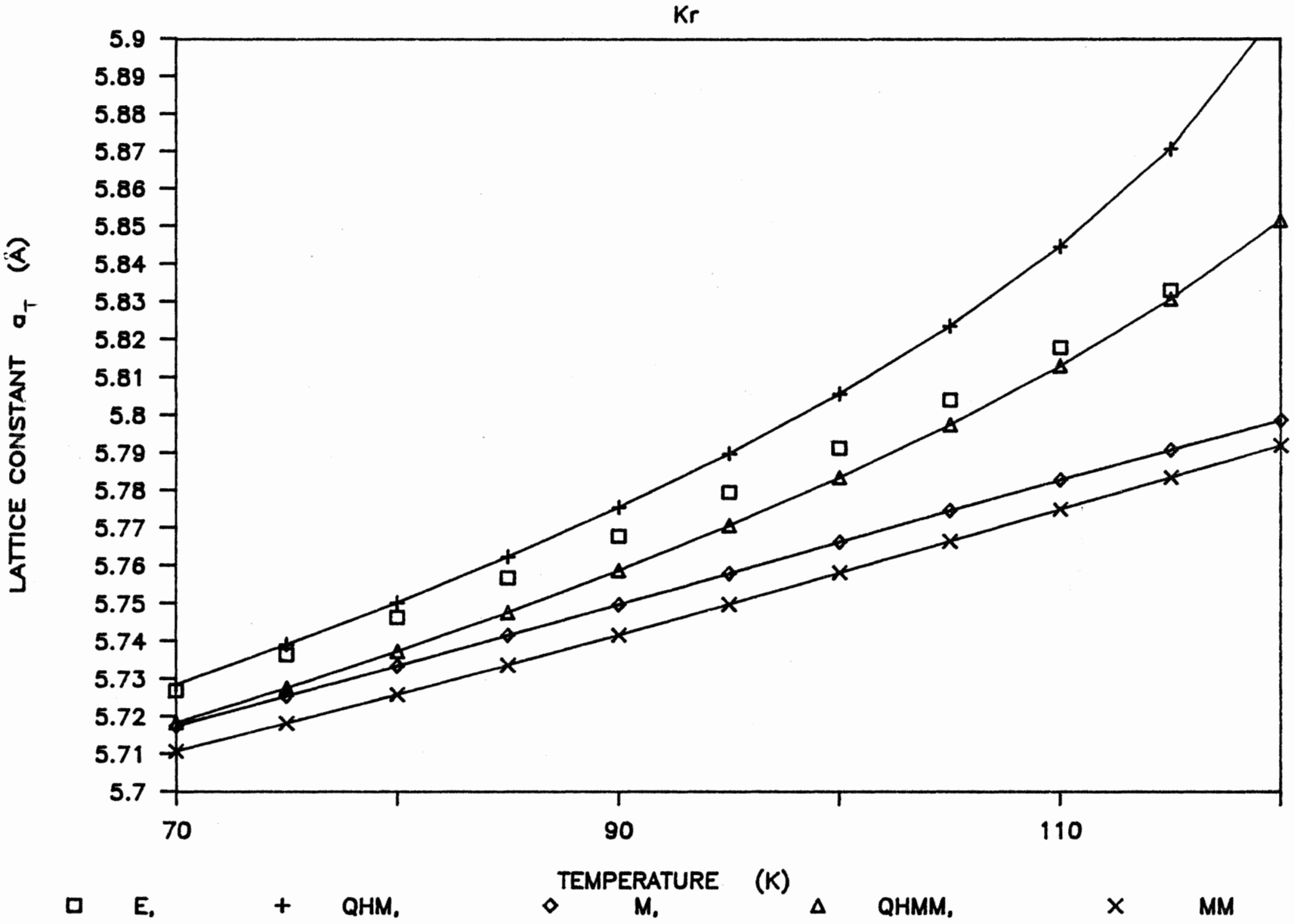
Kr
LATTICE CONSTANT a_T (Å)
5.9
5.89
5.88
5.87
5.86
5.85
5.84
5.83
5.82
5.81
5.8
5.79
5.78
5.77
5.76
5.75
5.74
5.73
5.72
5.71
5.7
70
90
110
TEMPERATURE (K)
E,
QHM,
M,
QHMM,
MM

Figure 3.2

Lattice Constant of Xe

With Morse (M) and Modified Morse (MM) Potentials.

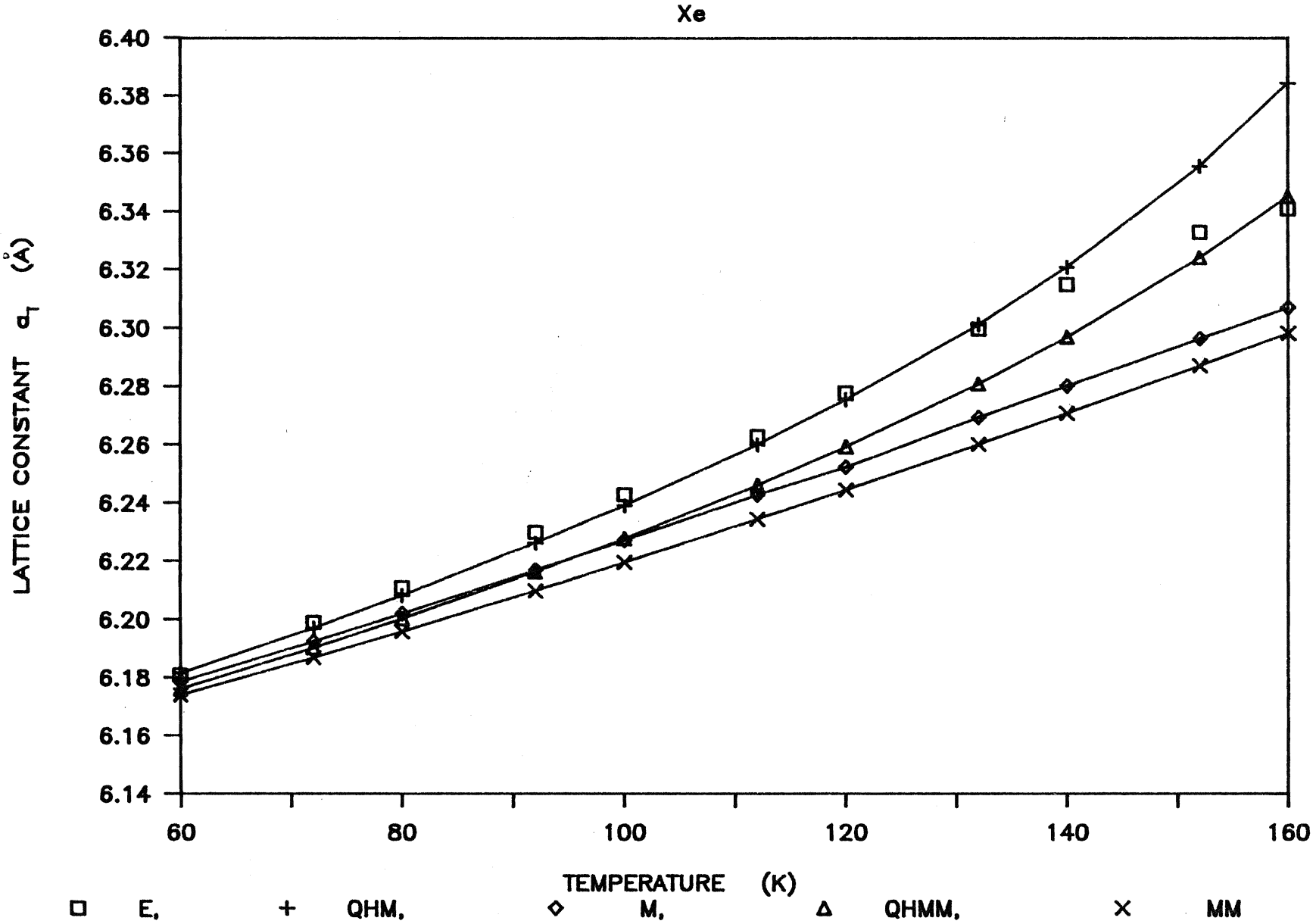
Xe
6.40
6.38
6.36
6.34
6.32
6.30
6.28
6.26
6.24
6.22
6.20
6.18
6.16
6.14
LATTICE CONSTANT a_T (Å)
60
80
100
120
140
160
TEMPERATURE (K)
E,
QHM,
M,
QHMM,
MM

Figure 3.3

Coefficient of Volume Expansion of Kr

With Morse (M) and Modified Morse (MM) Potentials.

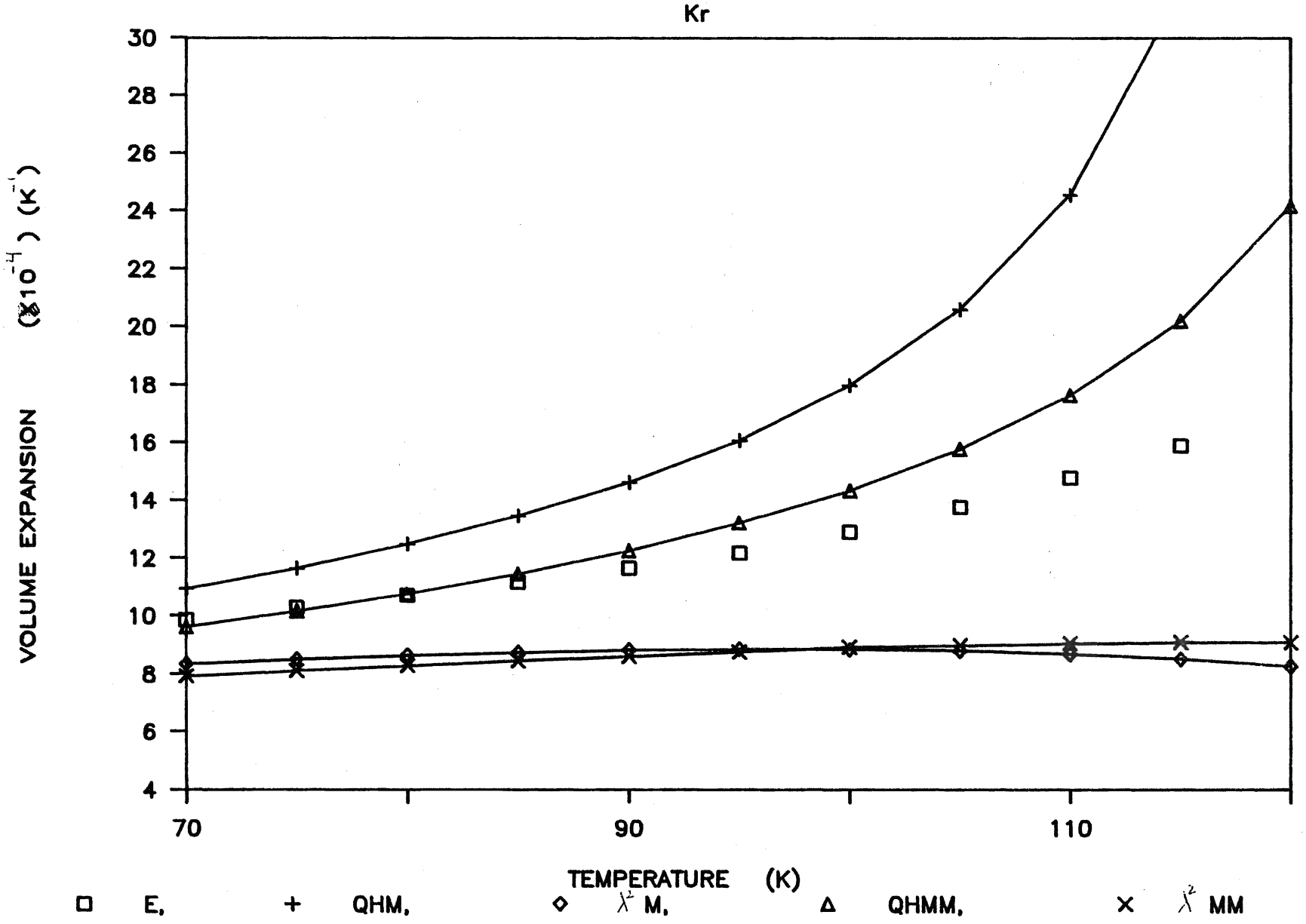
Kr
VOLUME EXPANSION (×10⁻⁴) (K⁻¹)
30
28
26
24
22
20
18
16
14
12
10
8
6
4
70
90
110
TEMPERATURE (K)
E,
QHM,
λ² M,
QHMM,
λ² MM

Figure 3.4

Coefficient of Volume Expansion of Xe

With Morse (M) and Modified Morse (MM) Potentials.

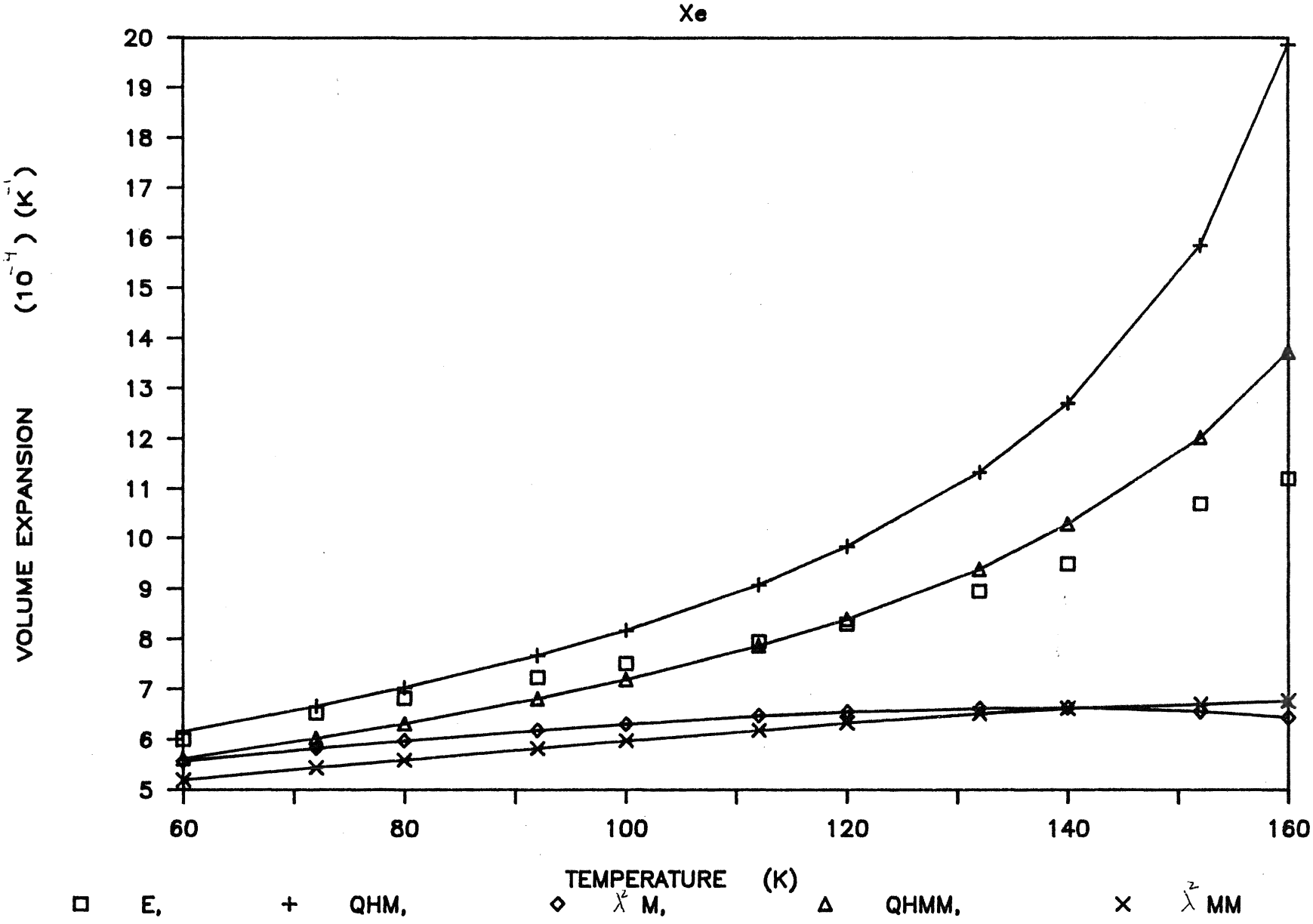
Xe
VOLUME EXPANSION (10^-4) (K^-1)
20
19
18
17
16
15
14
13
12
11
10
9
8
7
6
5
60
80
100
120
140
160
TEMPERATURE (K)
E,
QHM,
λ² M,
QHMM,
λ² MM

Figure 3.5

Specific Heat at Constant Volume of Kr

With Morse (M) and Modified Morse (MM) Potentials.

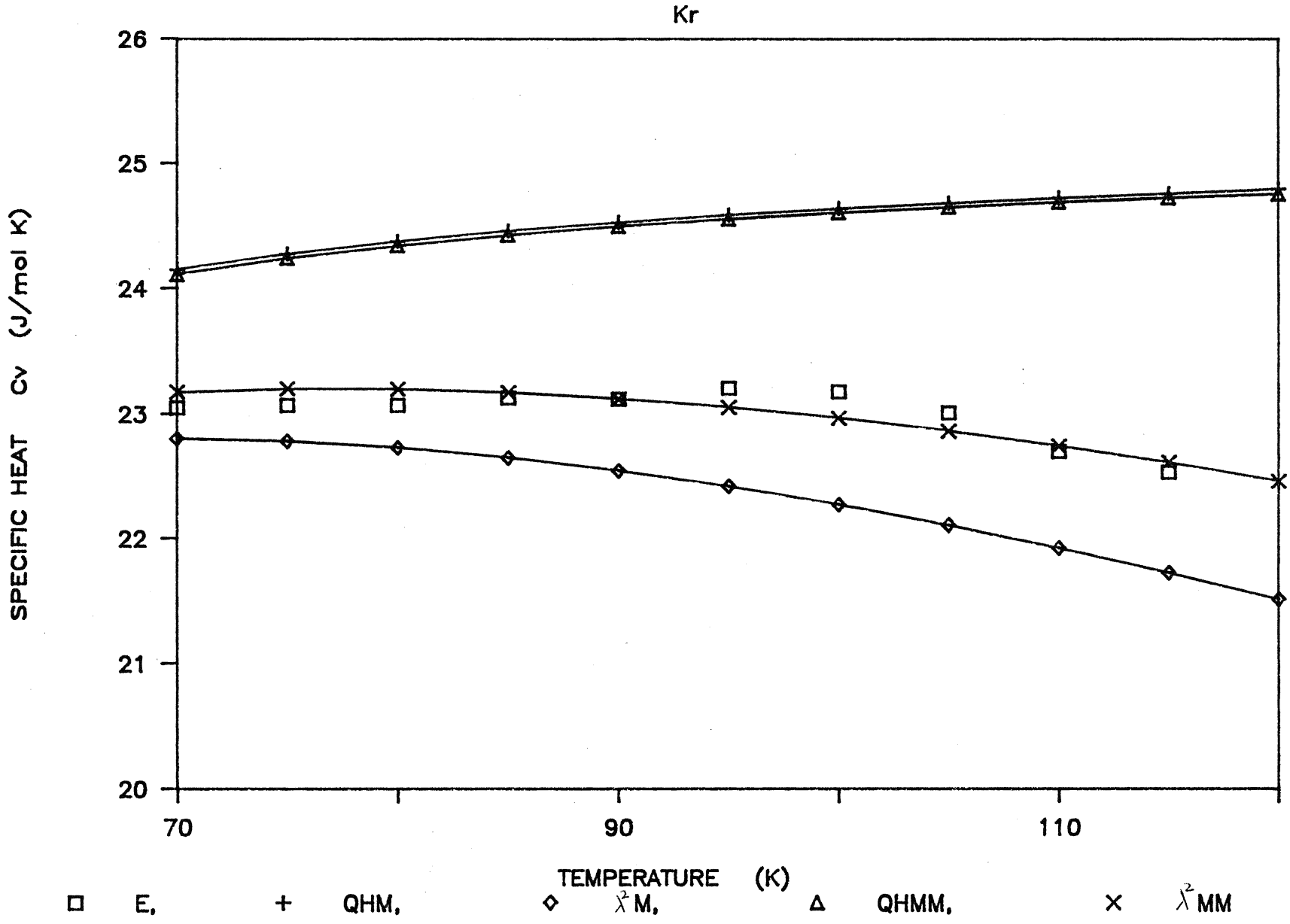
Kr
26
25
24
23
22
21
20
SPECIFIC HEAT Cv (J/mol K)
70
90
110
TEMPERATURE (K)
E,
QHM,
λ²M,
QHMM,
λ²MM

Figure 3.6

Specific Heat at Constant Volume of Xe

With Morse (M) and Modified Morse (MM) Potentials.

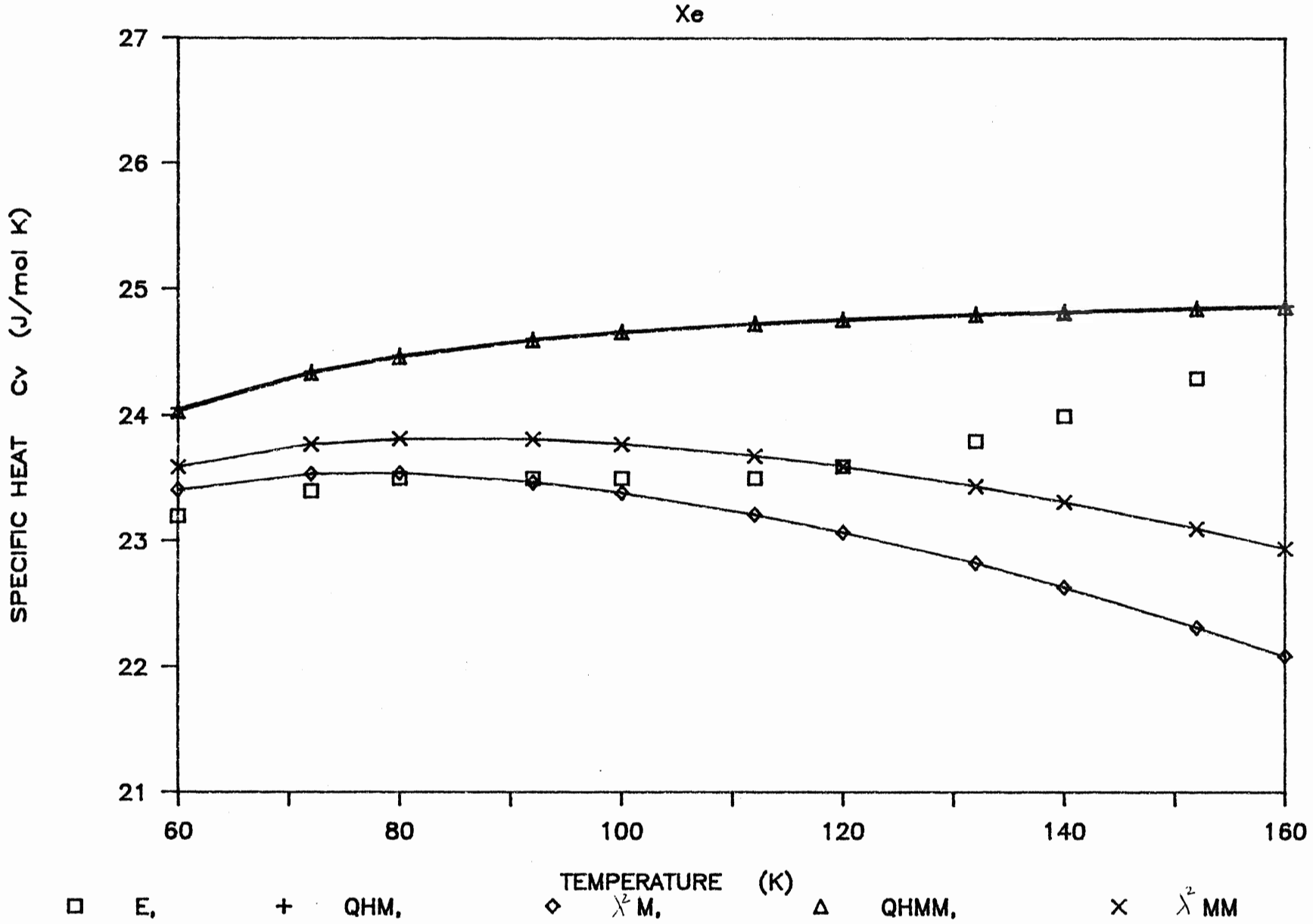
Xe
27
26
25
24
23
22
21
SPECIFIC HEAT Cv (J/mol K)
60
80
100
120
140
160
TEMPERATURE (K)
E,
QHM,
λ² M,
QHMM,
λ² MM

Figure 3.7

Specific Heat at Constant Pressure of Kr

With Morse (M) and Modified Morse (MM) Potentials.

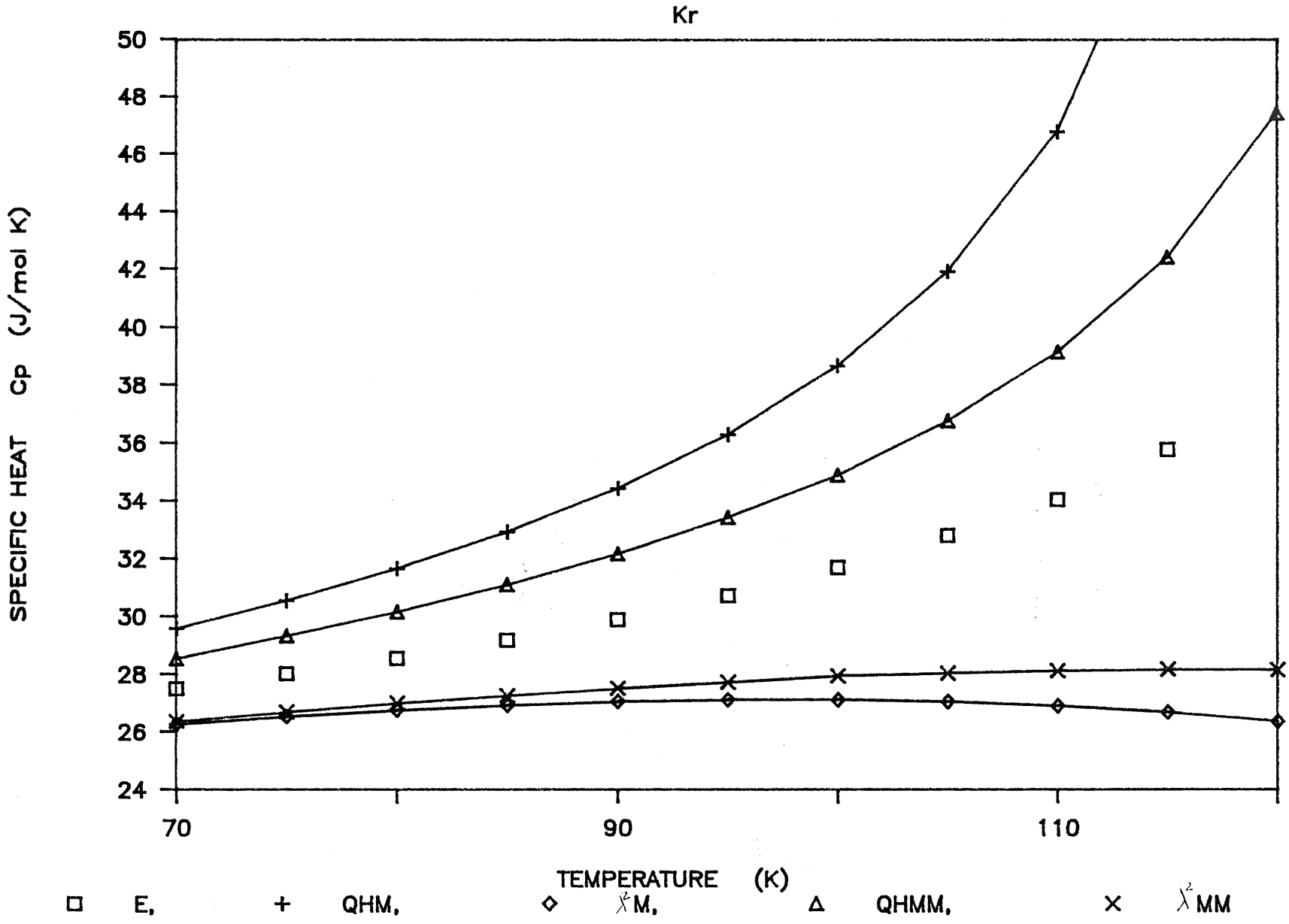
Kr
50
48
46
44
42
40
38
36
34
32
30
28
26
24
SPECIFIC HEAT Cp (J/mol K)
70
90
110
TEMPERATURE (K)
E,
QHM,
λ²M,
QHMM,
λ²MM

Figure 3.8

Specific Heat at Constant Pressure of Xe

With Morse (M) and Modified Morse (MM) Potentials.

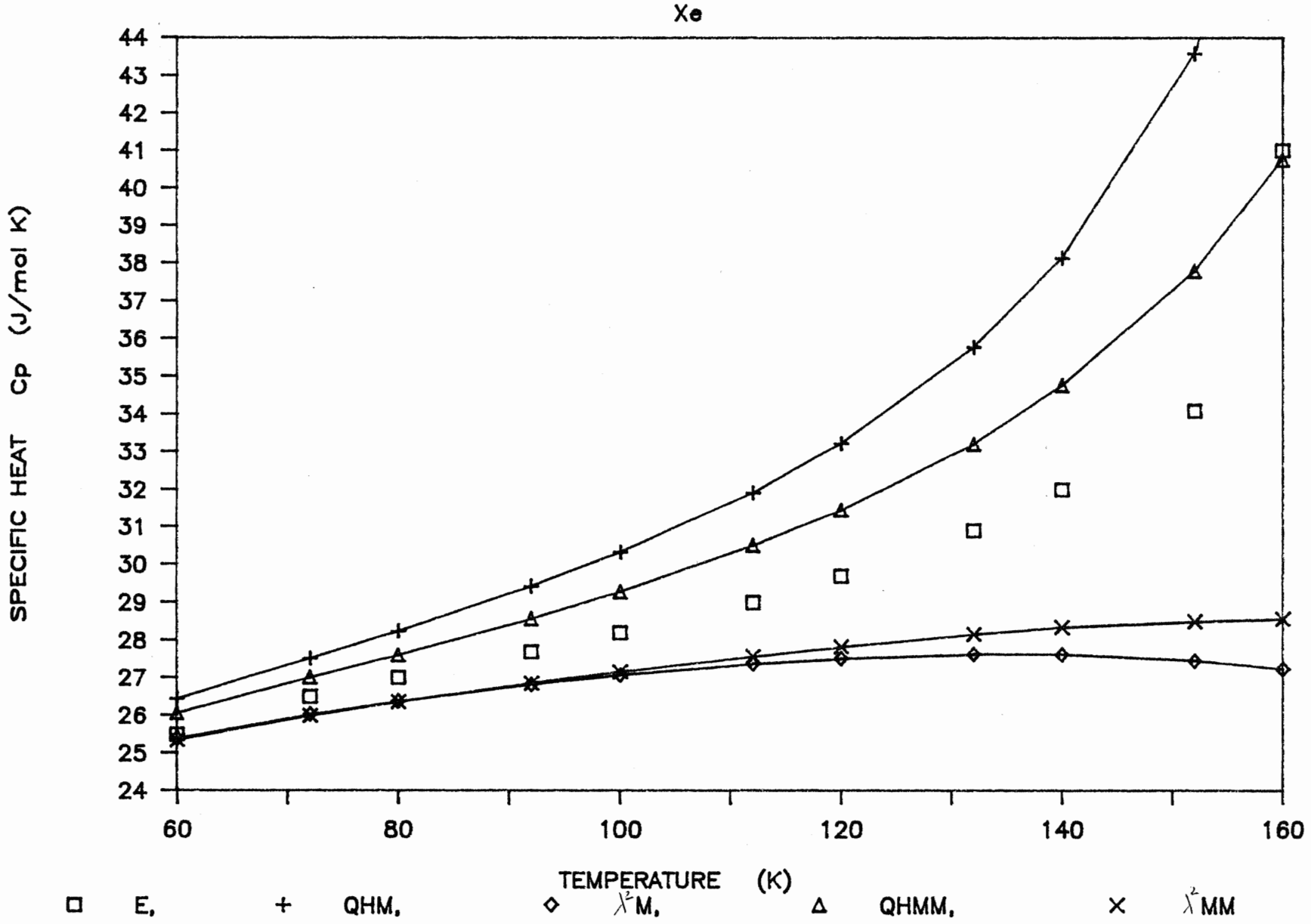
Xe
SPECIFIC HEAT Cp (J/mol K)
44
43
42
41
40
39
38
37
36
35
34
33
32
31
30
29
28
27
26
25
24
60
80
100
120
140
160
TEMPERATURE (K)
E,
QHM,
λ²M,
QHMM,
λ²MM

Figure 3.9

Isothermal Bulk Modulus of Kr

With Morse (M) and Modified Morse (MM) Potentials.

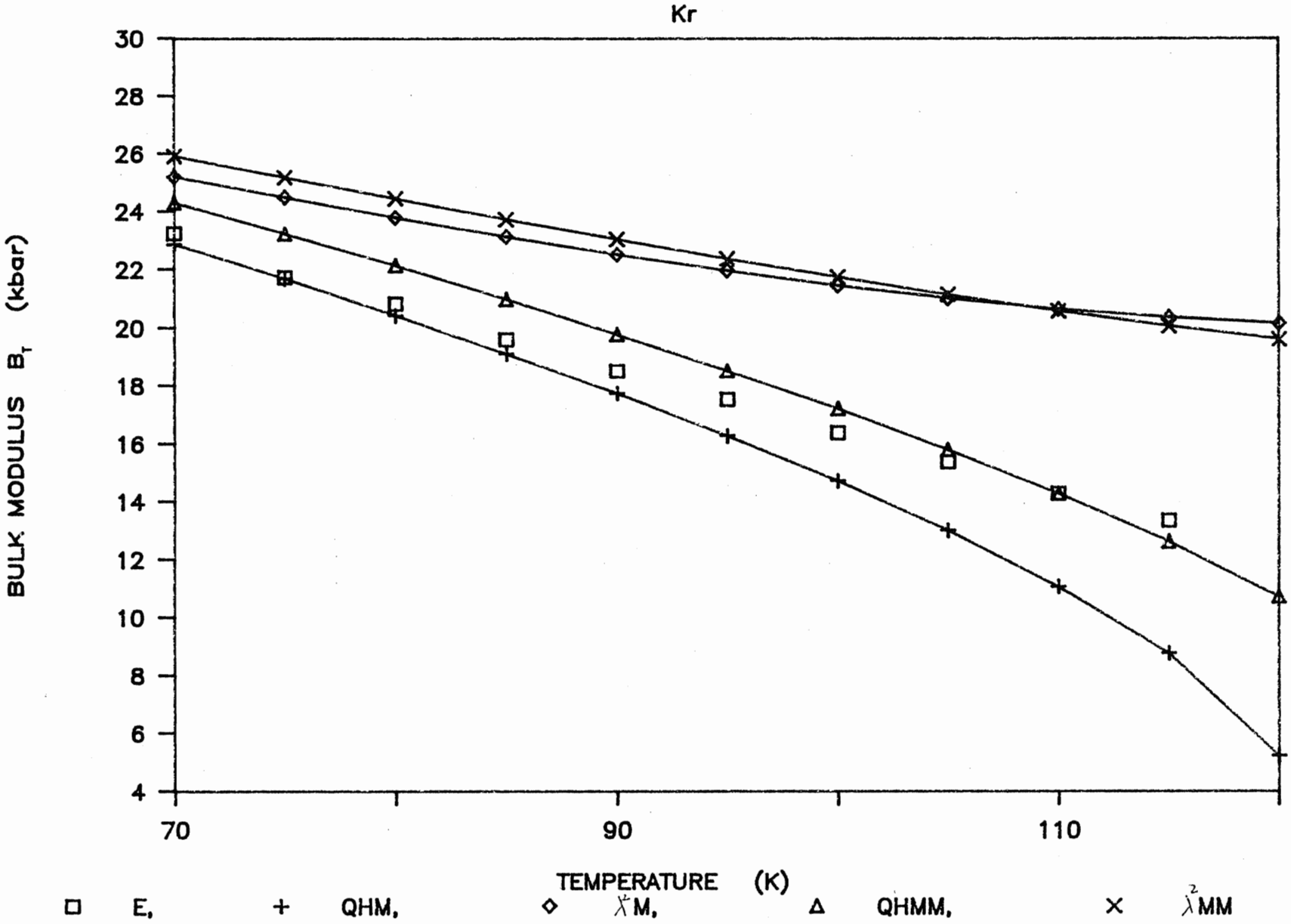
Kr
BULK MODULUS B_T (kbar)
30
28
26
24
22
20
18
16
14
12
10
8
6
4
70
90
110
TEMPERATURE (K)
E,
QHM,
λ^1M,
QHMM,
λ^2MM

Figure 3.10

Isothermal Bulk Modulus of Xe

With Morse (M) and Modified Morse (MM) Potentials.

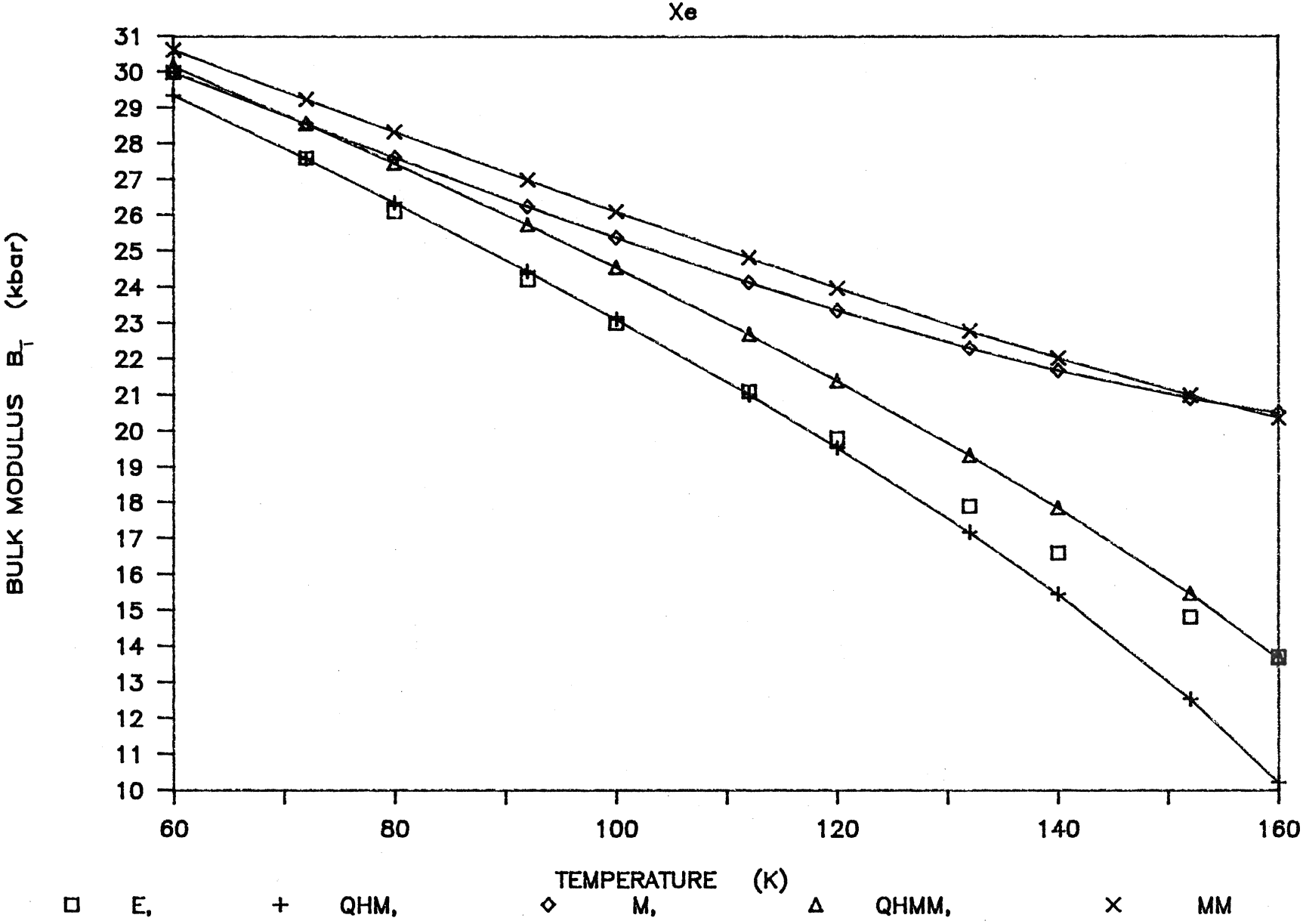
Xe
BULK MODULUS B_T (kbar)
31
30
29
28
27
26
25
24
23
22
21
20
19
18
17
16
15
14
13
12
11
10
60
80
100
120
140
160
TEMPERATURE (K)
E,
QHM,
M,
QHMM,
MM

Figure 3.11

Adiabatic Bulk Modulus of Kr

With Morse (M) and Modified Morse (MM) Potentials.

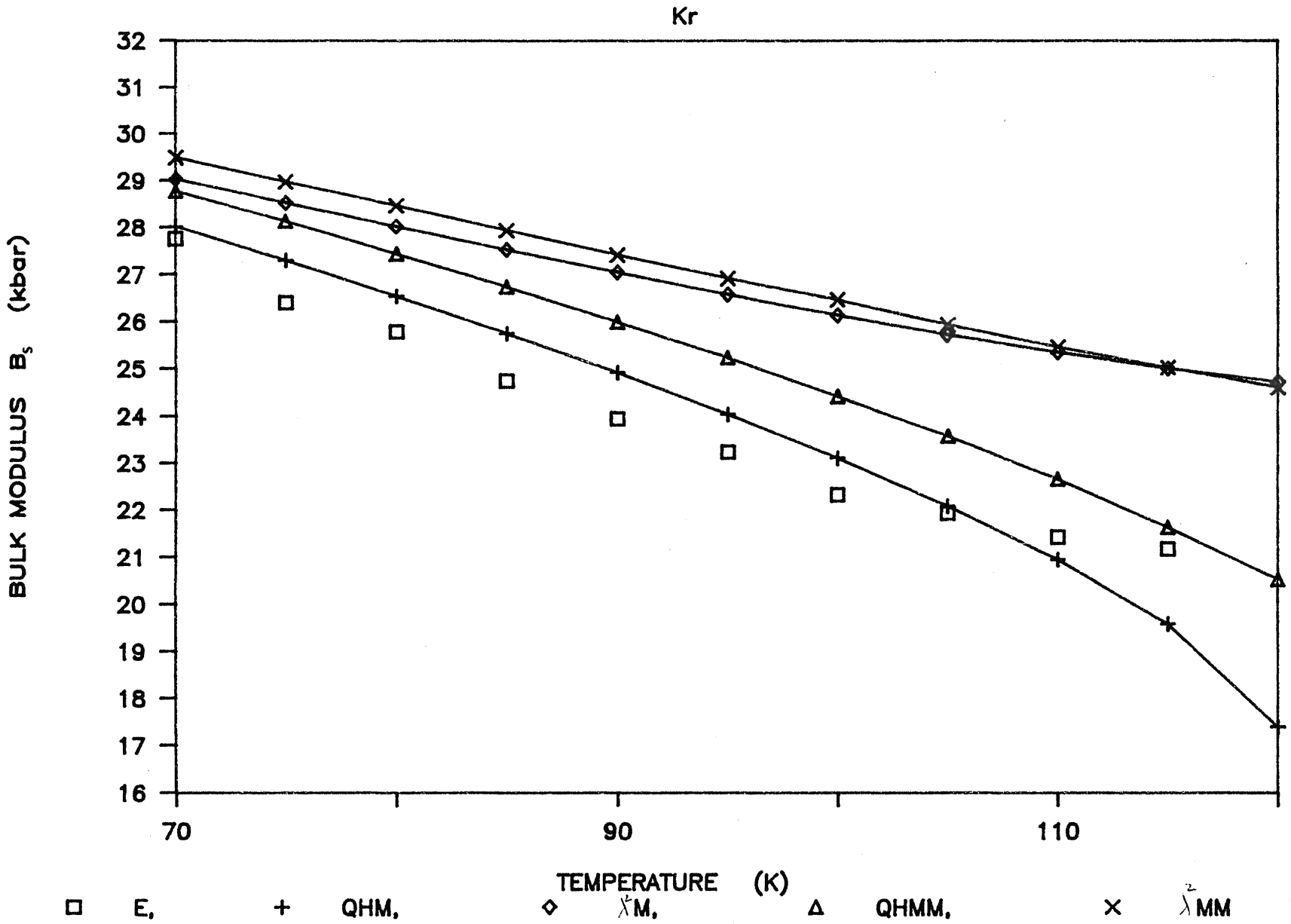
Kr
BULK MODULUS B_S (kbar)
32
31
30
29
28
27
26
25
24
23
22
21
20
19
18
17
16
70
90
110
TEMPERATURE (K)
E,
QHM,
λ^2M,
QHMM,
λ^2MM

Figure 3.12

Adiabatic Bulk Modulus of Xe

With Morse (M) and Modified Morse (MM) Potentials.

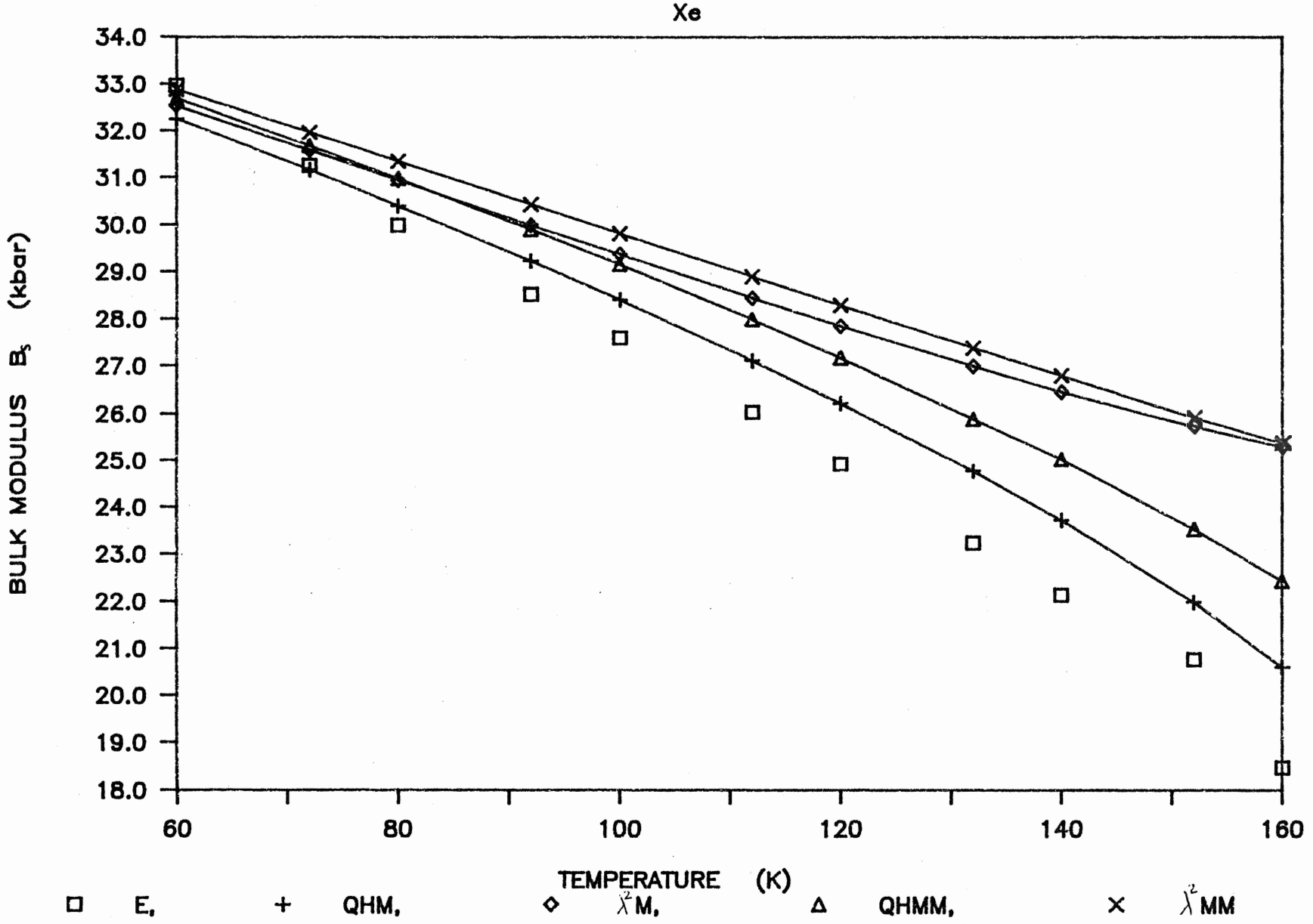
Xe
34.0
33.0
32.0
31.0
30.0
29.0
28.0
27.0
26.0
25.0
24.0
23.0
22.0
21.0
20.0
19.0
18.0
BULK MODULUS B_S (kbar)
60
80
100
120
140
160
TEMPERATURE (K)
E,
QHM,
λ^2M,
QHMM,
λ^2MM

Figure 3.13

Grüneisen Parameter of Kr

With Morse (M) and Modified Morse (MM) Potentials.

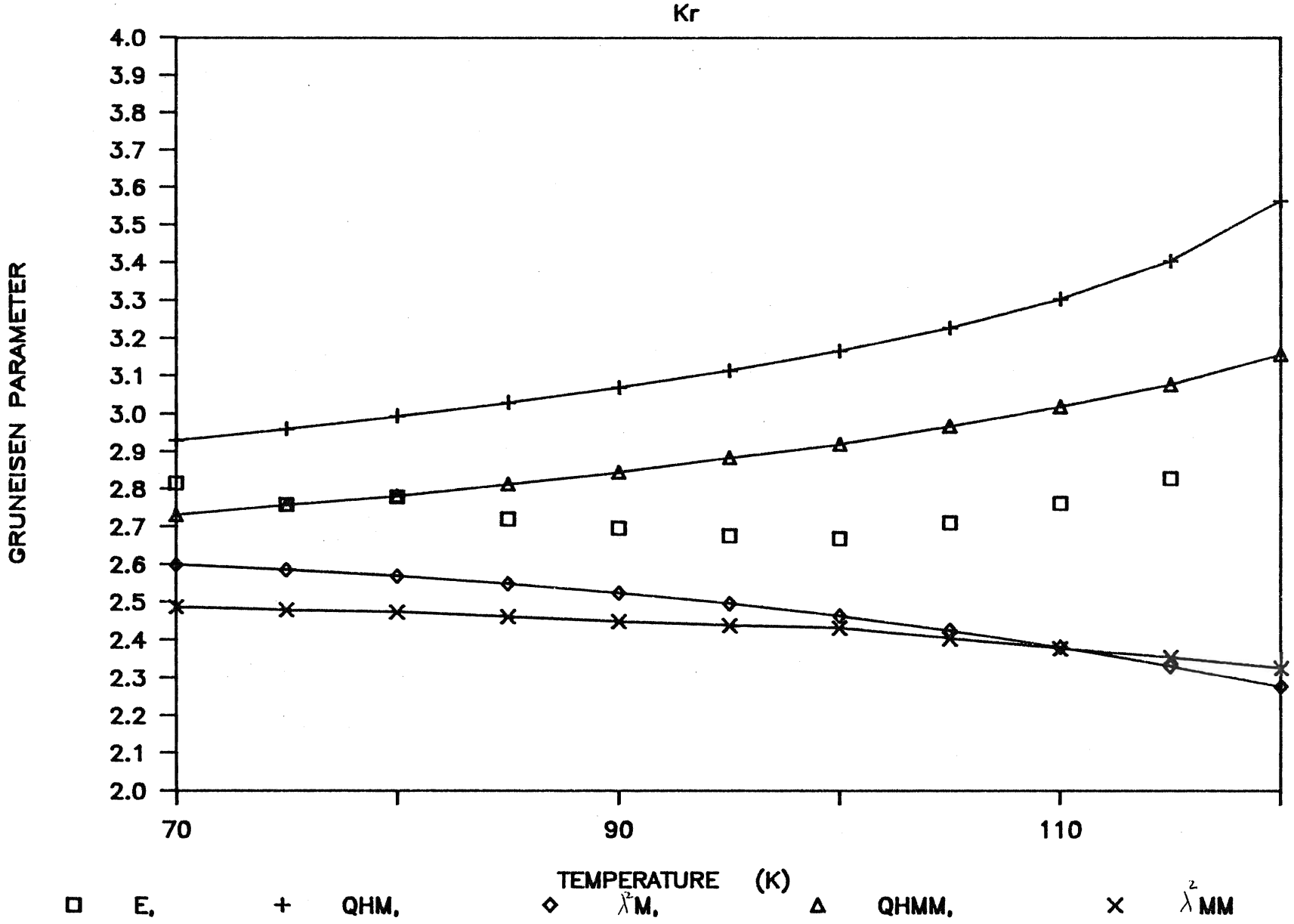
Kr
GRUNEISEN PARAMETER
4.0
3.9
3.8
3.7
3.6
3.5
3.4
3.3
3.2
3.1
3.0
2.9
2.8
2.7
2.6
2.5
2.4
2.3
2.2
2.1
2.0
70
90
110
TEMPERATURE (K)
E,
QHM,
λ²M,
QHMM,
λ²MM

Figure 3.14

Grüneisen Parameter of Xe

With Morse (M) and Modified Morse (MM) Potentials.

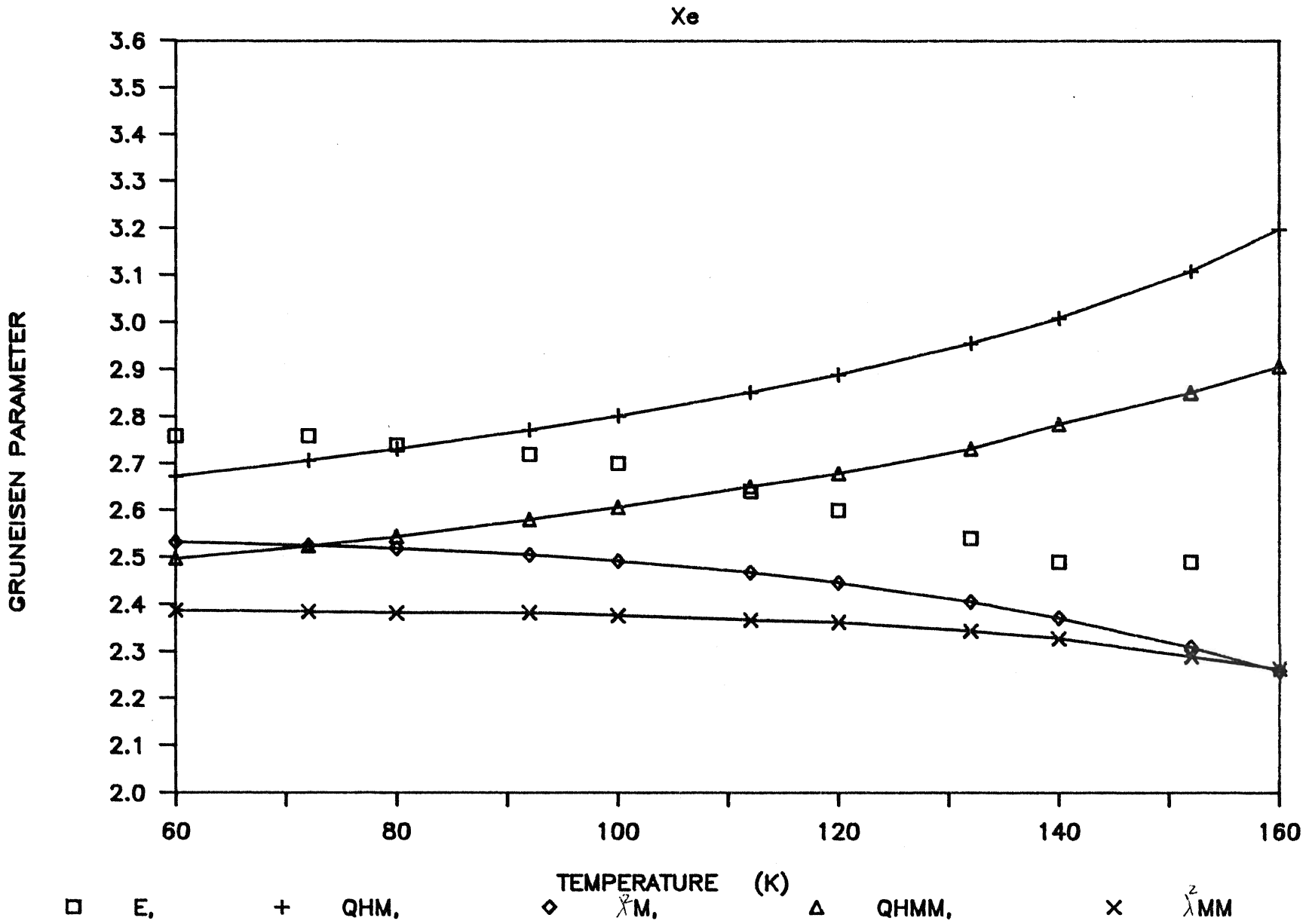
Xe
GRUNEISEN PARAMETER
3.6
3.5
3.4
3.3
3.2
3.1
3.0
2.9
2.8
2.7
2.6
2.5
2.4
2.3
2.2
2.1
2.0
60
80
100
120
140
160
TEMPERATURE (K)
E,
QHM,
QHMM,

The computed Grüneisen parameter for Kr which is shown in Figure 3.13, are in fair agreement with the experimental values; however, at higher temperatures this agreement between the calculated and the experimental values worsens. Whereas, for Xe, γ results for Xe are in fair agreement with the experimental values only at high temperature as shown in Figure 3.14.

In general, the thermodynamic properties calculated from $E(\lambda^2)$ equation of state are in good agreement with the experimental results near the Debye temperature. At temperature greater than $2/3T_m$, the thermal properties show a breakdown of the $O(\lambda^2)$ perturbation theory. This breakdown of the modified Morse potential, is not quite as serious as in the results for the Morse potential.

In comparison with the thermal properties calculated with the Lennard-Jones potential (Shukla and Shanes (1984)), we find that the results calculated with the Morse potential are qualitatively similar to those calculated with the Lennard-Jones potential. However, the results obtained with the two potentials are quantitatively different. For temperatures in the neighbourhood of θ_D the results calculated with the Lennard-Jones potential show a good agreement with the experimental values. At high temperatures the calculated thermal properties show a breakdown of the $O(\lambda^2)$ PT. This breakdown is more serious when the Lennard-Jones potential is used than when the Morse or the modified Morse potentials are used.

3.4.2. Thermodynamic Properties of Gold:

For the rare-gas solids, the interaction between the atoms was presented by the Morse potential and the modified Morse potential. However, for metals, in addition to the ion-ion interaction the effect of the electron gas should also be taken into account. The ion-ion interaction is represented by the Morse potential or the modified Morse potential. The effect of the electron gas is taken into account through the use of the free electron model. The electronic contribution to the isothermal bulk modulus is dependent on the crystal volume, which is calculated from the equation of state, and thus C_p^{el}, B_S^{el} and γ^{el} will also be affected by the equation of state used, since these properties depend on B_T^{el}.

The thermodynamic properties of the fcc metals: Pb, Al, Cu, Ag, Ni, Ca, and Sr were previously calculated for the modified Morse potential by MacDonald and MacDonald (1981). Following the same procedure we have calculated the thermodynamic properties of Au. These properties are presented in Figures 3.15 through 3.26. The lattice contribution and the lattice plus electronic contributions, which are obtained from the QH theory and the λ^2 PT, are shown on each figure, together with the experimental values.

The calculated thermal expansion for Au compared with experimental results (Touloukian et al. (1975)) is presented in Figure 3.15. The results of the modified Morse potential are in better agreement with experimental values than those of the Morse potential. This is so because the parameter b in the modified Morse potential was determined by matching the computed $\varepsilon(T)$ to the experimental value in the

neighbourhood of the Debye temperature. However, at higher temperatures, near T_m, the experimental values increase more rapidly than the computed $\varepsilon(T)$. This could be due to the omission of the vacancy contribution to the lattice constant.

The calculated linear expansion coefficient is shown in Figure 3.16. The results of the modified Morse potential are in fair agreement with experiment (Touloukian et al. (1975)) for temperatures up to $3/5T_m$. This disagreement could be due exclusion of the electronic contribution to the volume expansion.

The specific heat at constant volume is presented in Figures 3.17 and 3.18. The results from both potentials are in poor agreement with experimental results, calculated from the experimental values of C_p, B_T, and B_S. The specific heat at constant pressure is shown in Figure 3.19 and 3.20. The results of the Morse potential are in good agreement with experiment (Hultgren et al. (1973)) for temperatures up to $1/2T_m$. Whereas the results of the modified Morse potential are in better agreement with experiment for temperatures up to $2/3T_m$. The total C_p and Cv for both potentials show an improvement over the lattice contributions of these two properties in comparison with experimenatal results.

The isothermal and adiabatic bulk moduli are presented in Figures 3.21 through 3.24. The values of the parameter z, the effective number of free electrons per atom, is set equal to 1 for Au since it is known to be monovalent. The results obtained for both potentials are in poor agreement with experiment (Chang and Himmel (1966)). The added

electronic contribution to the lattice contribution shifted the the total bulk modulus up towards the experimental results.

The calculated Grüneisen parameter is presented in Figures 3.25 and 3.26. The lattice and the lattice plus electronic contributions are shown on the figures; however, the results are in poor agreement with the experimental values, calculated from experimental data.

Figure 3.15

Thermal Expansion of Au

With Morse (M) and Modified Morse (MM) Potentials.

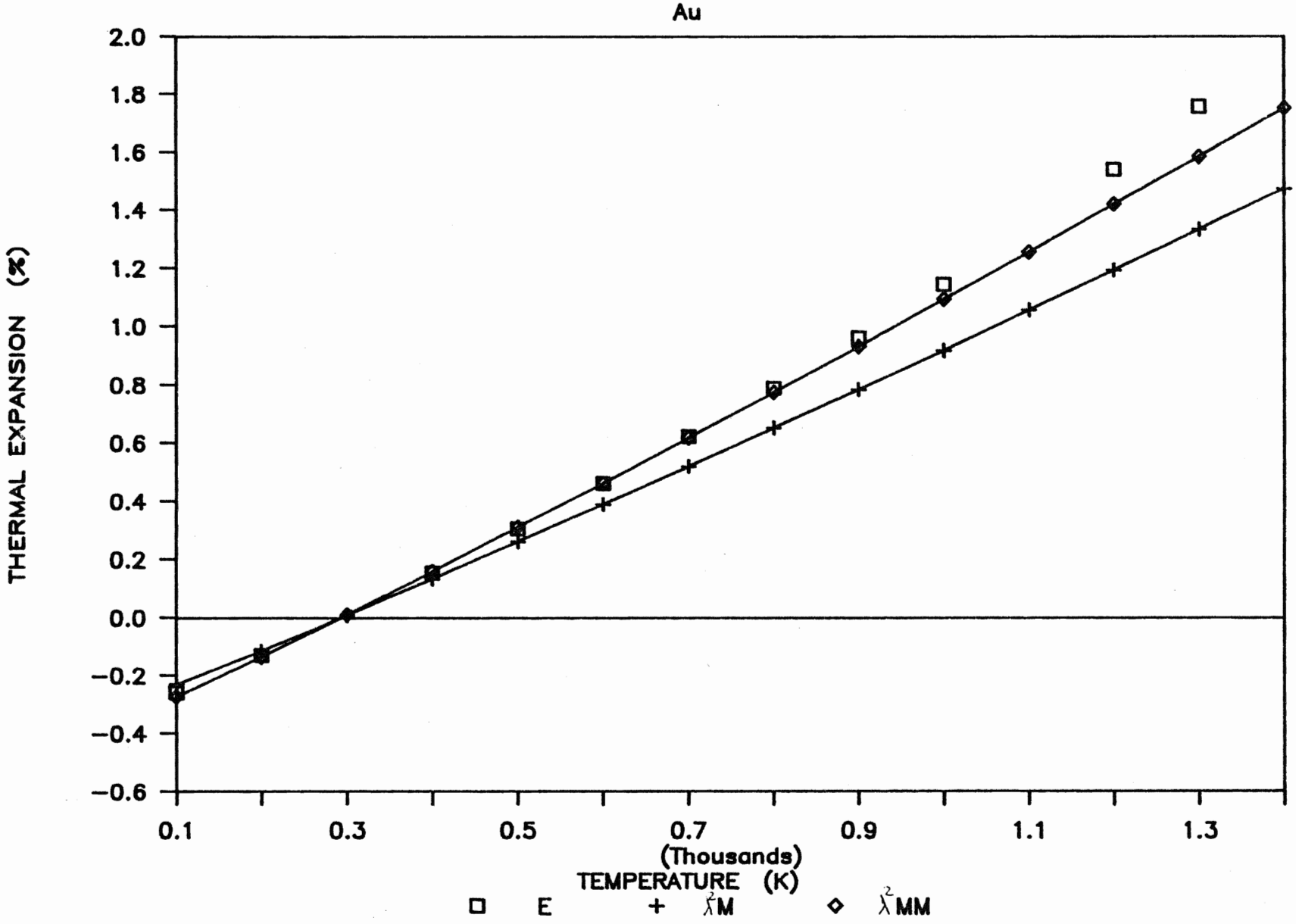
Au
2.0
1.8
1.6
1.4
1.2
1.0
0.8
0.6
0.4
0.2
0.0
−0.2
−0.4
−0.6
THERMAL EXPANSION (%)
0.1
0.3
0.5
0.7
0.9
1.1
1.3
(Thousands)
TEMPERATURE (K)
E
λ²M
λ²MM

Figure 3.16

Coefficient of Linear Expansion of Au

With Morse (M) and Modified Morse (MM) Potentials.

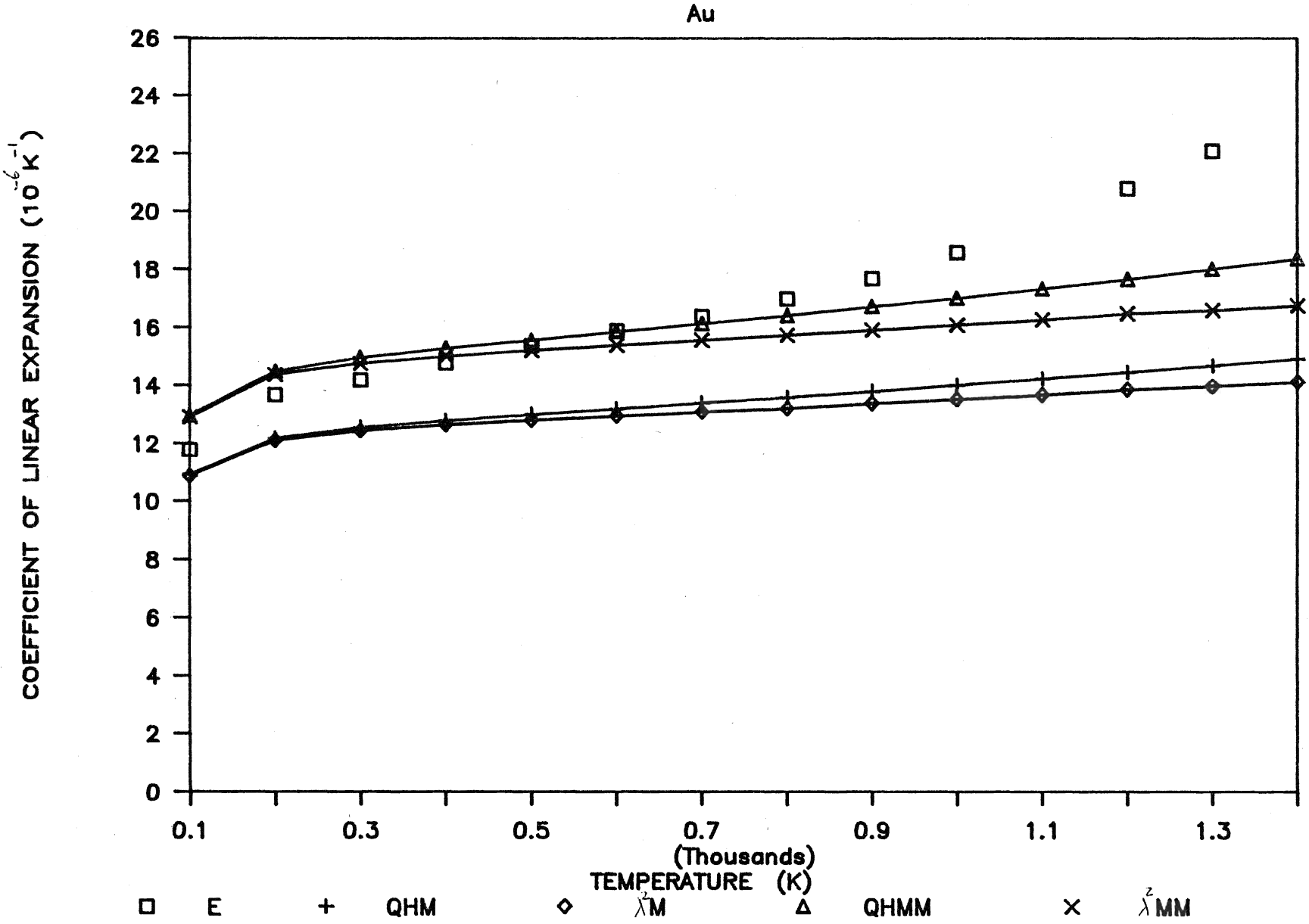
Au
COEFFICIENT OF LINEAR EXPANSION (10^{-6} K^{-1})
26
24
22
20
18
16
14
12
10
8
6
4
2
0
0.1
0.3
0.5
0.7
0.9
1.1
1.3
(Thousands)
TEMPERATURE (K)
E
QHM
λ^2M
QHMM
λ^2MM

Figure 3.17

Specific Heat at Constant Volume of Au With Morse Potential.

L denotes lattice contribution.

LE denotes lattice and electronic contributions.

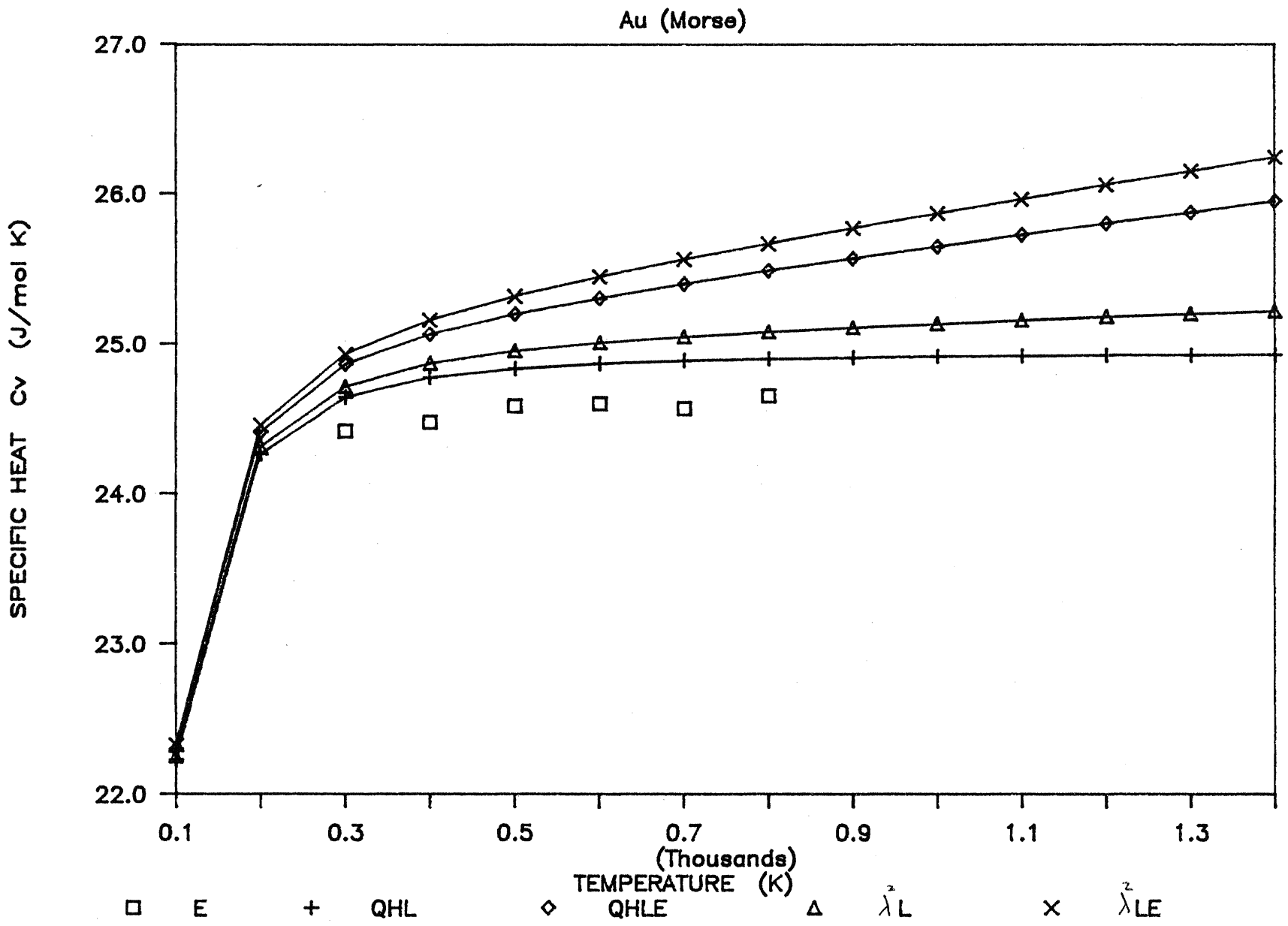
Au (Morse)
27.0
26.0
25.0
24.0
23.0
22.0
SPECIFIC HEAT Cv (J/mol K)
0.1
0.3
0.5
0.7
0.9
1.1
1.3
(Thousands)
TEMPERATURE (K)
E
QHL
QHLE
λ²L
λ²LE

Figure 3.18

Specific Heat at Constant Volume of Au With Modified Morse Potentials.

L denotes lattice contribution.

LE denotes lattice and electronic contributions.

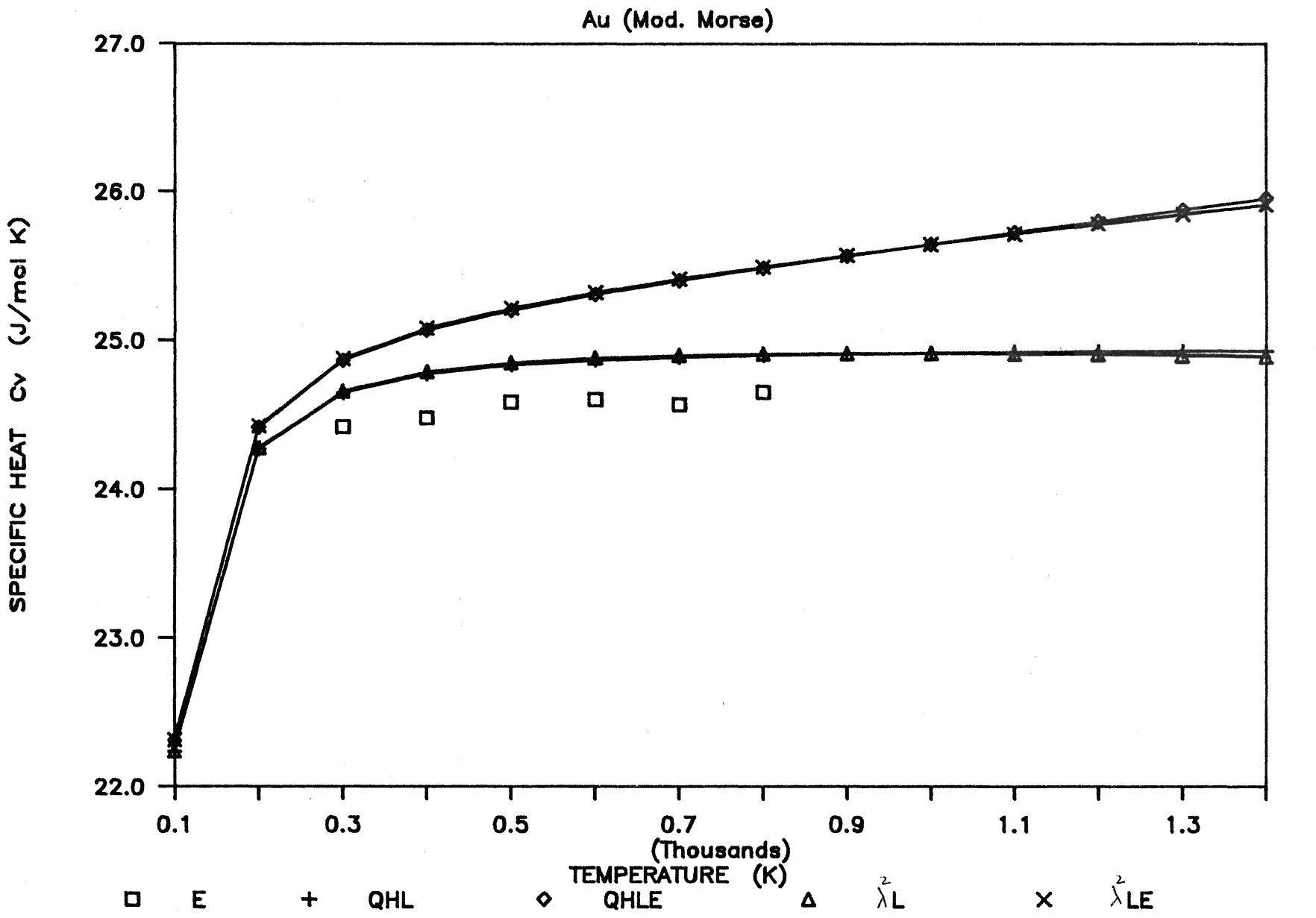
Au (Mod. Morse)
27.0
26.0
25.0
24.0
23.0
22.0
SPECIFIC HEAT Cv (J/mol K)
0.1
0.3
0.5
0.7
0.9
1.1
1.3
(Thousands)
TEMPERATURE (K)
E
QHL
QHLE
λ²L
λ²LE

Figure 3.19

Specific Heat at Constant Pressure of Au With Morse Potential.

L denotes lattice contribution.

LE denotes lattice and electronic contributions.

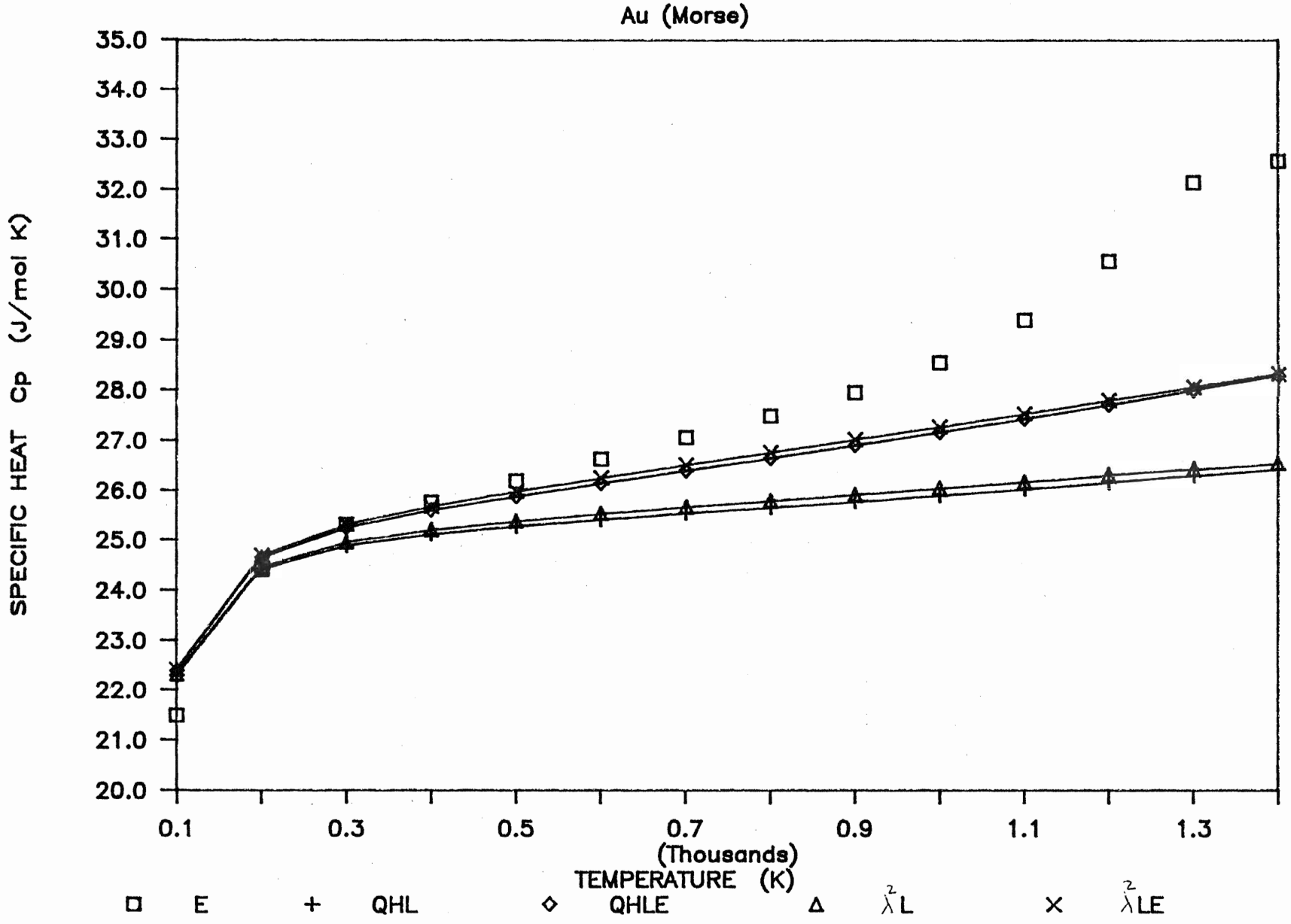
Au (Morse)
SPECIFIC HEAT Cp (J/mol K)
35.0
34.0
33.0
32.0
31.0
30.0
29.0
28.0
27.0
26.0
25.0
24.0
23.0
22.0
21.0
20.0
0.1
0.3
0.5
0.7
0.9
1.1
1.3
(Thousands)
TEMPERATURE (K)
E
QHL
QHLE
λ²L
λ²LE

Figure 3.20

Specific Heat at Constant Pressure of Au With Modified Morse Potential.

L denotes lattice contribution.

LE denotes lattice and electronic contributions.

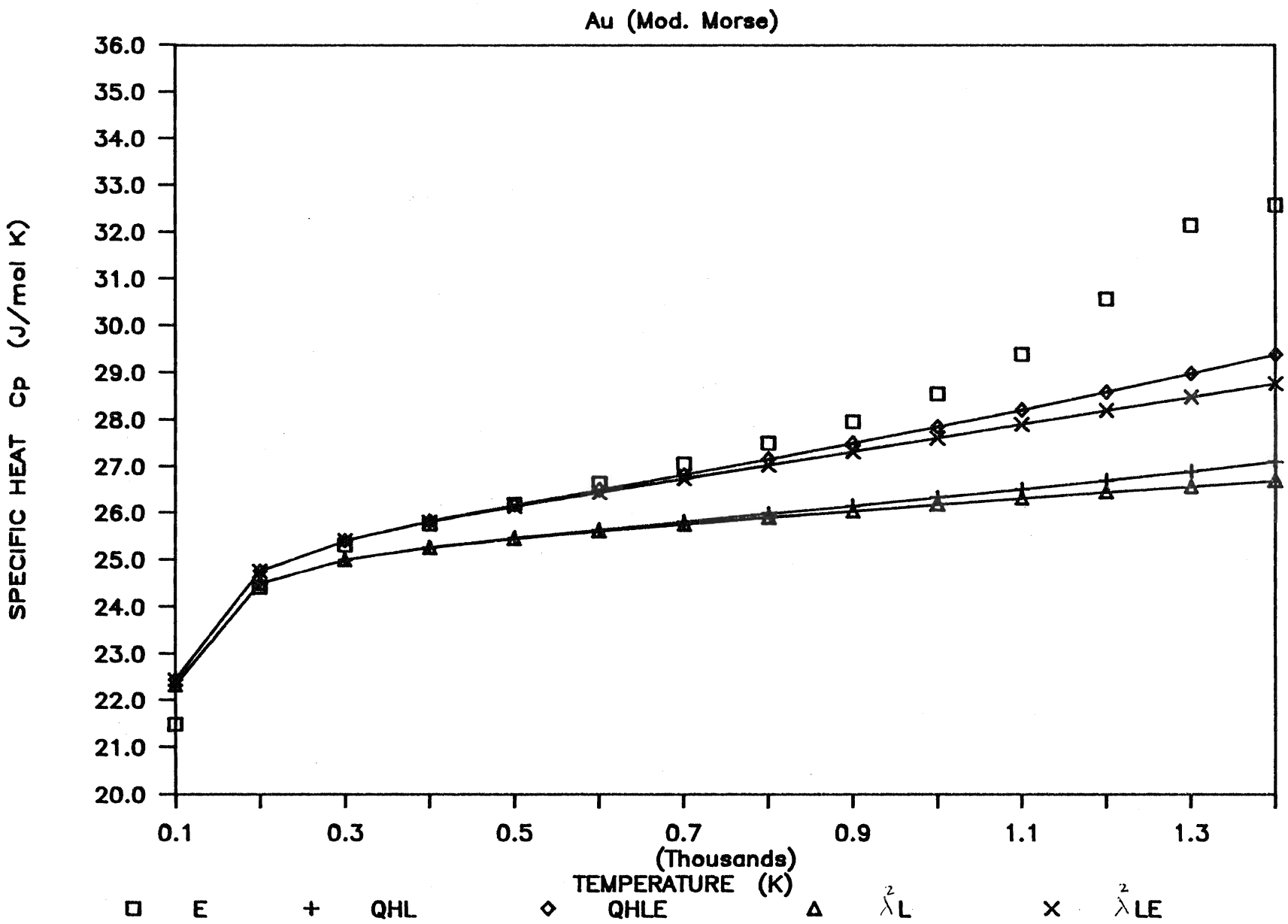
Au (Mod. Morse)
SPECIFIC HEAT Cp (J/mol K)
36.0
35.0
34.0
33.0
32.0
31.0
30.0
29.0
28.0
27.0
26.0
25.0
24.0
23.0
22.0
21.0
20.0
0.1
0.3
0.5
0.7
0.9
1.1
1.3
(Thousands)
TEMPERATURE (K)
E
QHL
QHLE
λ²L
λ²LE

Figure 3.21

Isothermal Bulk Modulus of Au With Morse Potential.

L denotes lattice contribution.

LE denotes lattice and electronic contributions.

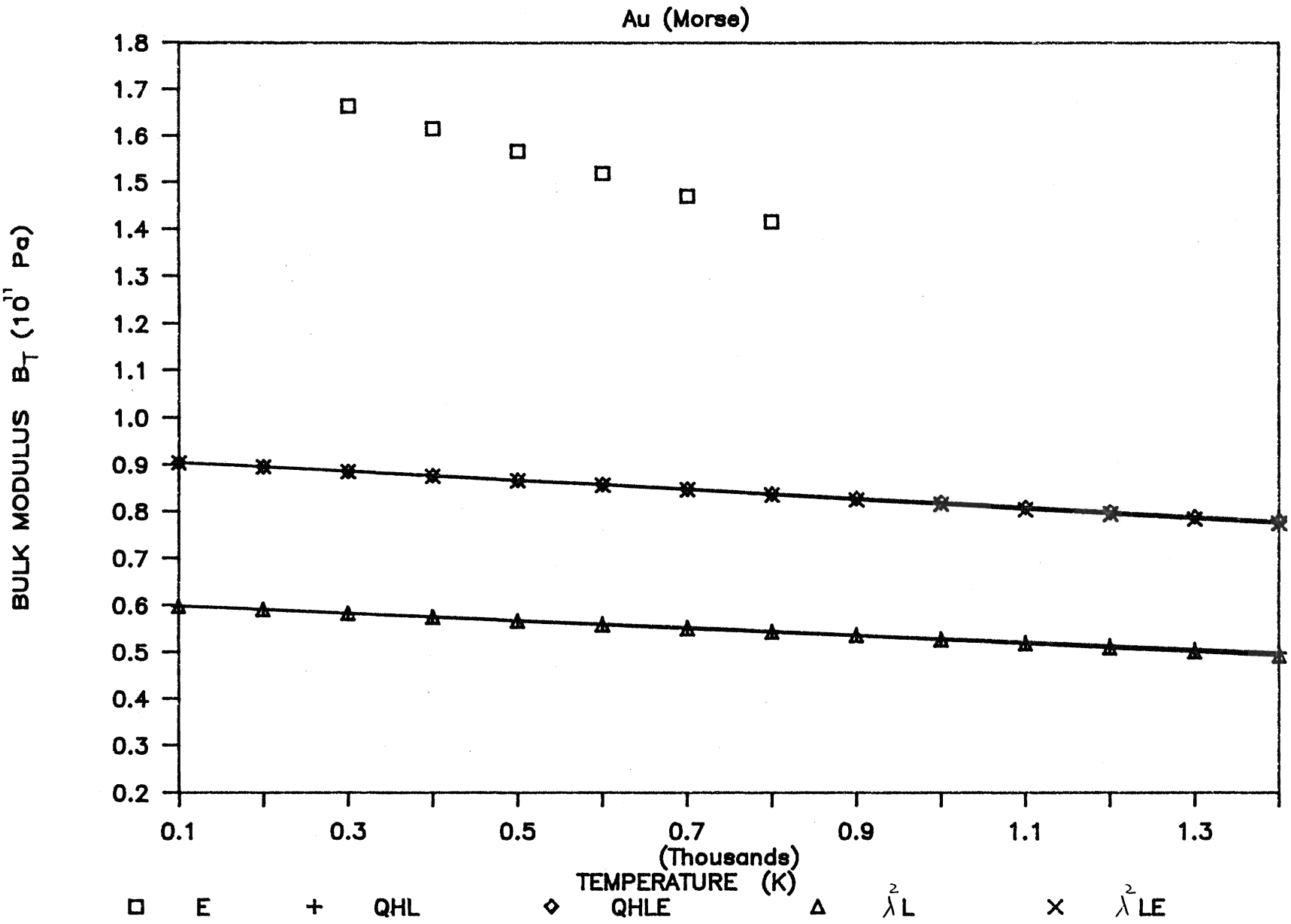
Au (Morse)
BULK MODULUS B_T (10^{11} Pa)
1.8
1.7
1.6
1.5
1.4
1.3
1.2
1.1
1.0
0.9
0.8
0.7
0.6
0.5
0.4
0.3
0.2
0.1
0.3
0.5
0.7
0.9
1.1
1.3
(Thousands)
TEMPERATURE (K)
E
QHL
QHLE
λ^2L
λ^2LE

Figure 3.22

Isothermal Bulk Modulus of Au With Modified Morse Potential.

L denotes lattice contribution.

LE denotes lattice and electronic contributions.

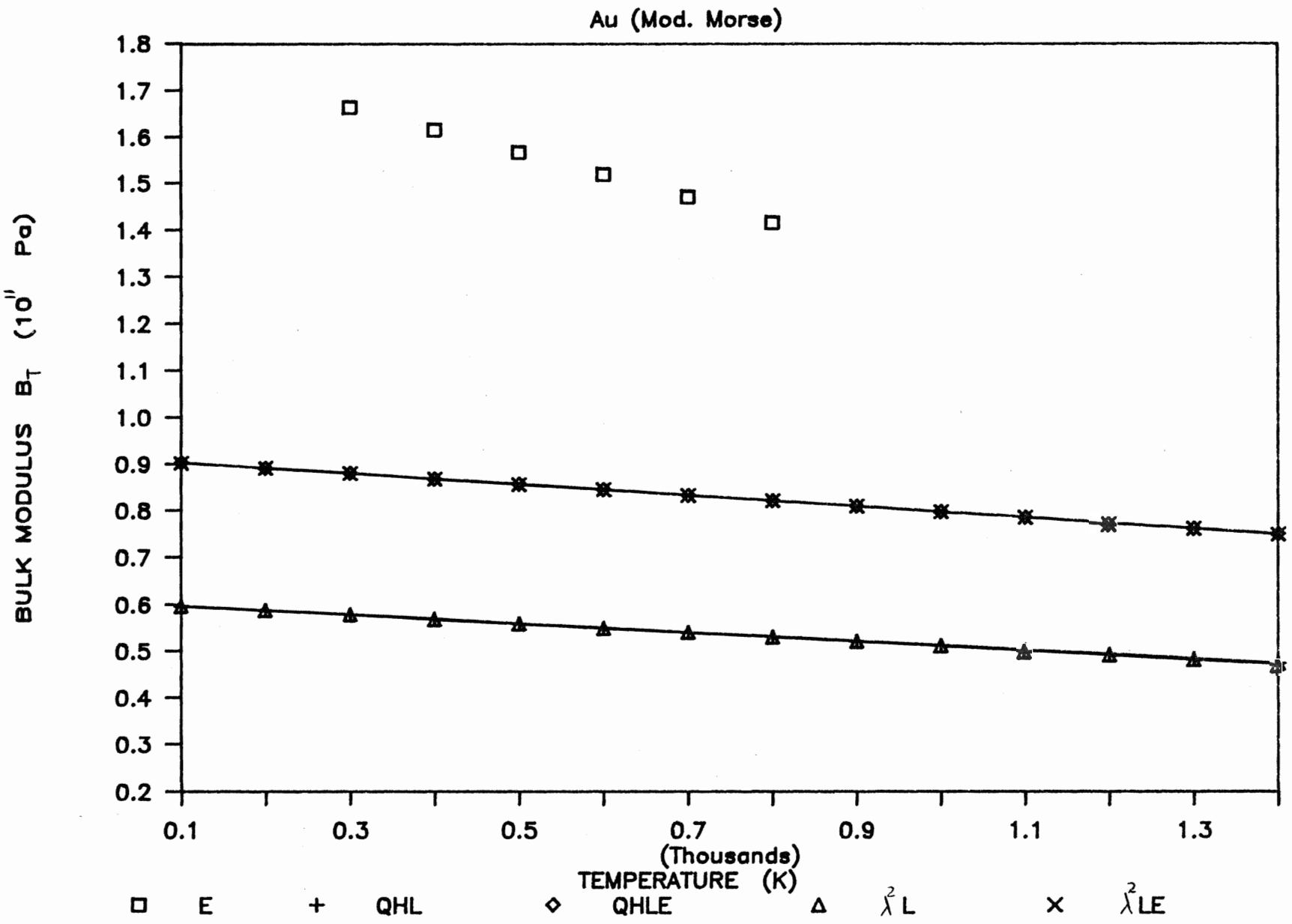
Au (Mod. Morse)
BULK MODULUS B_T (10^{11} Pa)
1.8
1.7
1.6
1.5
1.4
1.3
1.2
1.1
1.0
0.9
0.8
0.7
0.6
0.5
0.4
0.3
0.2
0.1
0.3
0.5
0.7
0.9
1.1
1.3
(Thousands)
TEMPERATURE (K)
E
QHL
QHLE
λ^2L
λ^2LE

Figure 3.23

Adiabatic Bulk Modulus of Au With Morse Potential.

L denotes lattice contribution.

LE denotes lattice and electronic contributions.

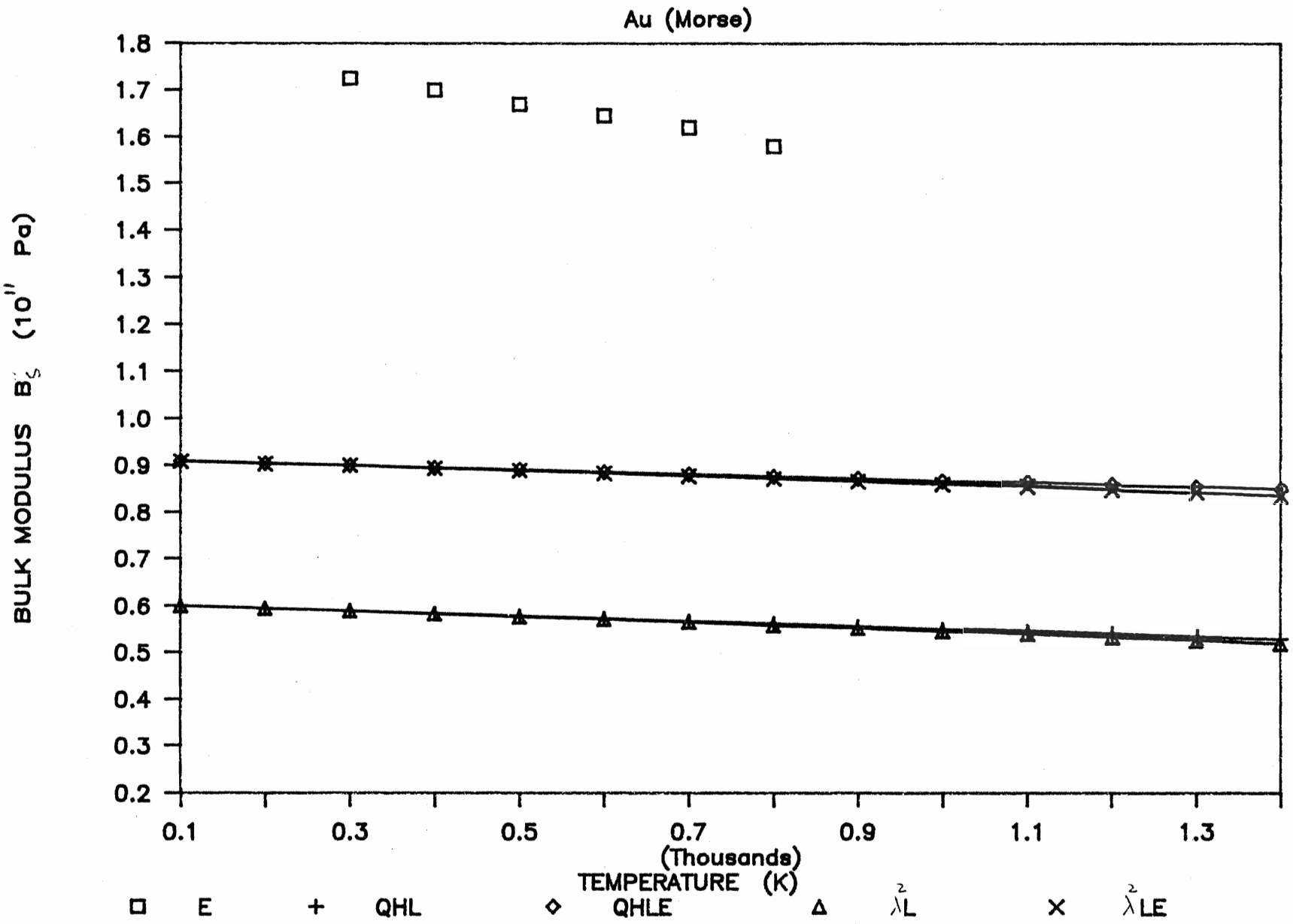
Au (Morse)
BULK MODULUS B_S (10^{11} Pa)
1.8
1.7
1.6
1.5
1.4
1.3
1.2
1.1
1.0
0.9
0.8
0.7
0.6
0.5
0.4
0.3
0.2
0.1
0.3
0.5
0.7
0.9
1.1
1.3
(Thousands)
TEMPERATURE (K)
E
QHL
QHLE
$\lambda^2 L$
$\lambda^2 LE$

Figure 3.24

Adiabatic Bulk Modulus of Au With Modified Morse Potential.

L denotes lattice contribution.

LE denotes lattice and electronic contributions.

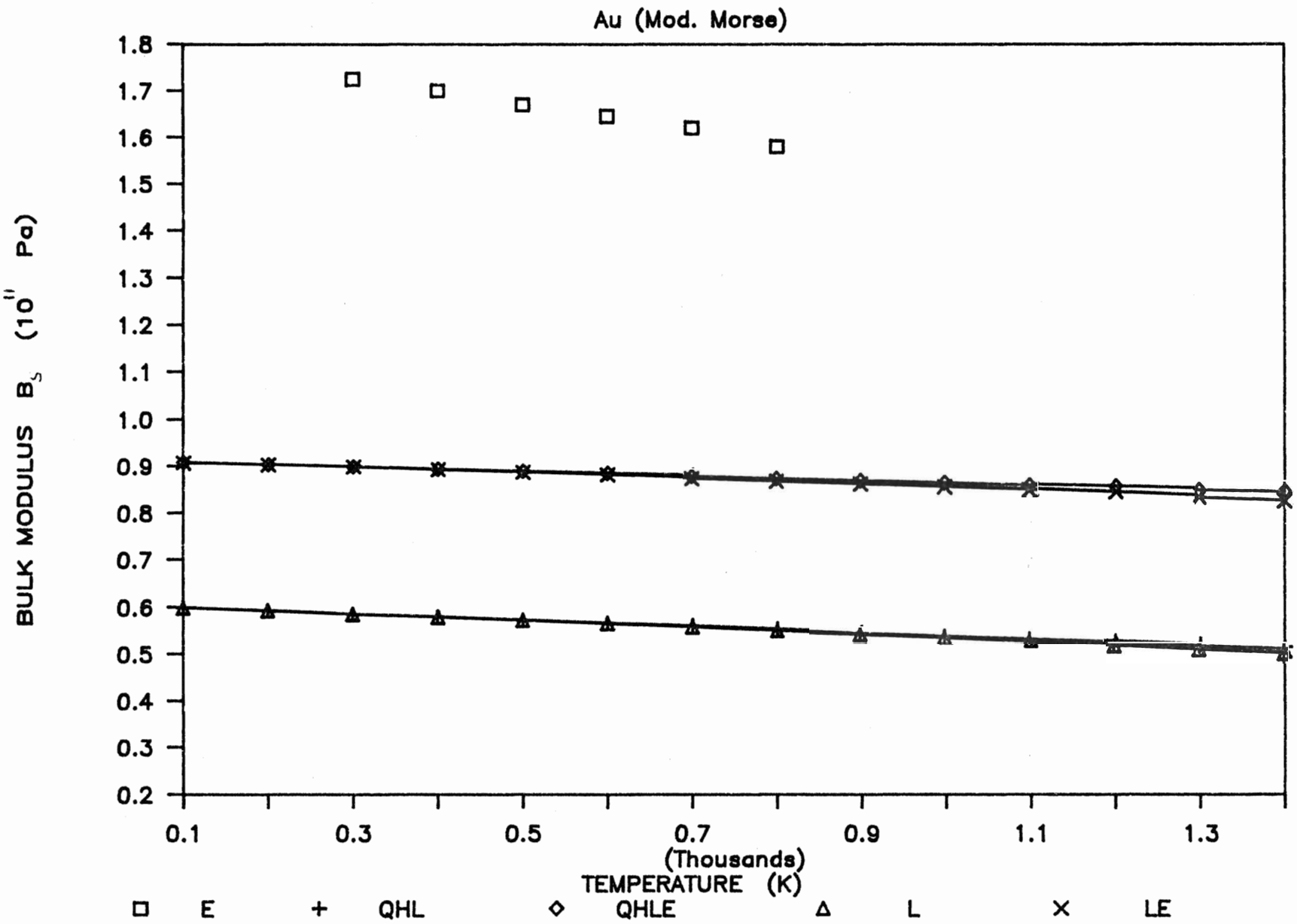
Au (Mod. Morse)
BULK MODULUS B_S (10^{11} Pa)
1.8
1.7
1.6
1.5
1.4
1.3
1.2
1.1
1.0
0.9
0.8
0.7
0.6
0.5
0.4
0.3
0.2
0.1
0.3
0.5
0.7
0.9
1.1
1.3
(Thousands)
TEMPERATURE (K)
E
QHL
QHLE
L
LE

Figure 3.25

Grüneisen Parameter of Au With Morse Potential.

L denotes lattice contribution.

LE denotes lattice and electronic contributions.

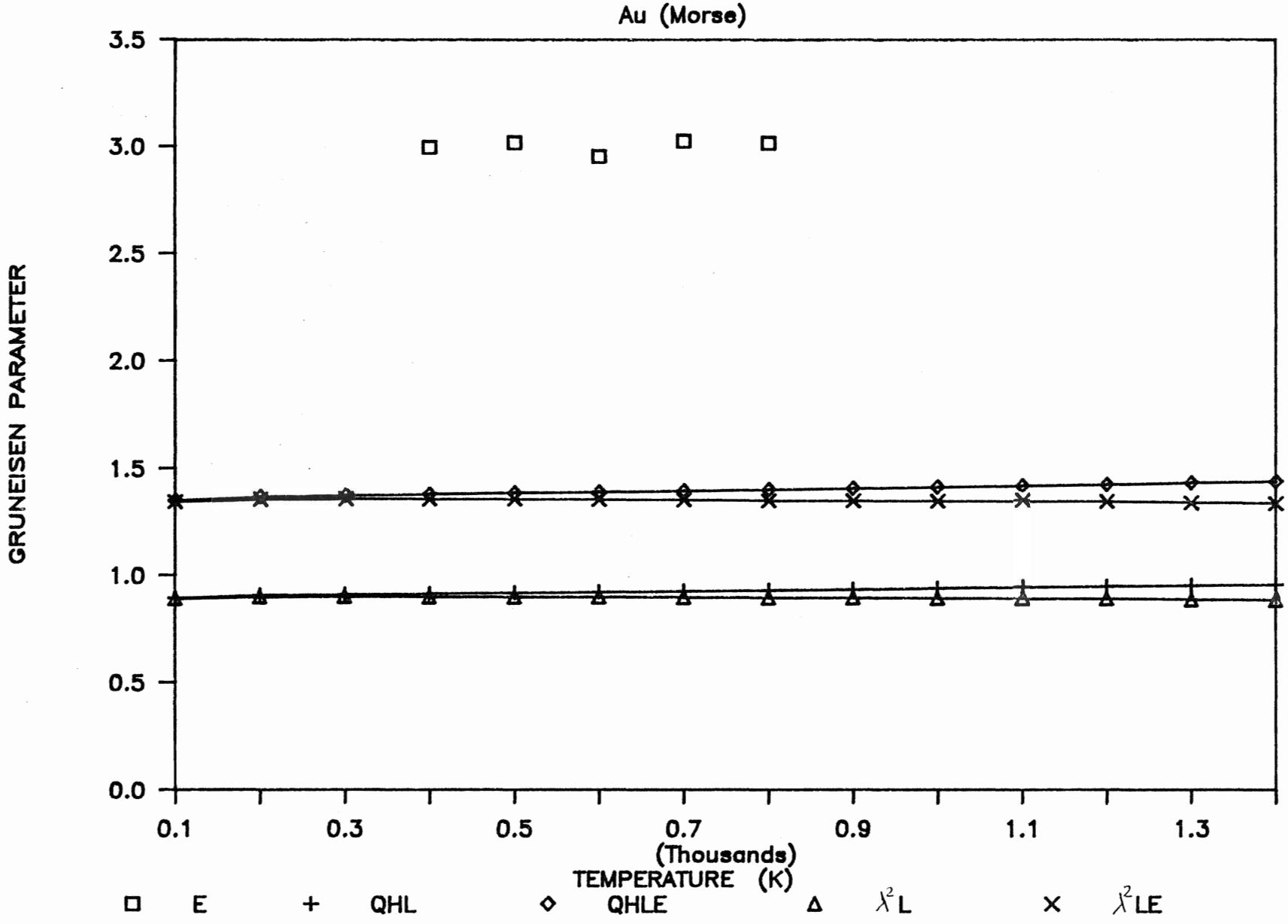
Au (Morse)
GRUNEISEN PARAMETER
3.5
3.0
2.5
2.0
1.5
1.0
0.5
0.0
0.1
0.3
0.5
0.7
0.9
1.1
1.3
(Thousands)
TEMPERATURE (K)
E
QHL
QHLE
λ²L
λ²LE

Figure 3.26

Grüneisen Parameter of Au With Modified Morse Potential.

L denotes lattice contribution.

LE denotes lattice and electronic contributions.

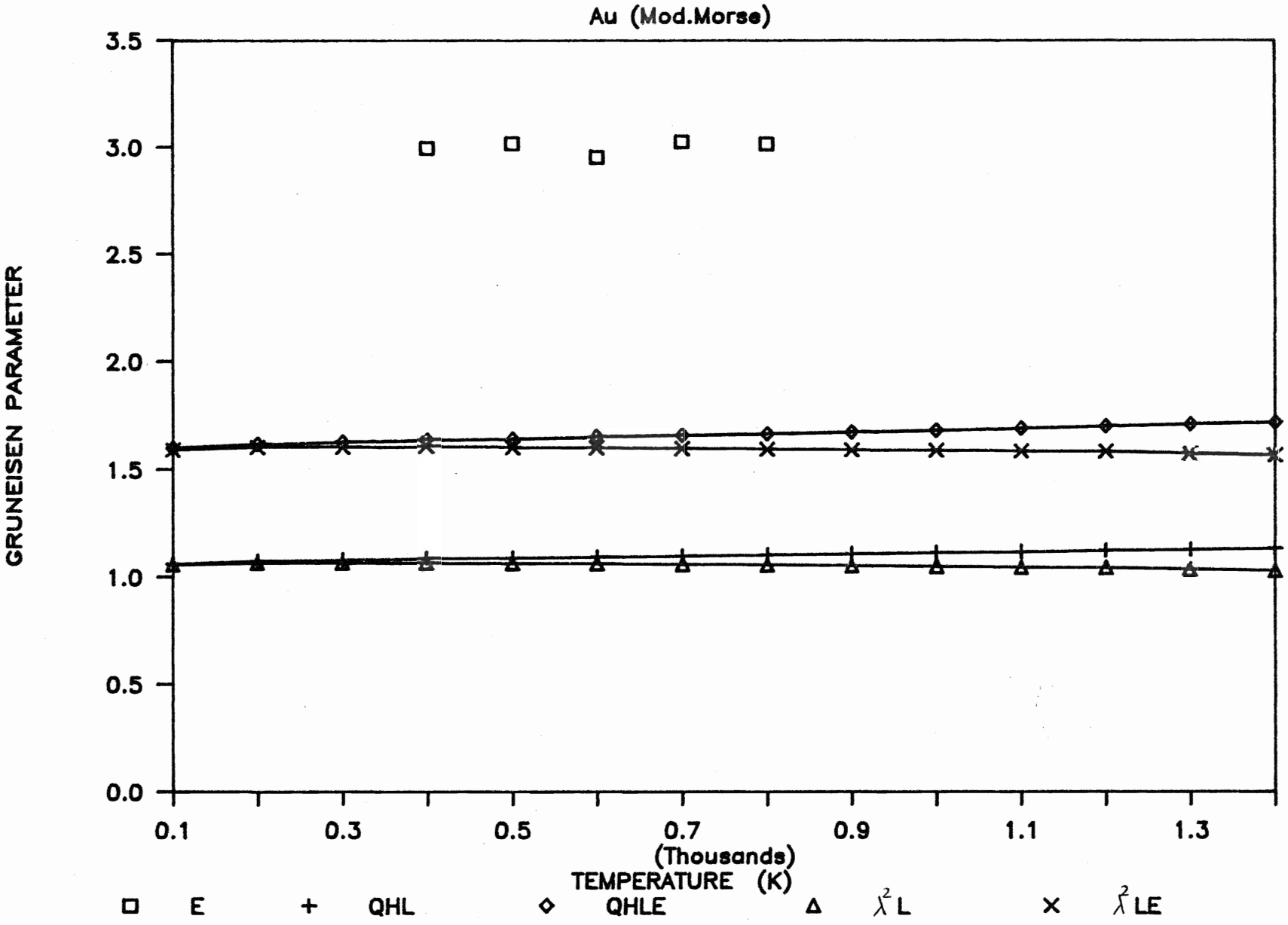
Au (Mod.Morse)
GRUNEISEN PARAMETER
3.5
3.0
2.5
2.0
1.5
1.0
0.5
0.0
0.1
0.3
0.5
0.7
0.9
1.1
1.3
(Thousands)
TEMPERATURE (K)
E
QHL
QHLE
λ² L
λ² LE

4. Calculation of Debye-Waller Factor

The objective of this section is to present the expressions developed by Shukla and Plint (1989), and to obtain numerical results for DWF or $< u^2 >$ for some fcc materials. In order to make these numerical calculations for any $\phi(r)$ and cubic crystal, we present the computational form of the harmonic and (λ^2) anharmonic contributions to DWF in the high temperature limit. These final results are expressed in terms of potential derivatives and a certain number of the BZ sums . The BZ sums are calculated by Shukla and Plint (1989) to a high degree of accuracy, and fitted to an exponential-type of form as a function of the parameter a_1.

After some algebraic manipulations done by Shukla and Plint (1989), the equations for $2M_{QH}(\mathbf{q})$, $2M_2(\mathbf{q})$, and $2M_1(\mathbf{q})$, can be reduced to the following forms for any application to any $\phi(r)$:

$$2M_{QH}(\mathbf{q}) = |\mathbf{q}|^2 \frac{3K_BT}{6B} S_{QH}(a_1) \tag{4.1}$$

$$2M_2(\mathbf{q}) = |\mathbf{q}|^2 \frac{(K_BT)^2}{F^4(r)} [\, C^2 S_{3A}(a_1) + \frac{2BC}{r} S_{3B}(a_1) + \frac{B^2}{r^2} S_{3C}(a_1) \,] \tag{4.2}$$

$$2M_1(\mathbf{q}) = - |\mathbf{q}|^2 \frac{(K_BT)^2}{3B^3} [\, D S_{4A}(a_1) + \frac{C}{r} S_{4B}(a_1) + \frac{B}{r^2} S_{4C}(a_1) \,] \tag{4.3}$$

where F(r) is a combination of the first and second derivatives of the potential function evaluated at the nearest-neighbour distance corresponding to temperature T, it is given by:

$$F(r) = \phi''(r) + \frac{1}{r}\phi'(r) \tag{4.4}$$

Table 4.1: Coefficients of The Least-Squares Fit of The Functions S_{QH}, etc.:

Function	b_0	b_1	b_2	b_3	b_4	b_5
S_{QH}	-0.174341	-4.45494	12.2157	-44.1948	126.459	-151.237
S_{4A}	-1.15553	-12.4982	35.4259	-141.374	514.150	-1037.31
S_{4B}	1.33303	-13.0698	37.5063	-150.333	554.644	-1150.08
S_{4C}	2.13851	-14.2170	41.4864	-165.353	596.810	-1195.17
S_{3A}	-3.00397	-8.12396	36.3668	-160.682	593.810	-1205.75
S_{3B}	-1.78646	-7.76336	34.9417	-155.390	583.985	-1213.79
S_{3C}	-0.035106	-8.31511	37.9244	-170.970	636.612	-1283.05

The BZ sums S_{QH}; S_{4A}, S_{4B}, S_{4C}; S_{3A}, S_{3B}, and S_{3C} are evaluated at the same temperature and fitted to the following form:

$$f(a_1) = \exp [\, P(a_1) \,] \tag{4.5}$$

where

$$P(a_1) = \sum_{n=0}^{5} b_n \, (a_1)^n. \tag{4.6}$$

Coefficients of the least-squares fit of these functions are presented in Table 4.1.

4.1. Mössbauer Recoilless Fraction for Kr and Xe:

The Debye-Waller factor (DWF) is related to the Mössbauer recoilless fraction (f) by

$$f = e^{-2W(T)} \tag{4.7}$$

where
$$2W(T) = \frac{1}{3} \left(\frac{E\gamma}{c\hbar} \right)^2 < u^2 > \tag{4.8}$$

$E\gamma$ is the energy of the γ-radiation scattered by the crystal, and c is the speed of light in vacuum. The theoretical values of f can be calculated using the MSD results obtained directly from the DWF calculation via the relation:

$$< u^2 > = \frac{3}{8\pi^2} B(T) \tag{4.9}$$

where B(T) is the experimental DWF, and it is defined as follows:

$$B(T) = 8\pi^2 \, (\, 2M_{QH}(\mathbf{q}) + 2M_1(\mathbf{q}) + 2M_2(\mathbf{q}) \,)$$

The MSD results, evaluated in the high temperature limit, were calculated for Morse potential, modified Morse potential, and Lennard-Jones potential using the volume obtained from the minimization of the quasiharmonic contribution, and the quasiharmonic and the anharmonic contributions of the total free energy. The graphs for the minimum volume at a given temperature for the Morse and modified Morse potentials have already been given in Figures 3.1 and 3.2 for Kr and Xe, respectively. Similar graphs for the L-J potential are not reproduced here because they can be found in Shukla and Shanes (1985). The L-J potential parameters for Kr and Xe are listed in Table 4.2.

4.1.1. Results and Discussion:

The calculated Mössbauer recoilless fraction is presented in Figures 4.1 through 4.4 for Kr and Xe. For Kr we compare our calculated values from three different potentials with experimental results obtained by Kolk (1971). The experimental results are available only at low temperatures. Since the DWF was calculated in the high temperature limit, we can only compare our results with those of Kolk in the neighborhood of Debye temperature. Morse potential and modified Morse potential have the same curvature, and they are higher the experimental values. The E(QH) L-J potential results agree excellently with the experimental results; whereas the $E(\lambda^2)$ results are in fair agreement over the range of temperatures near θ_D. For the case of Xe, experimental results were not available, therefore we can not conclude how good the calculated results are.

Table 4.2: Parameters of Lennard-Jones Potential For Kr and Xe.
The units of r_0, and U_0 are (Å), and (10^{-14} erg), respectively.

	LJ
Kr	$U_0 = 3.248$
	$r_0 = 3.965$
Xe	$U_0 = 4.577$
	$r_0 = 4.318$

Figure 4.1

Mössbauer Recoilless Fraction of Kr

With Morse (M) and Modified Morse (MM) Potentials.

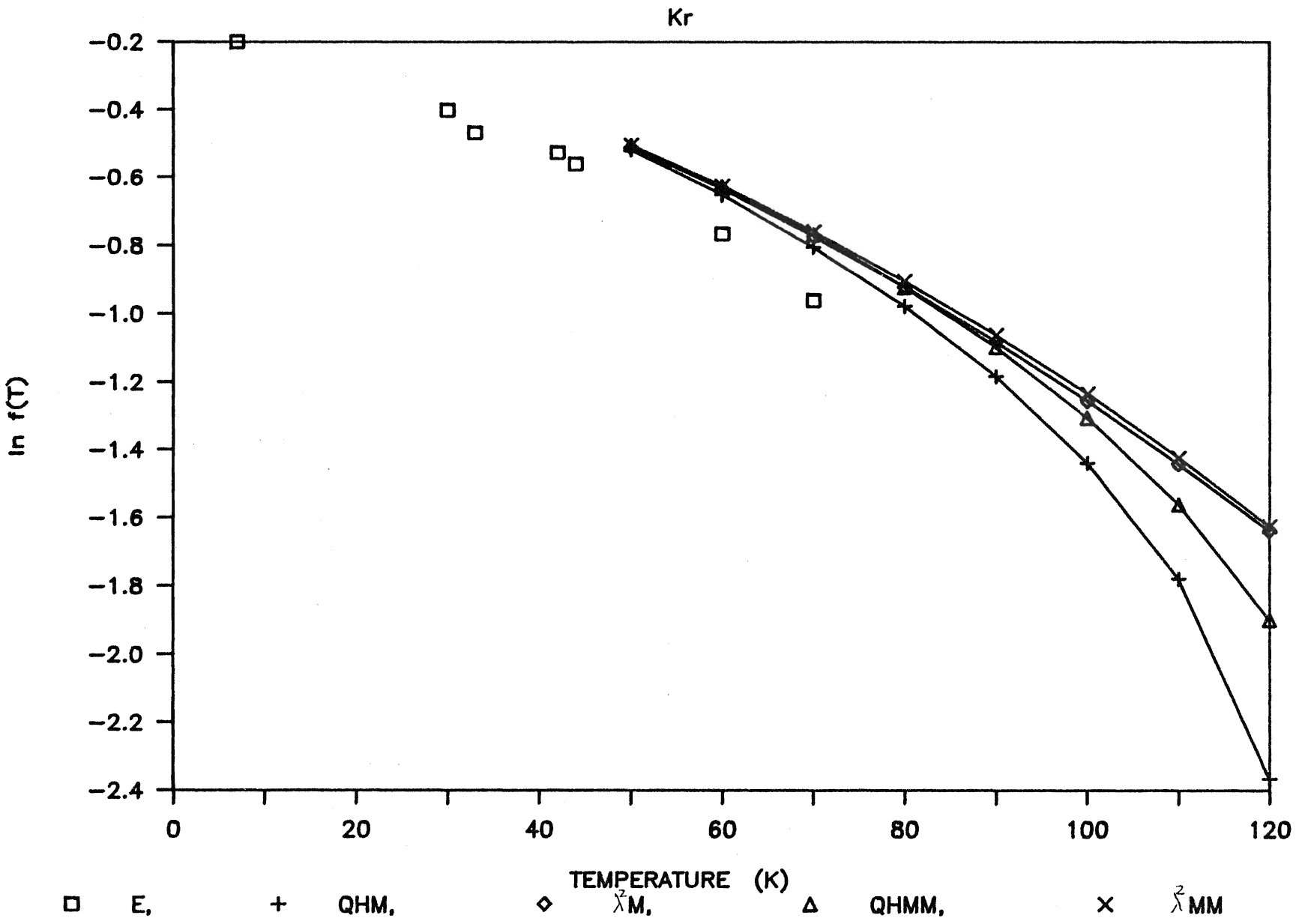
Kr
−0.2
−0.4
−0.6
−0.8
−1.0
−1.2
−1.4
−1.6
−1.8
−2.0
−2.2
−2.4
ln f(T)
0
20
40
60
80
100
120
TEMPERATURE (K)
E,
QHM,
λ²M,
QHMM,
λ²MM

Figure 4.2

Mössbauer Recoilless Fraction of Kr

With Morse (M) and Lennard-Jones (LJ) Potentials.

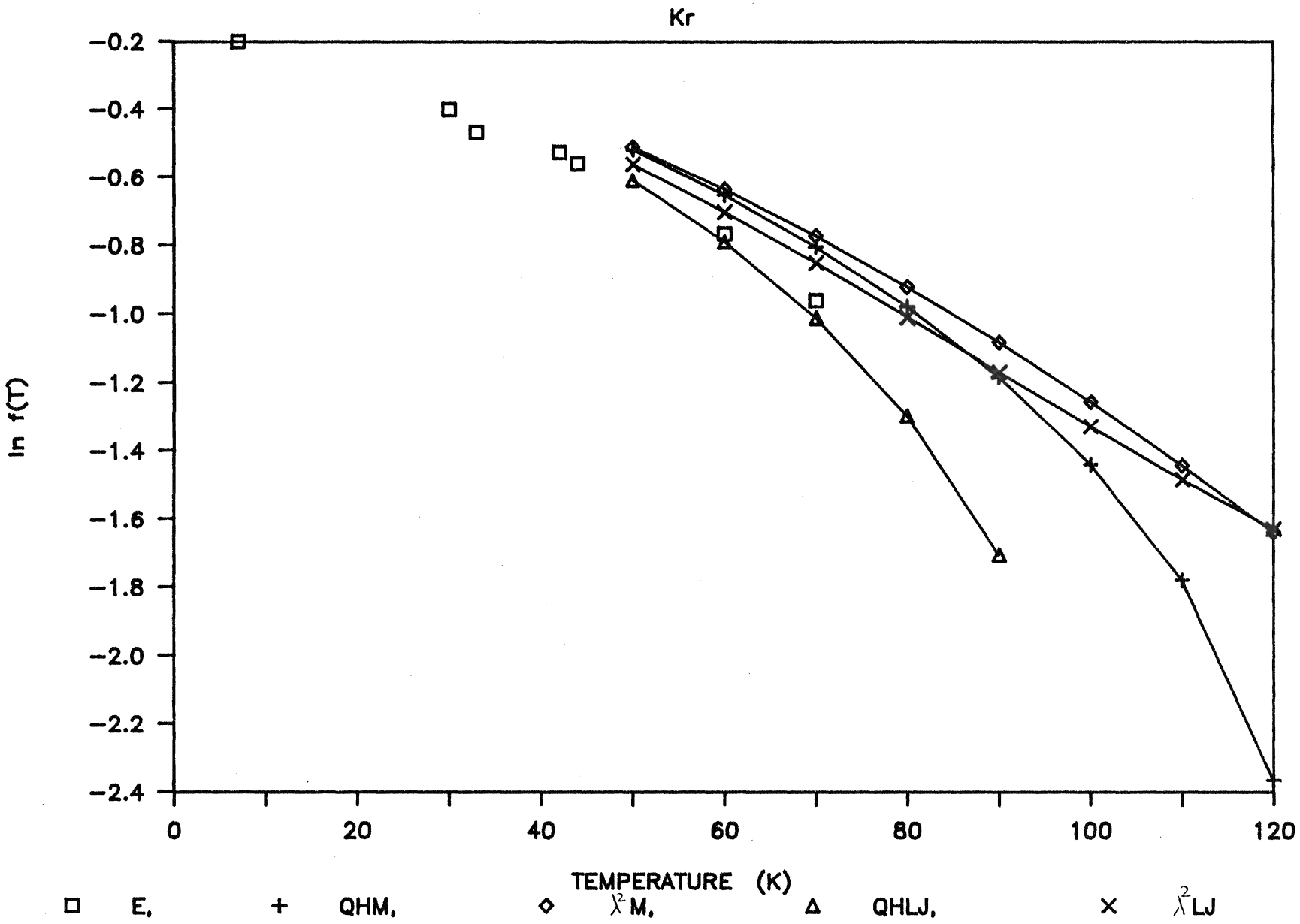
Kr
−0.2
−0.4
−0.6
−0.8
−1.0
−1.2
−1.4
−1.6
−1.8
−2.0
−2.2
−2.4
ln f(T)
0
20
40
60
80
100
120
TEMPERATURE (K)
E,
QHM,
λ² M,
QHLJ,
λ² LJ

Figure 4.3

Mössbauer Recoilless Fraction of Xe

With Morse (M) and Modified Morse (MM) Potentials.

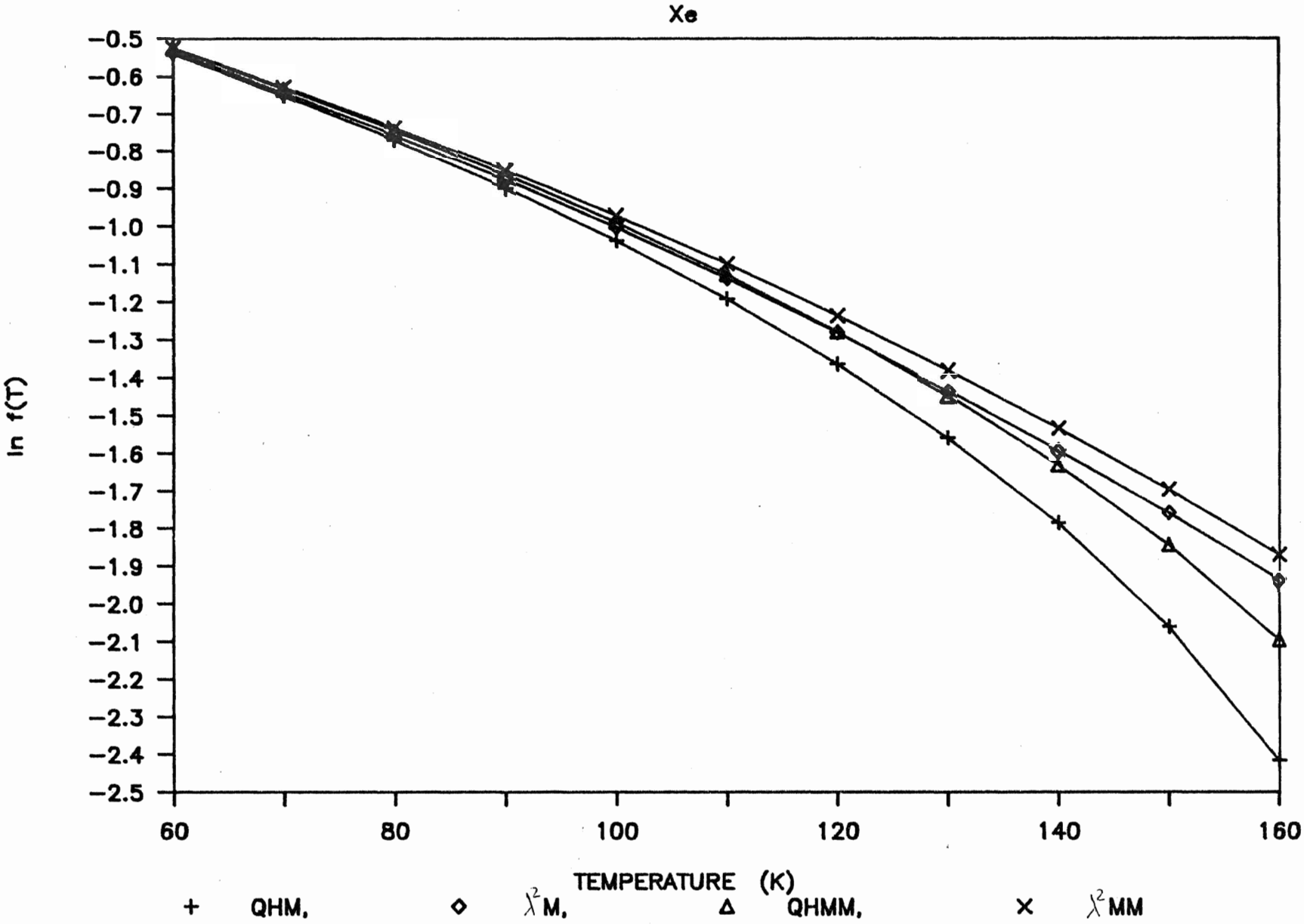
Xe
−0.5
−0.6
−0.7
−0.8
−0.9
−1.0
−1.1
−1.2
−1.3
−1.4
−1.5
−1.6
−1.7
−1.8
−1.9
−2.0
−2.1
−2.2
−2.3
−2.4
−2.5
ln f(T)
60
80
100
120
140
160
TEMPERATURE (K)
+ QHM,
◇ λ²M,
Δ QHMM,
× λ²MM

Figure 4.4

Mössbauer Recoilless Fraction of Xe

With Morse (M) and Lennard-Jones (LJ) Potentials.

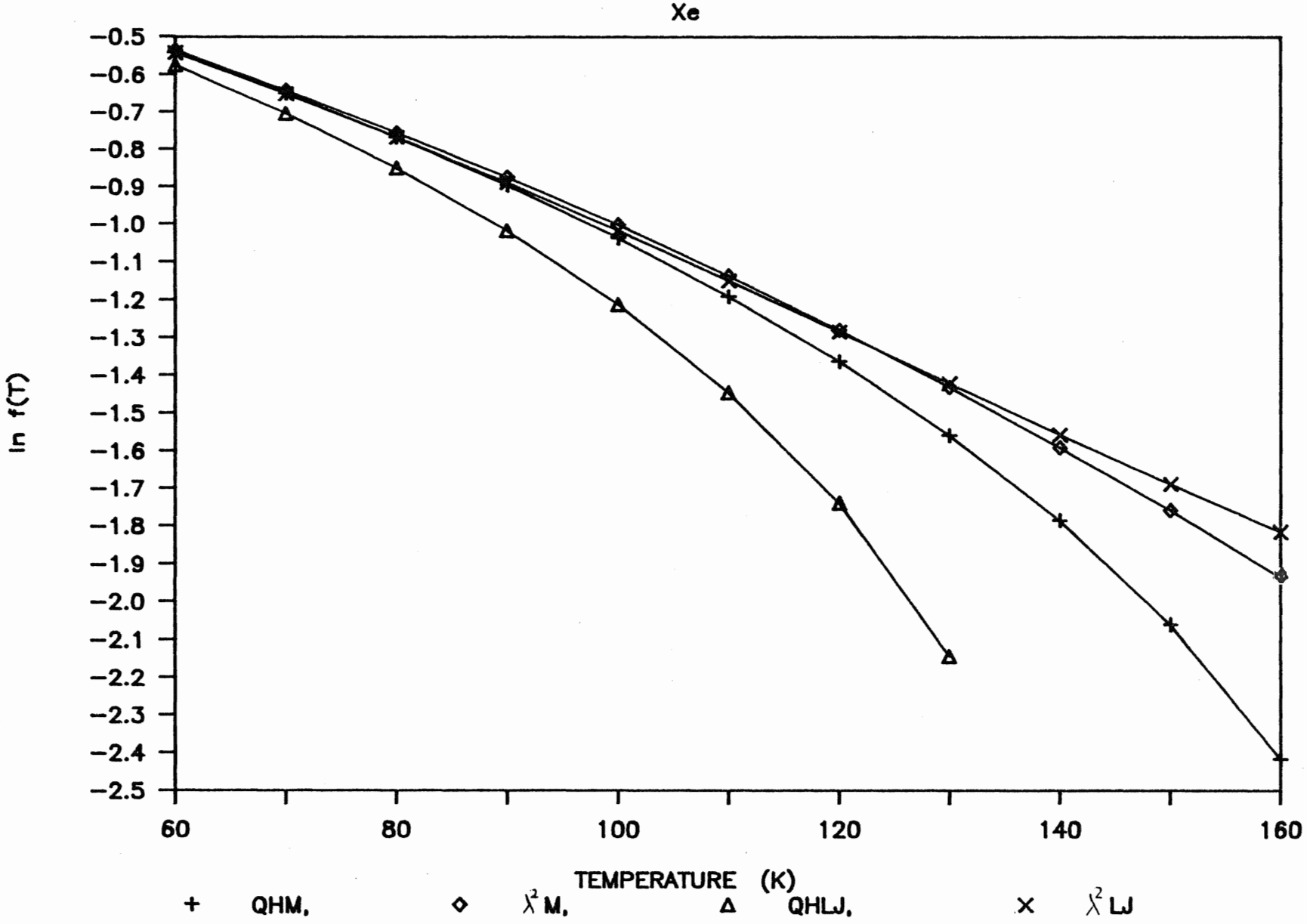
Xe
−0.5
−0.6
−0.7
−0.8
−0.9
−1.0
−1.1
−1.2
−1.3
−1.4
−1.5
−1.6
−1.7
−1.8
−1.9
−2.0
−2.1
−2.2
−2.3
−2.4
−2.5
ln f(T)
60
80
100
120
140
160
TEMPERATURE (K)
+ QHM,
◇ λ² M,
△ QHLJ,
× λ² LJ

4.3. DWF Results for fcc Metals:

The DWF was calculated for the following metals: Pb, Al,Cu, Ag, and Au with Morse potential and modified Morse potential from two different equations of state, E(QH) and $E(\lambda^2)$. The values of the nearest-neighbour distance are the same as determined in the previous section by minimizing the total free energy of the system for these potentials. The results of DWF for the metals are presented in Figures 4.5 through 4.9. For convenience, the results are given in terms of the experimental DWF, B. Whereas the quasiharmonic contribution of the Morse potential is less than that of the modified Morse, the anharmonic contributions are the other way around. In total the results obtained from the modified Morse potential are shifted up and closer to the experimental results, except in the case of Au. The calculated results for Pb, Al, and Cu are in good agreement with experiment at low temperature. However, at high temperature the experimental results (Chipman (1960), MacDonald (1967), and Martin and O'Connor (1978)), respectively, increase very rapidly. The experimental B(T) values of Ag (Simerska (1961)) were in a bad agreement with our calculated results. The computed results for Au are higher than the experimental values (Synecek and et al. (1970)) at all temperature.

Figure 4.5

Debye-Waller Factor of Pb

With Morse (M) and Modified Morse (MM) Potentials.

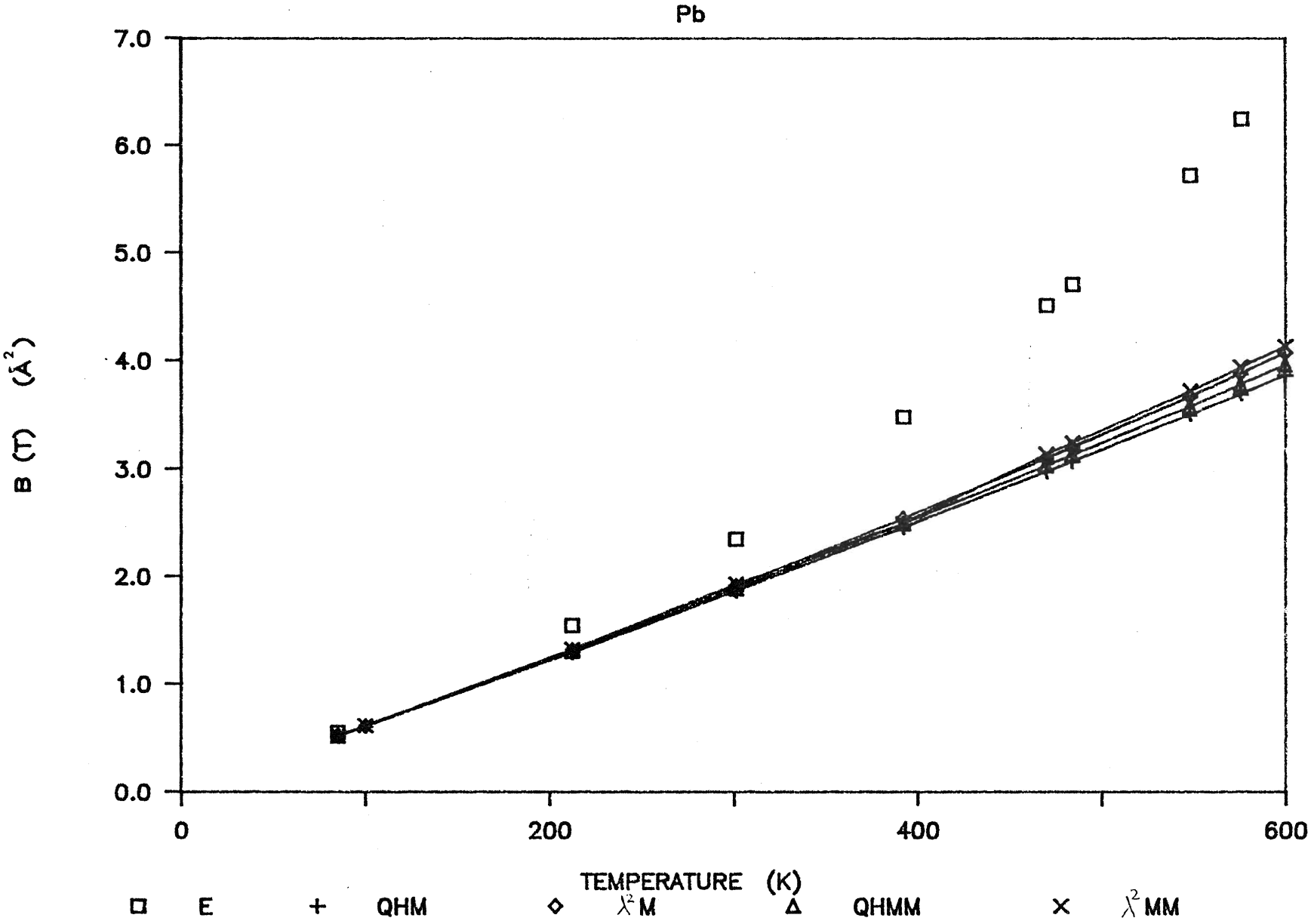
Pb
7.0
6.0
5.0
4.0
3.0
2.0
1.0
0.0
B (T) (Å²)
0
200
400
600
TEMPERATURE (K)
E
QHM
λ²M
QHMM
λ²MM

Figure 4.6

Debye-Waller Factor of Al

With Morse (M) and Modified Morse (MM) Potentials.

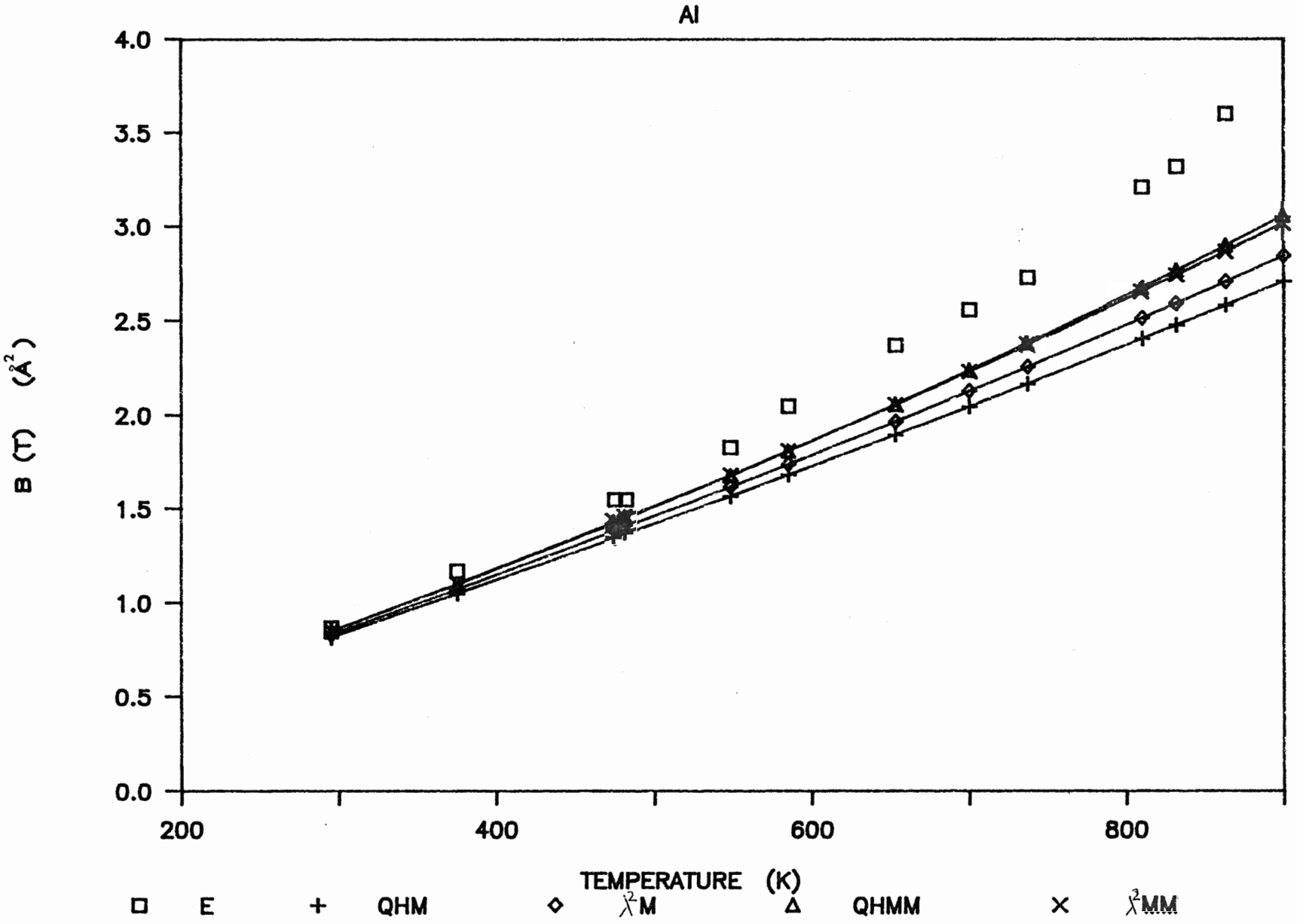
Al
4.0
3.5
3.0
2.5
2.0
1.5
1.0
0.5
0.0
B (T) (Å²)
200
400
600
800
TEMPERATURE (K)
E
QHM
λ²M
QHMM
λ³MM

Figure 4.7

Debye-Waller Factor of Cu

With Morse (M) and Modified Morse (MM) Potentials.

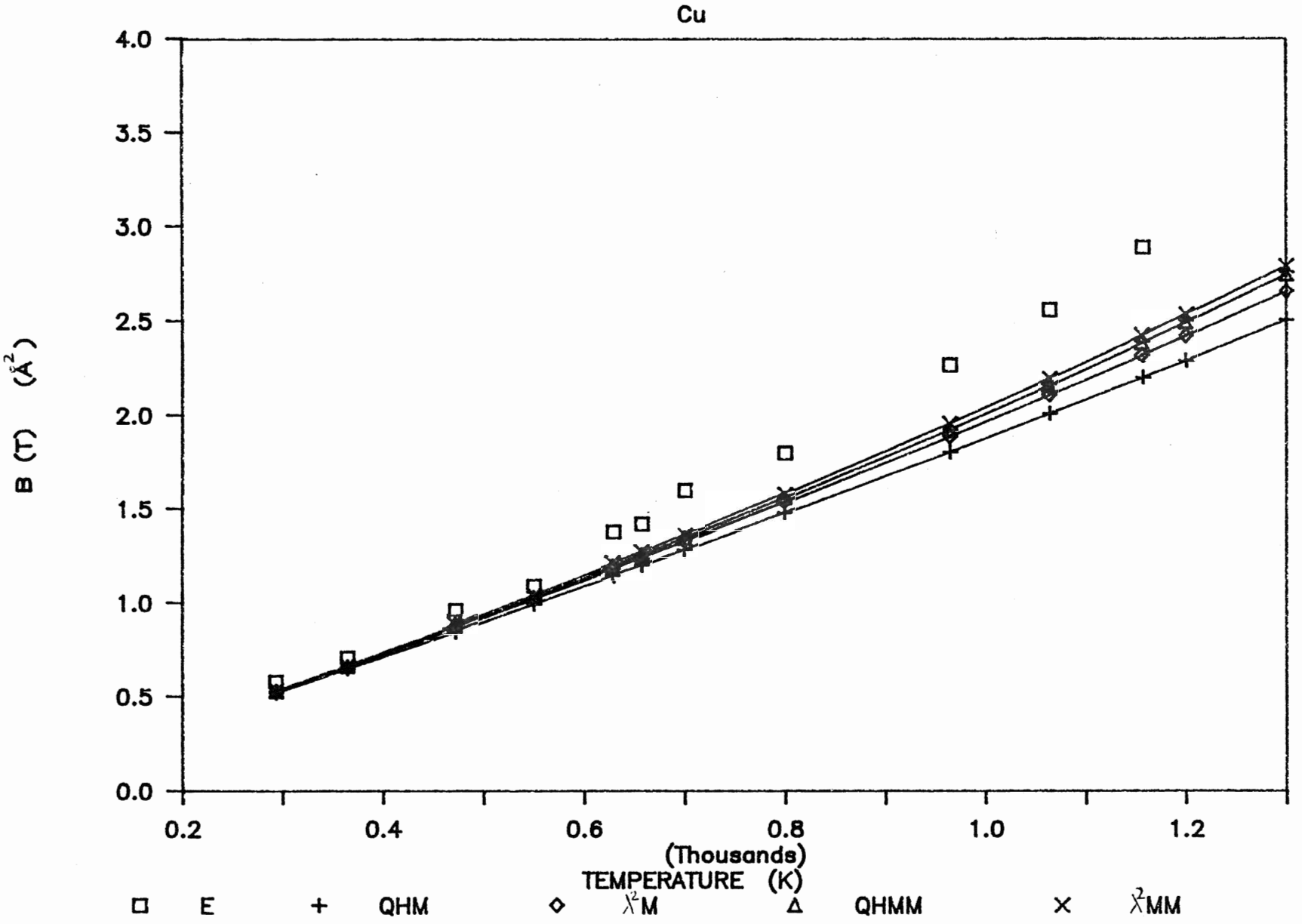
Cu
4.0
3.5
3.0
2.5
2.0
1.5
1.0
0.5
0.0
B (T) (Å^2)
0.2
0.4
0.6
0.8
1.0
1.2
(Thousands)
TEMPERATURE (K)
E
QHM
χ^2M
QHMM
χ^2MM

Figure 4.8

Debye-Waller Factor of Ag

With Morse (M) and Modified Morse (MM) Potentials.

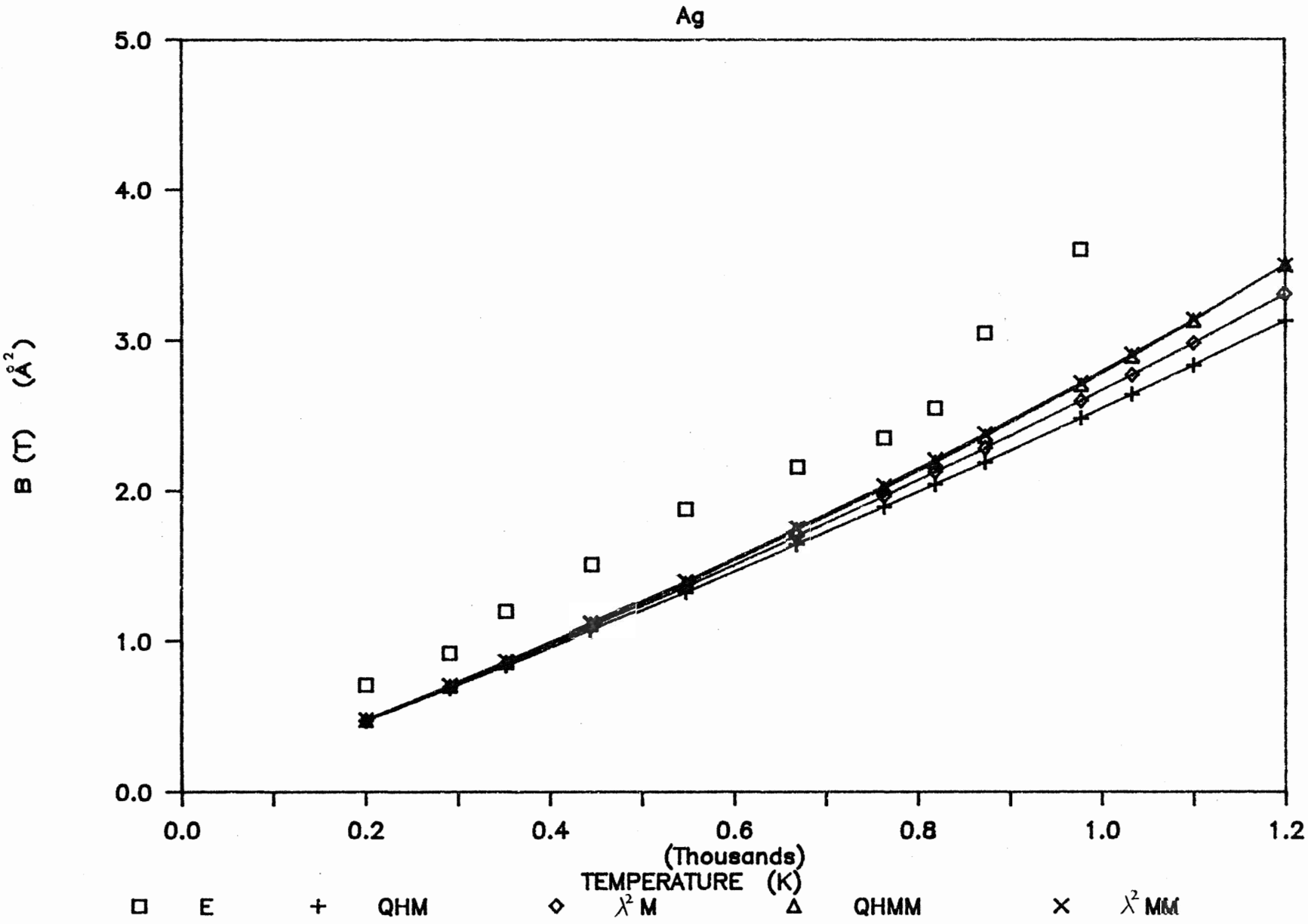
Ag
5.0
4.0
3.0
2.0
1.0
0.0
B (T) (Å²)
0.0
0.2
0.4
0.6
0.8
1.0
1.2
(Thousands)
TEMPERATURE (K)
E
QHM
λ² M
QHMM
λ² MM

Figure 4.9

Debye-Waller Factor of Au

With Morse (M) and Modified Morse (MM) Potentials.

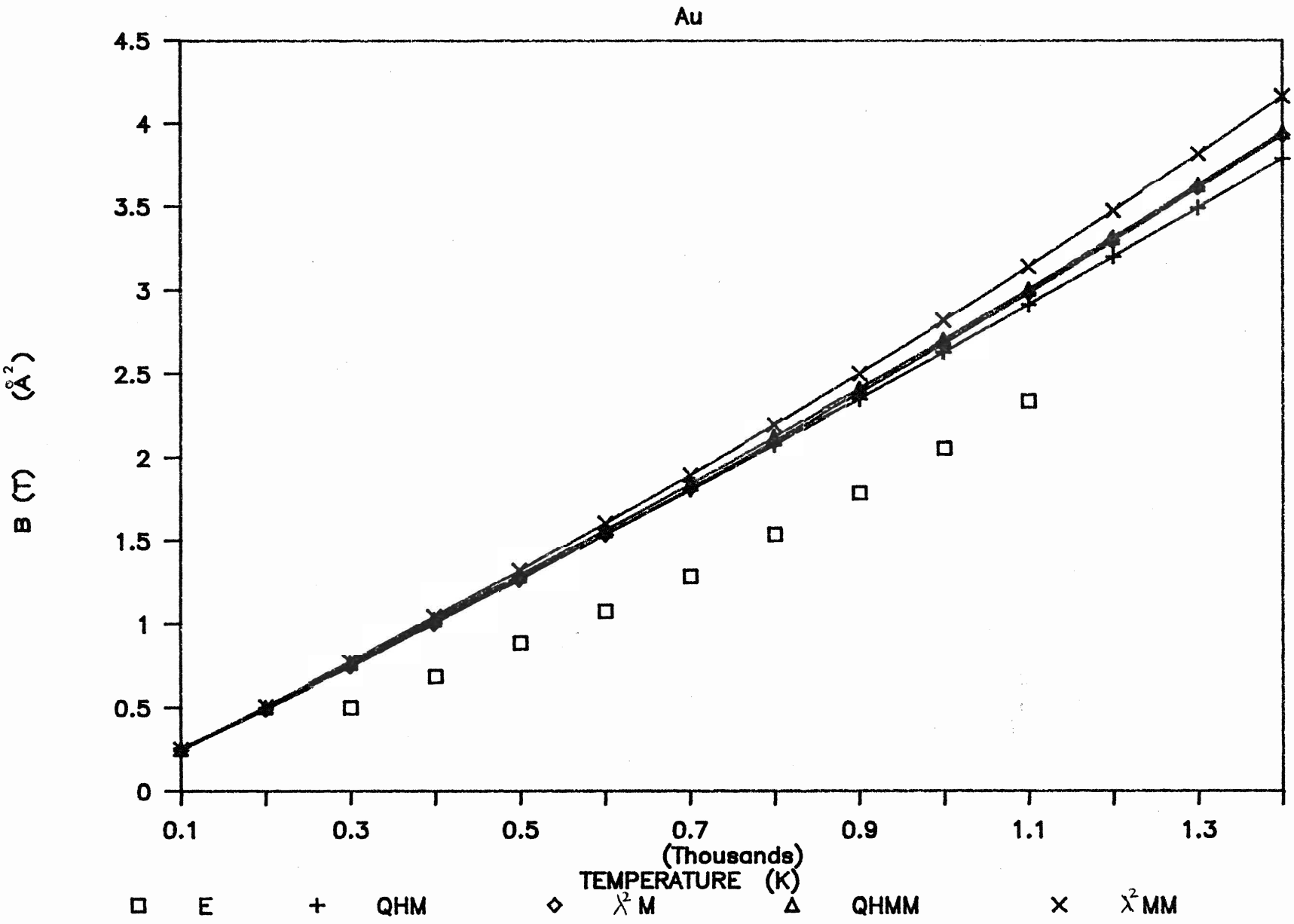
Au
4.5
4
3.5
3
2.5
2
1.5
1
0.5
0
B (Å²)
0.1
0.3
0.5
0.7
0.9
1.1
1.3
(Thousands)
TEMPERATURE (K)
E
QHM
χ² M
QHMM
χ² MM

5. Phonon Dispersion Curves

5.1. Quasiharmonic Phonon Frequency:

In this section we present the expression that is necessary to calculate the phonon dispersion curves for the wave vectors in the three symmetry principal directions. The quasiharmonic frequencies $\omega(\mathbf{q}j)$ for the normal mode $\mathbf{q}j$ are given by the following eigenvalue equation:

$$\omega_{\mathbf{q}j}^2 = \sum_{\alpha\beta} e_\alpha(\mathbf{q}j)\, D_{\alpha\beta}(\mathbf{q})\, e_\beta(\mathbf{q}j) \tag{5.1}$$

$D_{\alpha\beta}(\mathbf{q})$ is the dynamical matrix for the wave vector $\mathbf{q}$, and it is given by

$$D_{\alpha\beta}(\mathbf{q}) = \frac{1}{M} \sum_{l}{}' \phi_{\alpha\beta}(r_l)\, [1 - \cos(\mathbf{q}.\mathbf{r}_l)\,] \tag{5.2}$$

5.2. Renormalized Phonon Frequency:

In this section we outline the theory required for the calculation of the cubic and the quartic frequency shifts. This calculation of the phonon frequencies includes the quasiharmonic and the two lowest-order anharmonic contributions. The sum of these three contributions is defined as the renormalized phonon frequency. This renormalized frequency is obtained by means of the Green's function method at a finite temperature (Shukla and Muller (1971)). Shukla and Hübschle (1989) have

employed the high temperature limit and used the static approximation by setting $\omega = 0$. Here, we give some feedback for the Green's function method carried out by Shukla and Muller (1971).

5.2.1. The Green's Function Method:

For an anharmonic crystal the quasiharmonic and interaction parts of the Hamiltonian are given by:

$$H = H_0 + H' \tag{5.3}$$

where

$$H_0 = \sum_{qj} \hbar\, \omega_{qj} \left(a^{\dagger}_{qj}\, a_{qj} + \frac{1}{2} \right), \tag{5.4}$$

$$H' = \lambda \sum_{q_1 j_1} \sum_{q_2 j_2} \sum_{q_3 j_3} V^3(q_1 j_1, q_2 j_2, q_3 j_3)\, A_{q_1 j_1}\, A_{q_2 j_2}\, A_{q_3 j_3} +$$

$$+ \lambda^2 \sum_{q_1 j_1} \sum_{q_2 j_2} \sum_{q_3 j_3} \sum_{q_4 j_4} V^4(q_1 j_1, q_2 j_2, q_3 j_3, q_4 j_4)\, A_{q_1 j_1}\, A_{q_2 j_2}\, A_{q_3 j_3}\, A_{q_4 j_4} \tag{5.5}$$

$$= \lambda\, V^3 + \lambda^2\, V^4 = H_3 + H_4 \tag{5.6}$$

The various symbols arising in the above equations are: $a^{\dagger}_{qj}$ and a_{qj} are the phonon creation and annihilation operators for the mode qj, $\omega(qj)$ is the angular frequency for the normal mode qj, λ is an order parameter which should be set equal to unity at the end of the calculation. The coefficients V^3 and V^4 are completely symmetric in their indices (qj) and are related to the atomic force constants by:

$$V^n(q_1j_1,\ldots,q_nj_n) = \frac{N^{1-n/2}}{n!}\,\Delta(q_1,\ldots,q_n)\left[\frac{\hbar^n}{2^n\,\omega_{q_1j_1}\ldots\omega_{q_nj_n}}\right]^{1/2}$$

$$\times\ \Phi(q_1j_1,\ldots,q_nj_n). \tag{5.7}$$

The operator A_{qj} introduced in Eq. (5.5) is defined here as:

$$A_{qj} = a_{qj} + a^{\dagger}_{qj} \tag{5.8}$$

Following Zubarev (1960) the one-phonon double-time temperature-dependent Green's function is defined as

$$G_{qjq'j'}(t - t') = \ll A_{qj}(t)\ ;\ A^{\dagger}_{qj}(t') \gg$$

$$= -\,i\,\theta(t - t') \langle [\ A_{qj}(t)\ ,\ A^{\dagger}_{qj}(t')\ ] \rangle, \tag{5.9}$$

where the square bracket is the commutator:

$$[\ A\ ,\ B\ ] = AB - BA, \tag{5.10}$$

and $\theta(t)$ is the Heaviside unit step function.

The Fourier transform $G_{qjq'j'}(\omega)$ of the one particle Green's function is give by

$$G_{qjq'j'}(t - t') = \int_{-\infty}^{+\infty} G_{qjq'j'}(\omega)\,\exp\{-\,i\omega(t - t')\}\,d\omega \tag{5.11}$$

The Green's function $G_{qjq'j'}(\omega)$ can be generated by employing the equation of motion as described by Zubarev (1960). Thus, the Fourier transform of the Green's function, derived by Shukla and Muller (1971), has the following form

$$G_{qjq'j'}(\omega) = \frac{\omega_{qj}\,\delta_{qq'}\delta_{jj'}}{\pi\,[\omega^2 - \omega_{qj}^2 - 2\omega_{qj}\Pi_{qj}(\omega)]} \tag{5.12}$$

where $\Pi_{qj}(\omega)$ is the phonon self-energy term, defined by

$$\Pi_{qj}(\omega) = \Pi_{qj}^3(\omega) + \Pi_{qj}^4 \tag{5.13}$$

$$\Pi_{qj}^3(\omega) = \frac{18\lambda^2}{\hbar^2} \sum_{q_1 j_1} \sum_{q_2 j_2} |\, V^3(-qj, q_1 j_1, q_2 j_2)\,|^2 \times$$

$$\times \left[(N_1 + N_2)\, \frac{\omega_1 + \omega_2}{\omega^2 - (\omega_1 + \omega_2)^2} + (N_2 - N_1)\, \frac{\omega_1 - \omega_2}{\omega^2 - (\omega_1 - \omega_2)^2} \right] \tag{5.14}$$

$$\Pi_{qj}^4 = \frac{12\lambda^2}{\hbar} \sum_{q_1 j_1} V^4(q_1 j_1, -q_1 j_1, qj, -qj)\, N_1 \tag{5.15}$$

In the above equations ω_i and N_i are abbreviations for $\omega(q_i j_i)$ and $N(q_i j_i) = \coth(\frac{1}{2}\beta\hbar\omega_i)$, respectively (i=1,2).

Since Π^4, the quartic part, is independent of ω, it is assumed that the dependence of $\Pi^3(\omega)$ on ω is also weak (Shukla and Hübschle (1989)), therefore ω is set equal to zero in $\Pi^3(\omega)$ (static approximation). With this approximation and taking the high temperature limit, $G(\omega)$ simplifies significantly:

$$G_{qjq'j'}(\omega) = \frac{\omega_{qj}\,\delta_{qq'}\delta_{jj'}}{\pi\,[\omega^2 - \Omega_{qj}^2(\omega=0)]} \tag{5.16}$$

where

$$\Omega_{qj}^2\,(\omega=0) = \omega_{qj}^2 - \frac{\lambda^2}{2\beta N} \sum_{q_1 j_1} \sum_{q_2 j_2} \Delta(q_1+q_2-q) \times \frac{|\,\Phi(q_1 j_1, -q_2 j_2, -qj)\,|^2}{\omega_{q_1 j_1}^2\, \omega_{q_2 j_2}^2} +$$

$$+ \frac{\lambda^2}{2\beta N} \sum_{q_1 j_1} \frac{\Phi(q_1 j_1, qj, -q_1 j_1, -qj)}{\omega_{q_1 j_1}{}^2} ,$$

$$= \omega_{qj}{}^2 + \Delta_3(qj) + \Delta_4(qj). \qquad (5.17)$$

Ω_{qj} is the renormalized frequency of the phonon (qj) and Δ_3 and Δ_4 are the cubic and quartic frequency shifts, respectively. The quasiharmonic contribution is represented by ω_{qj}.

The cubic shift contains a Δ function which can be represented by plane waves

$$\Delta(q) = \frac{1}{N} \sum_{l} \exp[i(q.r_l)] \qquad (5.18)$$

Substituting for $\Phi(q_1 j_1, -q_2 j_2, -qj)$ from Eq. (2.5) and using the representation (5.18) for Δ we obtain the following expression for the cubic shift:

$$\Delta_3(qj) = - \frac{K_B T}{32 N^2 M B^2} \sum_{l} \sum_{l_1}{}' \sum_{l_2}{}' g(q;l,l_1,l_2) \sum_{\alpha\beta} e_\alpha(qj)\, e_\beta(qj)$$

$$\times \sum_{\gamma\lambda} \sum_{\sigma\delta} \phi_{\gamma\delta\alpha}(l_1)\, \phi_{\lambda\sigma\beta}(l_2)\, F_{\gamma\lambda}(l,l_1,l_2)\, F_{\delta\sigma}(l,l_1,l_2) \qquad (5.19)$$

where

$$g(q;l,l_1,l_2) = \cos(q.r_l) - \cos[q.(r_l - r_{l_1})] - \cos[q.(r_l + r_{l_2})] +$$
$$+ \cos[q.(r_l - r_{l_1} + r_{l_2})] \qquad (5.20)$$

$F_{\alpha\beta}(l,l_1,l_2)$ is a combination of tensors, i.e.,

$$F_{\alpha\beta}(l,l_1,l_2) = S_{\alpha\beta}(l) - S_{\alpha\beta}(l - l_1) - S_{\alpha\beta}(l + l_2) + S_{\alpha\beta}(l - l_1 + l_2) \qquad (5.21)$$

and the tensors $S_{\alpha\beta}(l)$ are defined as (Shukla and Wilk (1974)):

$$S_{\alpha\beta}(l) = \sum_{qj} \frac{e_\alpha(qj)\, e_\beta(qj)}{\omega_{qj}^2} \cos(\mathbf{q}.\mathbf{r}_l) \tag{5.22}$$

The quartic shift is obtained by substituting for $\Phi(q_1j_1,qj,-q_1j_1,-qj)$ from Eq. (2.5):

$$\Delta_4(qj) = \frac{K_B T}{2NMB} \sum_{l}{}' [1 - \cos(\mathbf{q}.\mathbf{r}_l)] \sum_{\alpha\beta} e_\alpha(qj)\, e_\beta(qj) \times$$

$$\times \sum_{\gamma\delta} \phi_{\alpha\beta\gamma\delta}(l) [S_{\gamma\delta}(0) - S_{\gamma\delta}(l)] \tag{5.23}$$

The expressions for the tensors, $\phi_{\alpha\beta}(l)$, $\phi_{\alpha\beta\gamma}(l)$, and $\phi_{\alpha\beta\gamma\delta}(l)$, introduced in Eqs. (5.2), (5.19), and (5.23) are given by, for any $\phi(r)$,

$$\phi_{\alpha\beta}(l) = \frac{\alpha_l\beta_l}{r_l^2} B(r_l) + \delta_{\alpha\beta} \frac{1}{r_l} \phi'(r_l) \tag{5.24}$$

$$\phi_{\alpha\beta\gamma}(l) = \frac{\alpha_l\beta_l\gamma_l}{r_l^3} C(r_l) + (\alpha_l\delta_{\beta\gamma}+\beta_l\delta_{\gamma\alpha}+\gamma_l\delta_{\alpha\beta}) \frac{B(r_l)}{r_l^2} \tag{5.25}$$

$$\phi_{\alpha\beta\gamma\delta}(l) = \frac{\alpha_l\beta_l\gamma_l\delta_l}{r_l^4} D(r_l) + (\alpha_l\beta_l\delta_{\gamma\delta} + \beta_l\gamma_l\delta_{\alpha\delta} + \alpha_l\gamma_l\delta_{\beta\delta}$$

$$+ \alpha_l\delta_l\delta_{\beta\gamma} + \beta_l\delta_l\delta_{\alpha\gamma} + \gamma_l\delta_l\delta_{\alpha\beta}) \frac{C(r_l)}{r_l^3} +$$

$$+ (\delta_{\alpha\beta}\delta_{\gamma\delta} + \delta_{\beta\gamma}\delta_{\alpha\delta} + \delta_{\alpha\gamma}\delta_{\beta\delta}) \frac{B(r_l)}{r_l^2} \tag{5.26}$$

where α, β, γ, δ are each assigned the values of x, y, z, respectively, and α_l, β_l ,γ_l, δ_l are the corresponding components of the direct lattice vector r_l. B, C, D are combinations of derivatives of $\phi(r)$ evaluated at $r_l=|r_l|$.

5.3. Results and Discussion:

Since the basic ingredient in all the thermodynamic calculations is the phonon frequency, we have calculated the phonon dispersion curves for the three principal symmetry directions, by using Morse potential and modified Morse potential. The quasiharmonic frequencies were calculated for the lattice spacing at 10K, and the results are presented in Figures 5.1 through 5.8 for Kr and Xe. The dispersion curves calculated from both potentials seem to have the correct shape as compared to the experimental curves (Skalyo jr and et al. (1974) and Lurie and et al. (1974)). This indicates that the first and the second derivatives of the potentials, which enter in the calculation of the quasiharmonic frequencies, are of the correct order of magnitude The dispersion curves calculated from both potential for Kr and Xe did not show any disagreement.

Similarly, the phonon dispersion curves for the fcc metals: Cu, Ag, and Au were calculated and presented in Figures 5.9 through 5.20. The quasiharmonic frequencies were calculated with the lattice spacing at 673K, 293K, and 298K for Cu, Ag, and Au, respectively. The experimental results for Cu, Ag, and Au are obtained from Miller and Brockhouse (1971), Kamitakahara and Brockhouse (1969), and Lynn and et al. (1973), respectively. To investigate the effect of the anharmonic (cubic and quartic shifs) contributions to the phonon frequency, we have calculated these shifts for Cu and added them up to the quasiharmonic frequencies as shown in Figures 5.9 through 5.12. The anharmonic shifts did not affect the longitudinal mode because the cancellation of the cubic

and quartic shifts is almost complete. However, in the case of the transverse mode the cubic shift being negative is greater in magnitude than the quartic shift, and this resulted in lowering the total for the transverse mode from its quasiharmonic value. In general the results of the transverse mode for all elements were in good agreement with experiment. However, the longitudinal mode results were less than the experimental values, especially for Au.

Figure 5.1

QH Phonon Dispersion Curves for Kr Along the [1 0 0] Direction With Morse (M) and Modified Morse (MM) Potentials.

T denotes Transverse mode.

L denotes Longitudinal mode.

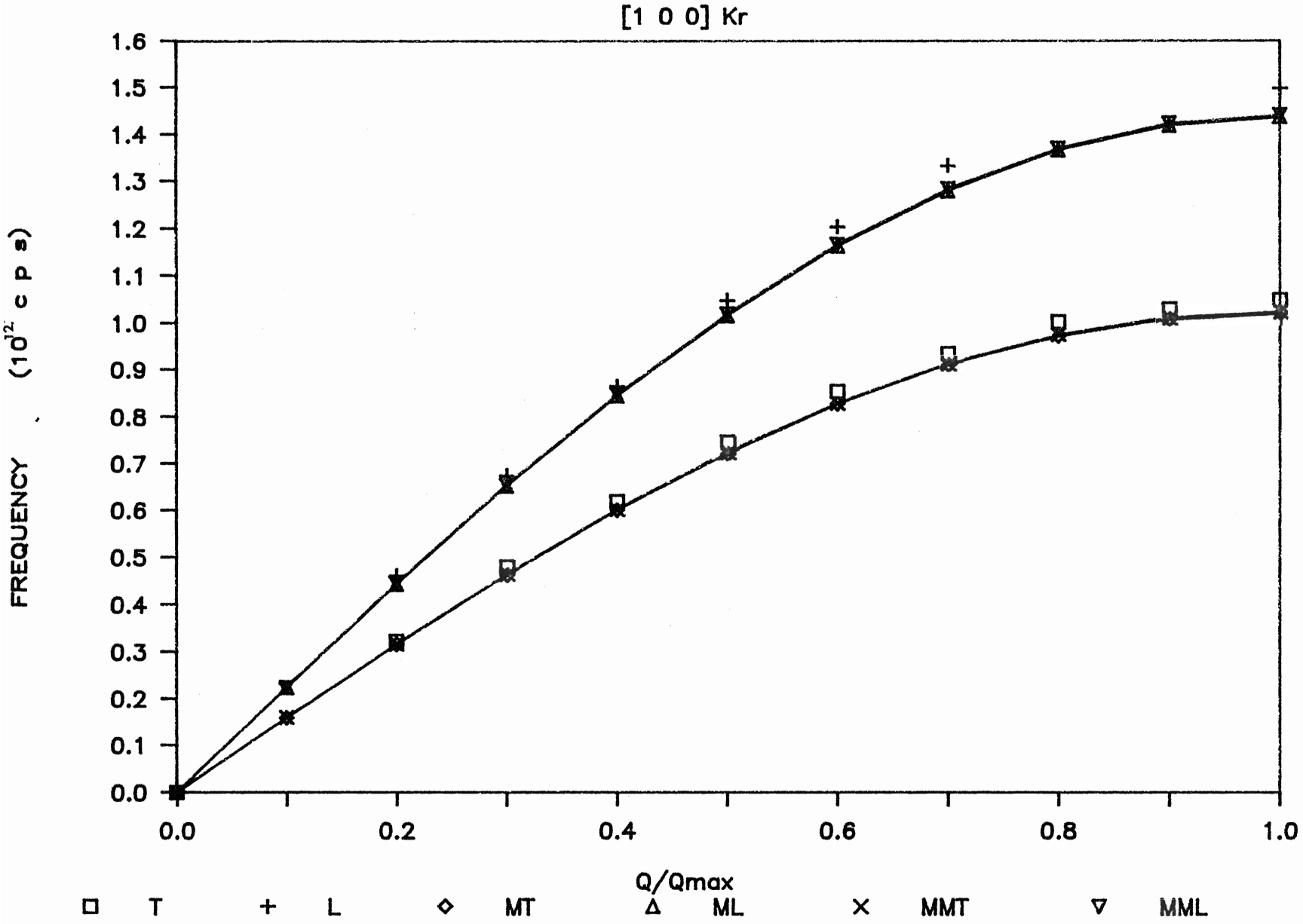
[1 0 0] Kr
FREQUENCY (10^12 c p s)
1.6
1.5
1.4
1.3
1.2
1.1
1.0
0.9
0.8
0.7
0.6
0.5
0.4
0.3
0.2
0.1
0.0
0.0
0.2
0.4
0.6
0.8
1.0
Q/Qmax
T
L
MT
ML
MMT
MML

Figure 5.2

QH Phonon Dispersion Curves for Kr Along the [1 1 0] Direction With Morse (M) Potential.

T denotes Transverse mode.

L denotes Longitudinal mode.

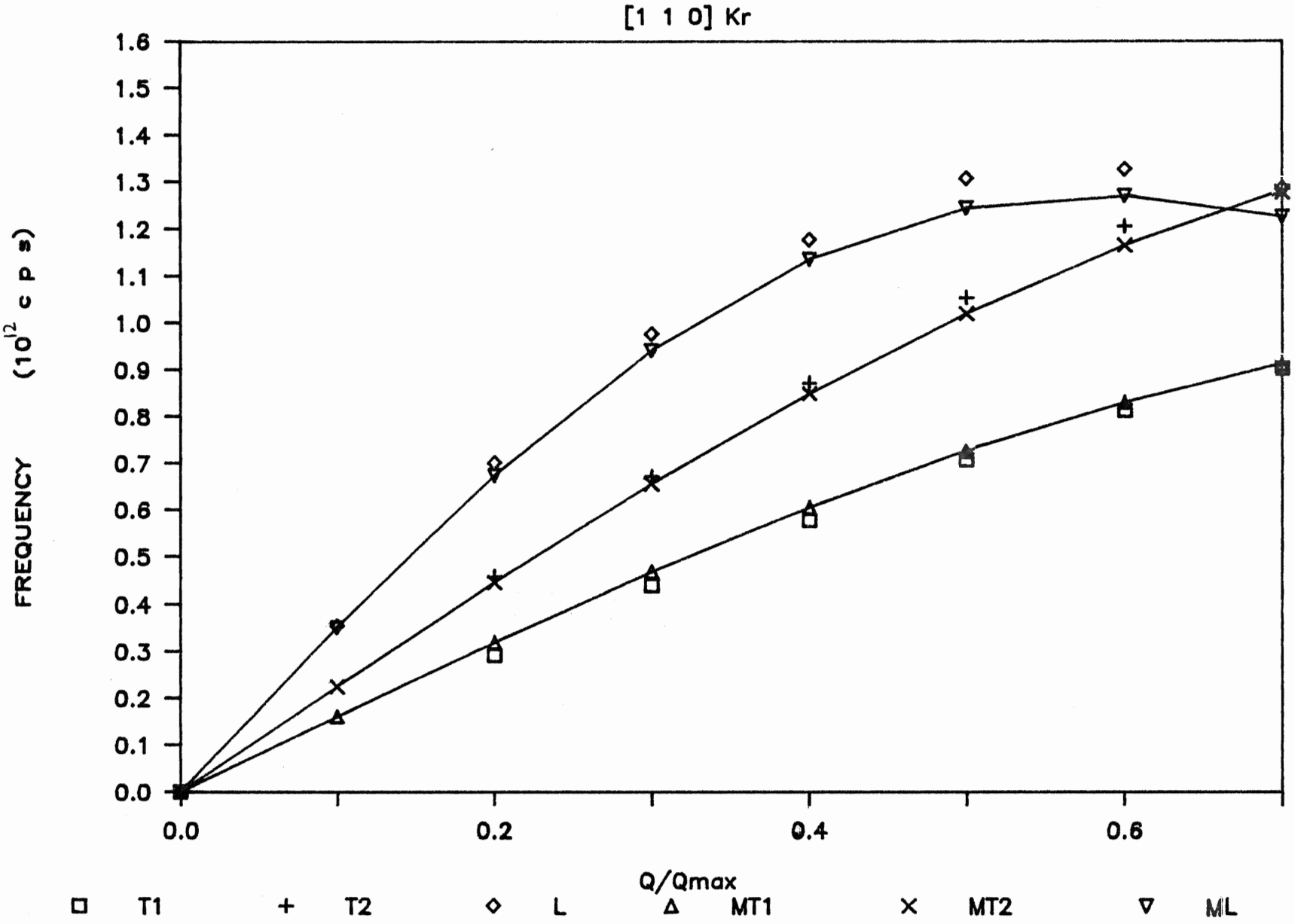
[1 1 0] Kr
FREQUENCY (10^12 c p s)
1.6
1.5
1.4
1.3
1.2
1.1
1.0
0.9
0.8
0.7
0.6
0.5
0.4
0.3
0.2
0.1
0.0
0.0
0.2
0.4
0.6
Q/Qmax
T1
T2
L
MT1
MT2
ML

Figure 5.3

QH Phonon Dispersion Curves for Kr Along the [1 1 0] Direction With Modified Morse (MM) Potential.

T denotes Transverse mode.

L denotes Longitudinal mode.

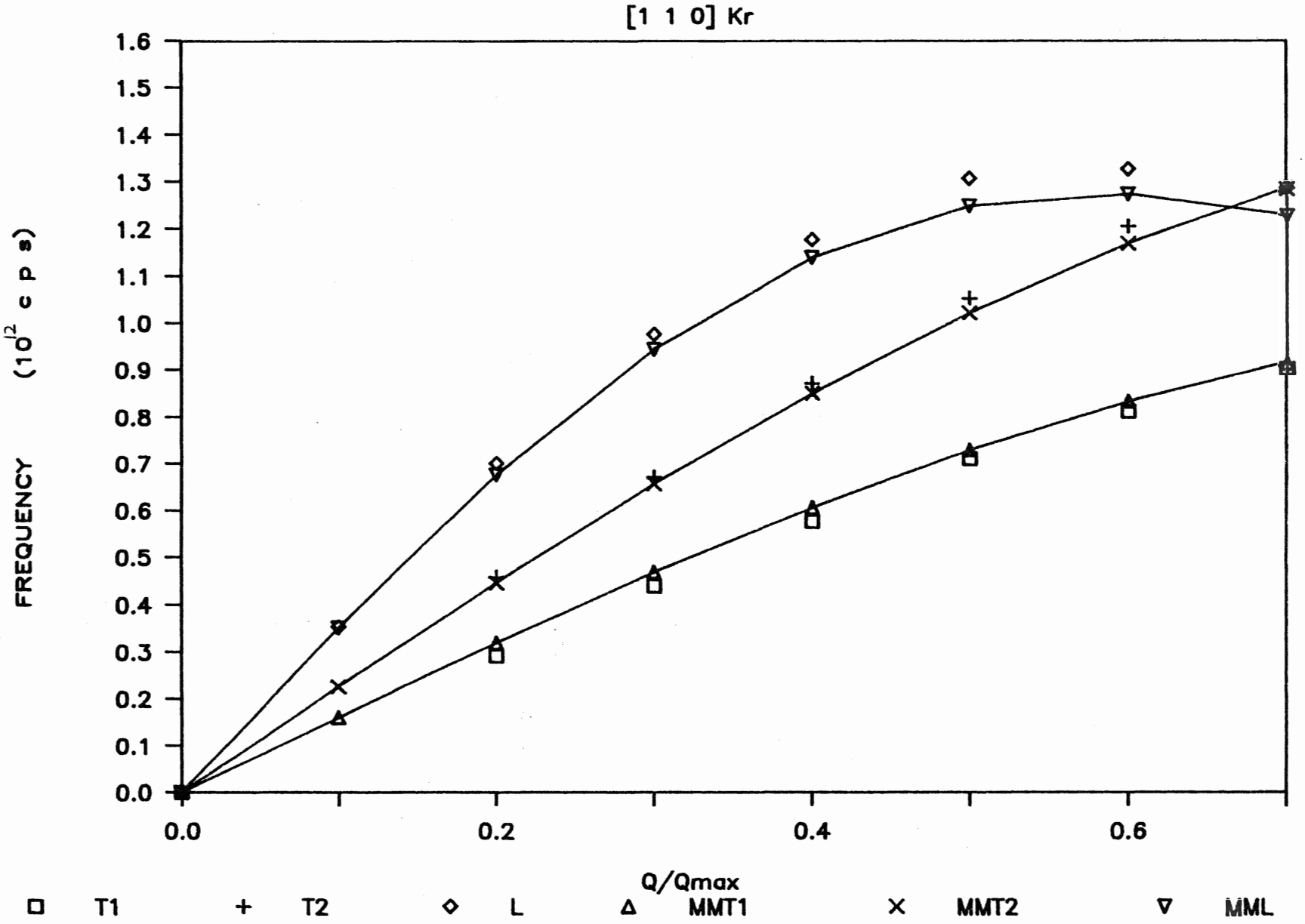
[1 1 0] Kr
FREQUENCY (10^12 c p s)
1.6
1.5
1.4
1.3
1.2
1.1
1.0
0.9
0.8
0.7
0.6
0.5
0.4
0.3
0.2
0.1
0.0
0.0
0.2
0.4
0.6
Q/Qmax
T1
T2
L
MMT1
MMT2
MML

Figure 5.4

QH Phonon Dispersion Curves for Kr Along the [1 1 1] Direction With Morse (M) and Modified Morse (MM) Potentials.

T denotes Transverse mode.

L denotes Longitudinal mode.

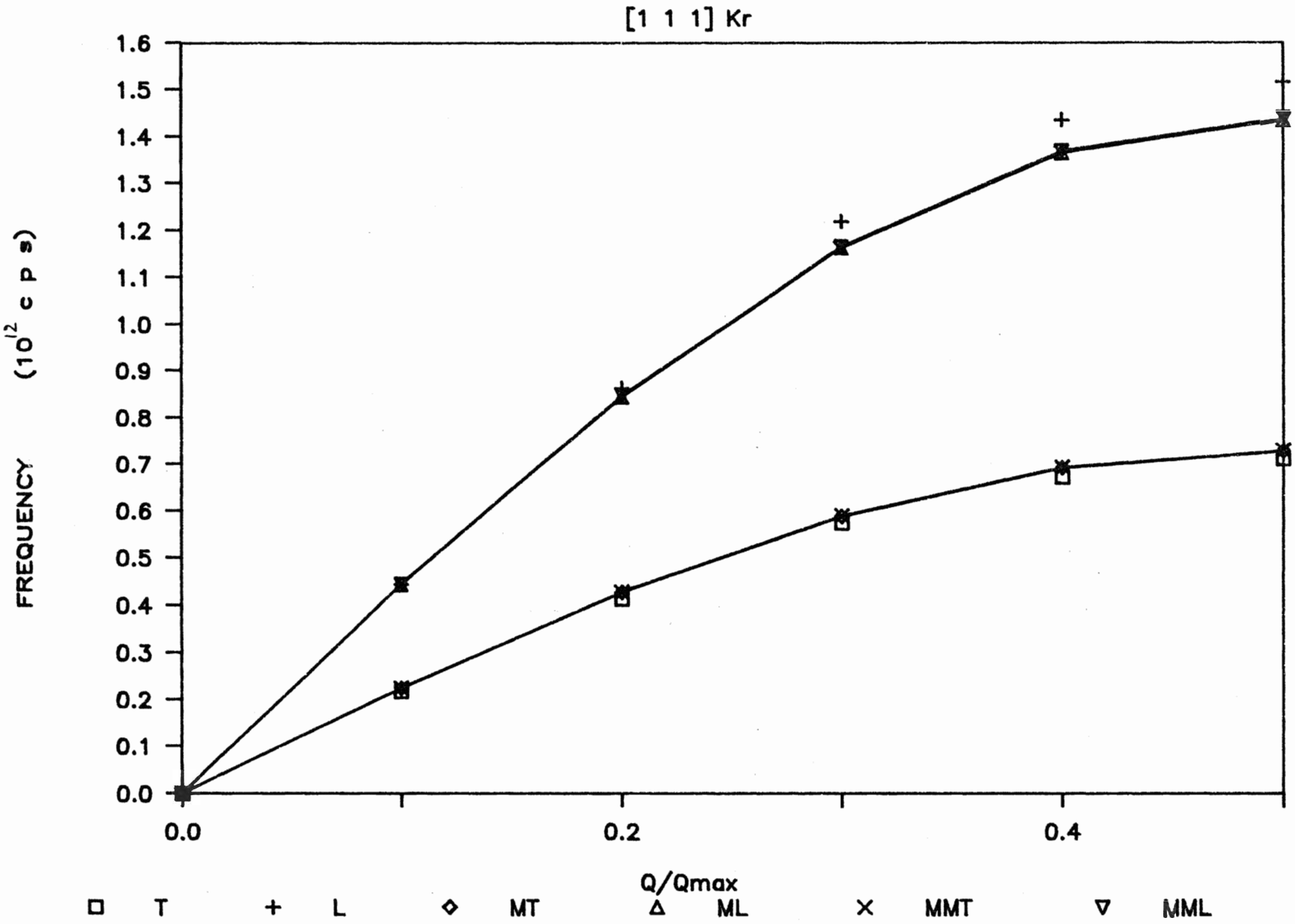
[1 1 1] Kr
FREQUENCY (10^12 c p s)
1.6
1.5
1.4
1.3
1.2
1.1
1.0
0.9
0.8
0.7
0.6
0.5
0.4
0.3
0.2
0.1
0.0
0.0
0.2
0.4
Q/Qmax
T
L
MT
ML
MMT
MML

Figure 5.5

QH Phonon Dispersion Curves for Xe Along the [1 0 0] Direction
With Morse (M) and Modified Morse (MM) Potentials.

T denotes Transverse mode.

L denotes Longitudinal mode.

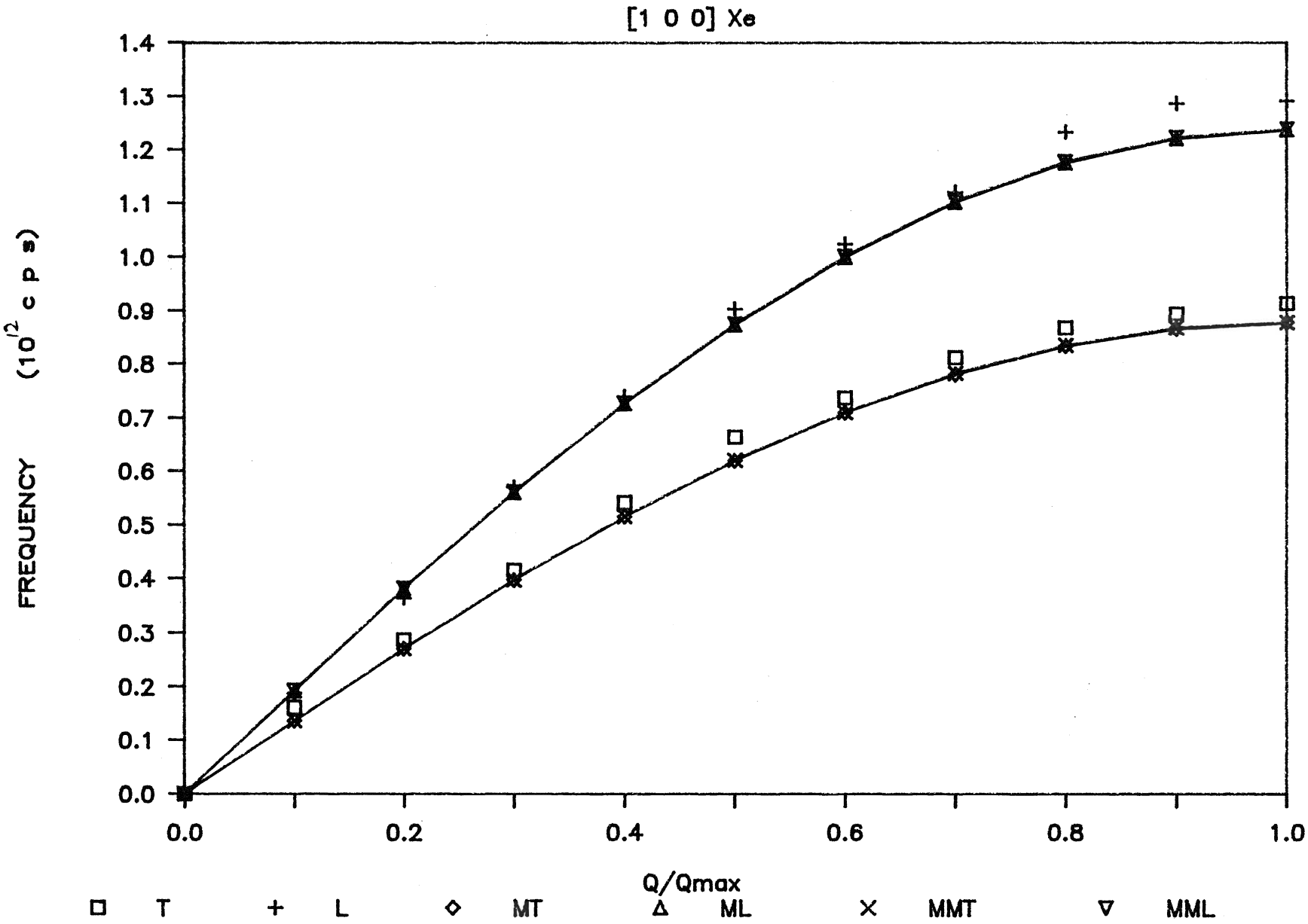
[1 0 0] Xe
FREQUENCY (10^12 c p s)
1.4
1.3
1.2
1.1
1.0
0.9
0.8
0.7
0.6
0.5
0.4
0.3
0.2
0.1
0.0
0.0
0.2
0.4
0.6
0.8
1.0
Q/Qmax
T
L
MT
ML
MMT
MML

Figure 5.6

QH Phonon Dispersion Curves for Xe Along the [1 1 0] Direction With Morse (M) Potential.

T denotes Transverse mode.

L denotes Longitudinal mode.

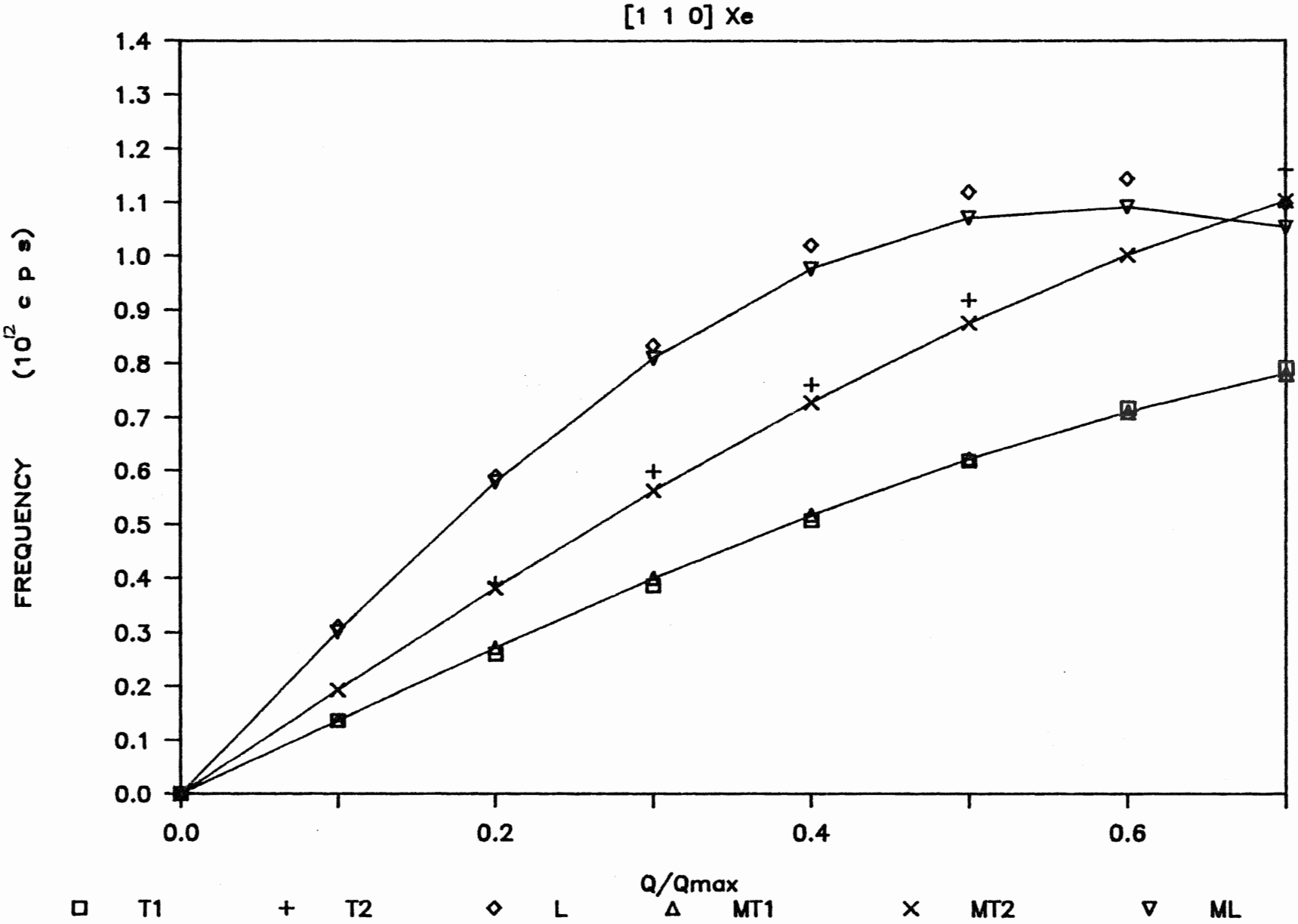
[1 1 0] Xe
FREQUENCY (10^12 c p s)
1.4
1.3
1.2
1.1
1.0
0.9
0.8
0.7
0.6
0.5
0.4
0.3
0.2
0.1
0.0
0.0
0.2
0.4
0.6
Q/Qmax
T1
T2
L
MT1
MT2
ML

Figure 5.7

QH Phonon Dispersion Curves for Xe Along the [1 1 0] Direction With Modified Morse (MM) Potential.

T denotes Transverse mode.

L denotes Longitudinal mode.

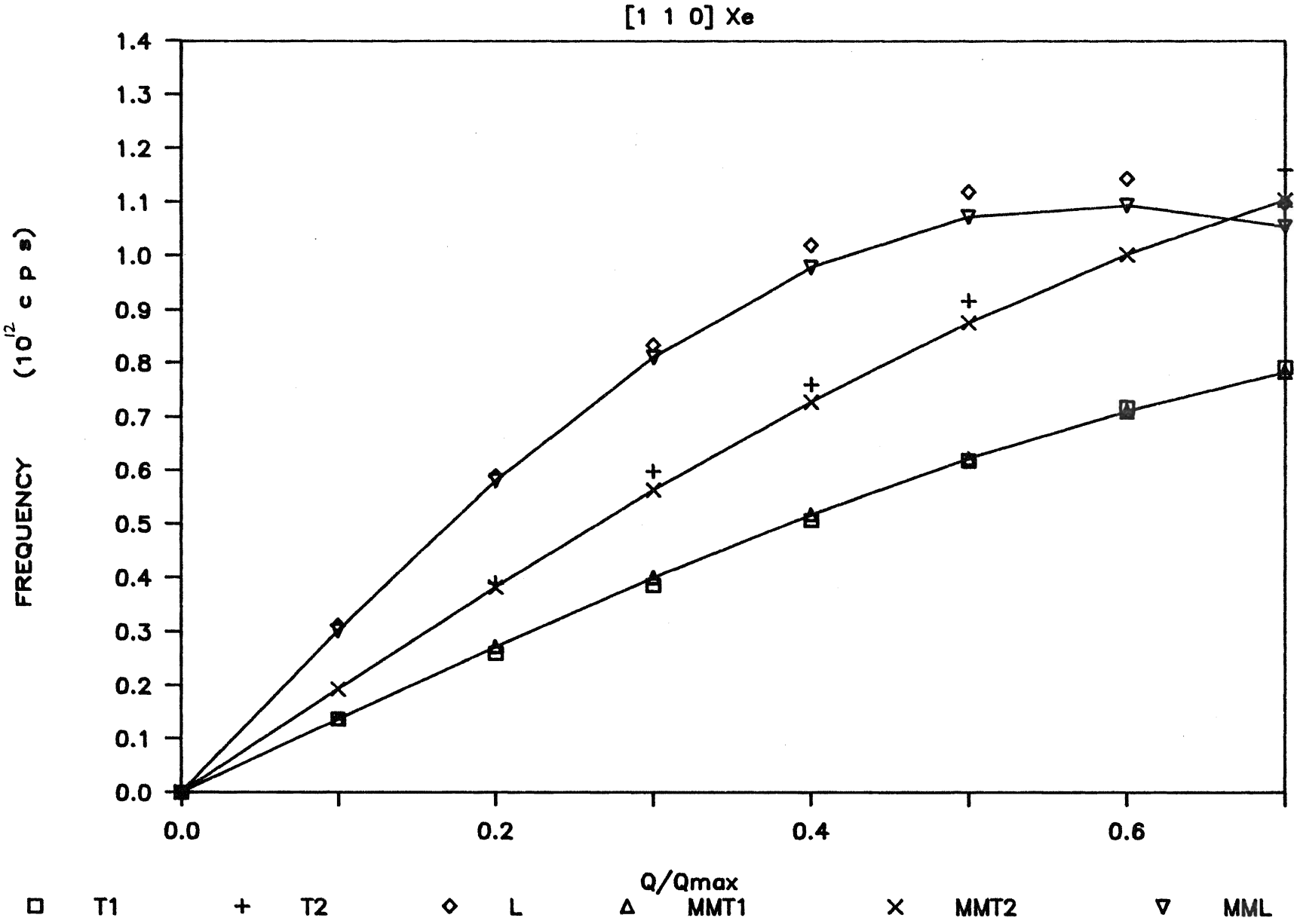
[1 1 0] Xe
FREQUENCY (10^12 c p s)
1.4
1.3
1.2
1.1
1.0
0.9
0.8
0.7
0.6
0.5
0.4
0.3
0.2
0.1
0.0
0.0
0.2
0.4
0.6
Q/Qmax
T1
T2
L
MMT1
MMT2
MML

Figure 5.8

QH Phonon Dispersion Curves for Xe Along the [1 1 1] Direction
With Morse (M) and Modified Morse (MM) Potentials.

T denotes Transverse mode.
L denotes Longitudinal mode.

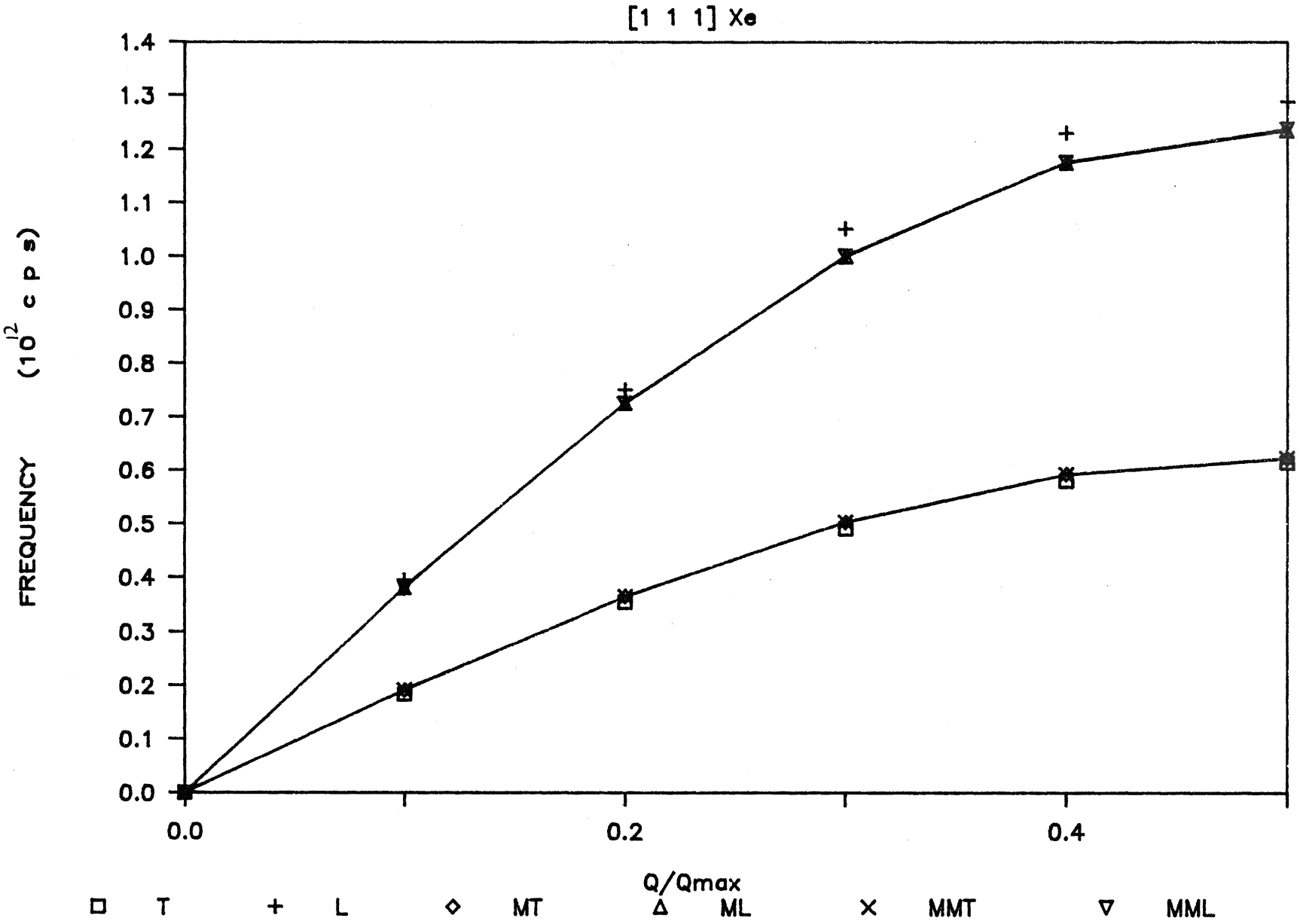
[1 1 1] Xe
FREQUENCY (10^12 c p s)
1.4
1.3
1.2
1.1
1.0
0.9
0.8
0.7
0.6
0.5
0.4
0.3
0.2
0.1
0.0
0.0
0.2
0.4
Q/Qmax
T
L
MT
ML
MMT
MML

Figure 5.9

QH and λ^2 Phonon Dispersion Curves for Cu Along the [1 0 0] Direction With Morse (M) Potential.

T denotes Transverse mode.

L denotes Longitudinal mode.

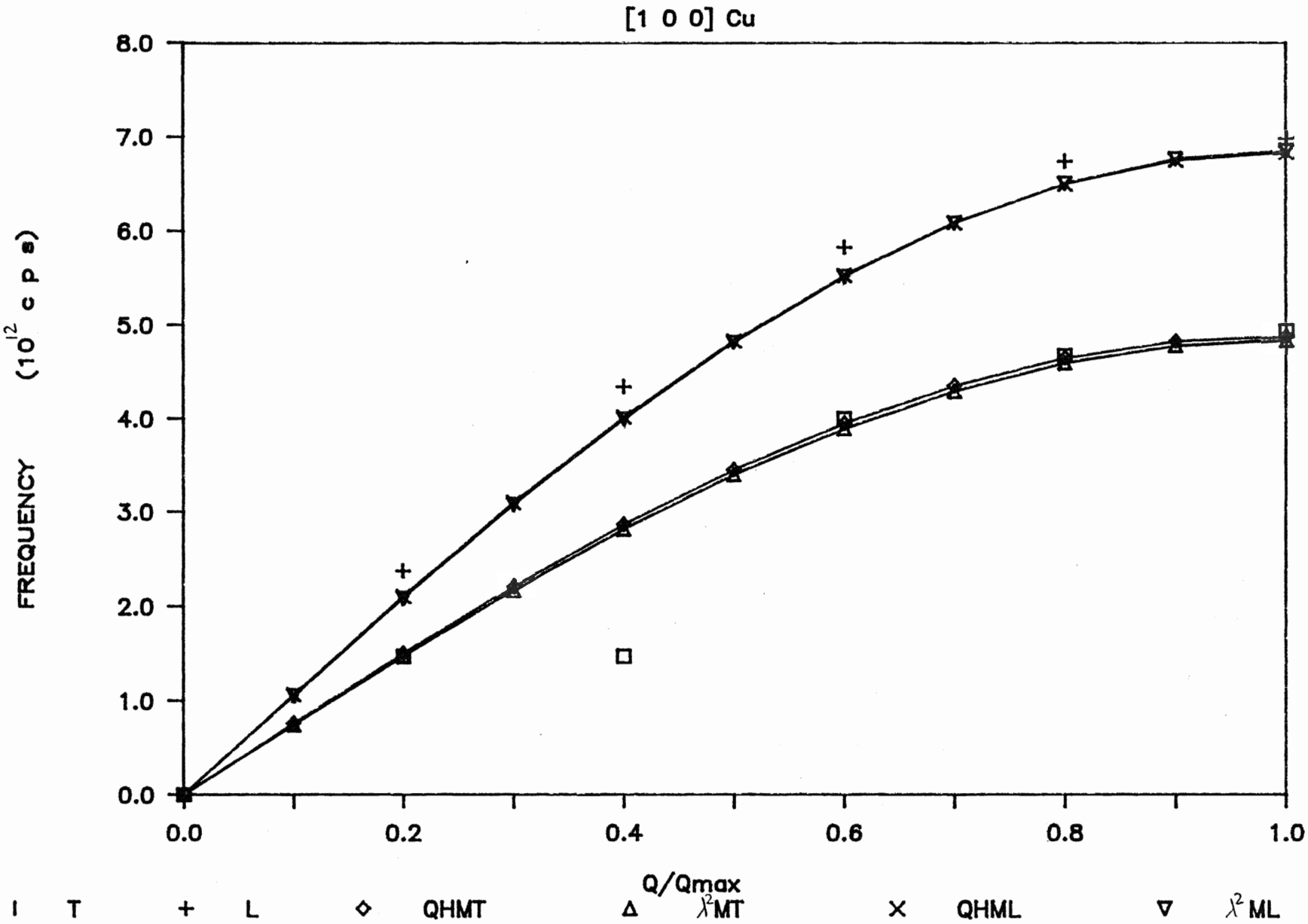
[1 0 0] Cu
FREQUENCY (10^12 c p s)
8.0
7.0
6.0
5.0
4.0
3.0
2.0
1.0
0.0
0.0
0.2
0.4
0.6
0.8
1.0
Q/Qmax
I
T
+
L
◇
QHMT
△
χ²MT
×
QHML
▽
χ² ML

Figure 5.10

QH Phonon Dispersion Curves for Cu Along the [1 1 0] Direction With Morse (M) Potential.

T denotes Transverse mode.

L denotes Longitudinal mode.

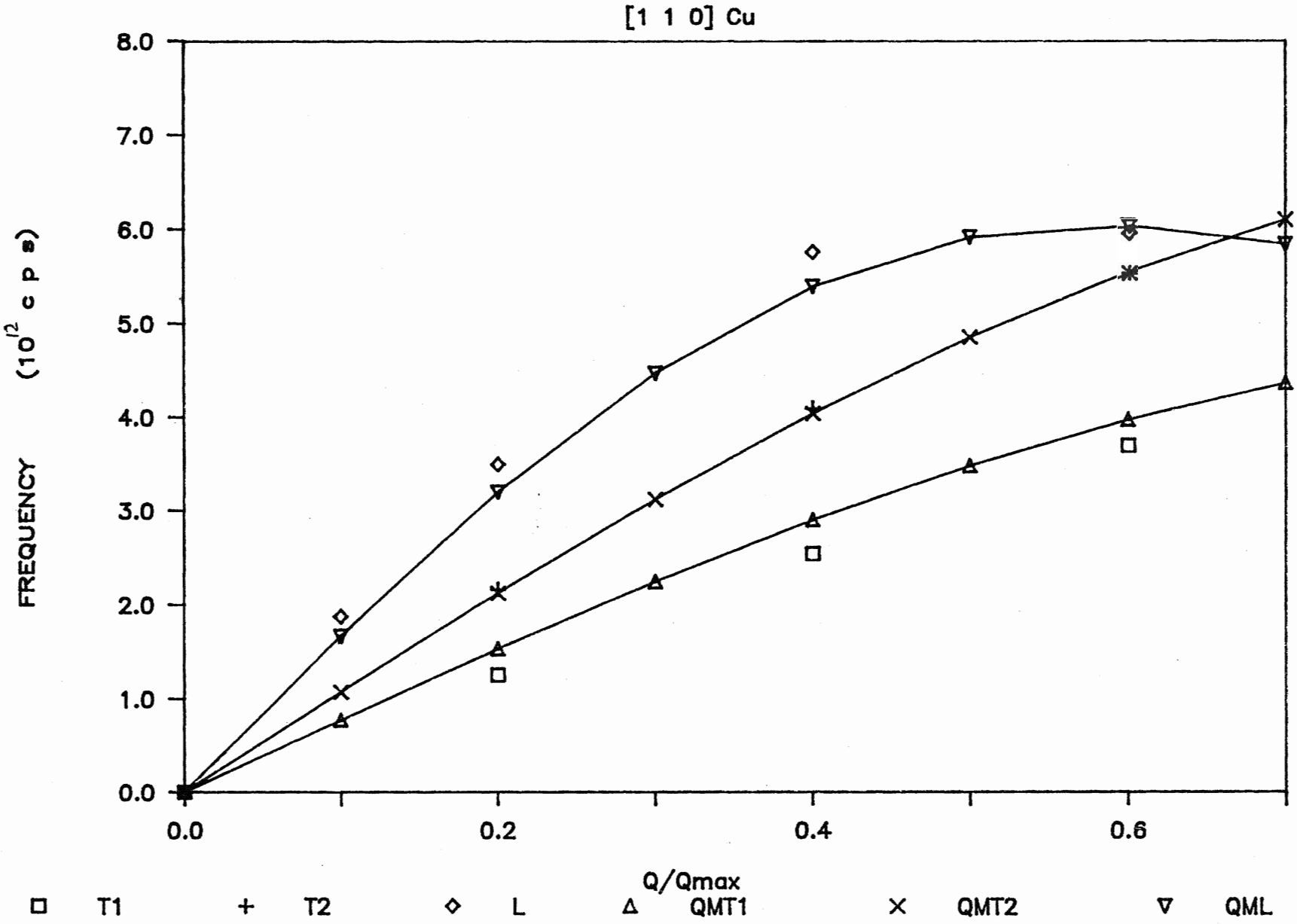
[1 1 0] Cu
8.0
7.0
6.0
5.0
4.0
3.0
2.0
1.0
0.0
FREQUENCY (10^2 c p s)
0.0
0.2
0.4
0.6
Q/Qmax
T1
T2
L
QMT1
QMT2
QML

Figure 5.11

λ^2 Phonon Dispersion Curves for Cu Along the [1 1 0] Direction With Morse (M) Potential.

T denotes Transverse mode.

L denotes Longitudinal mode.

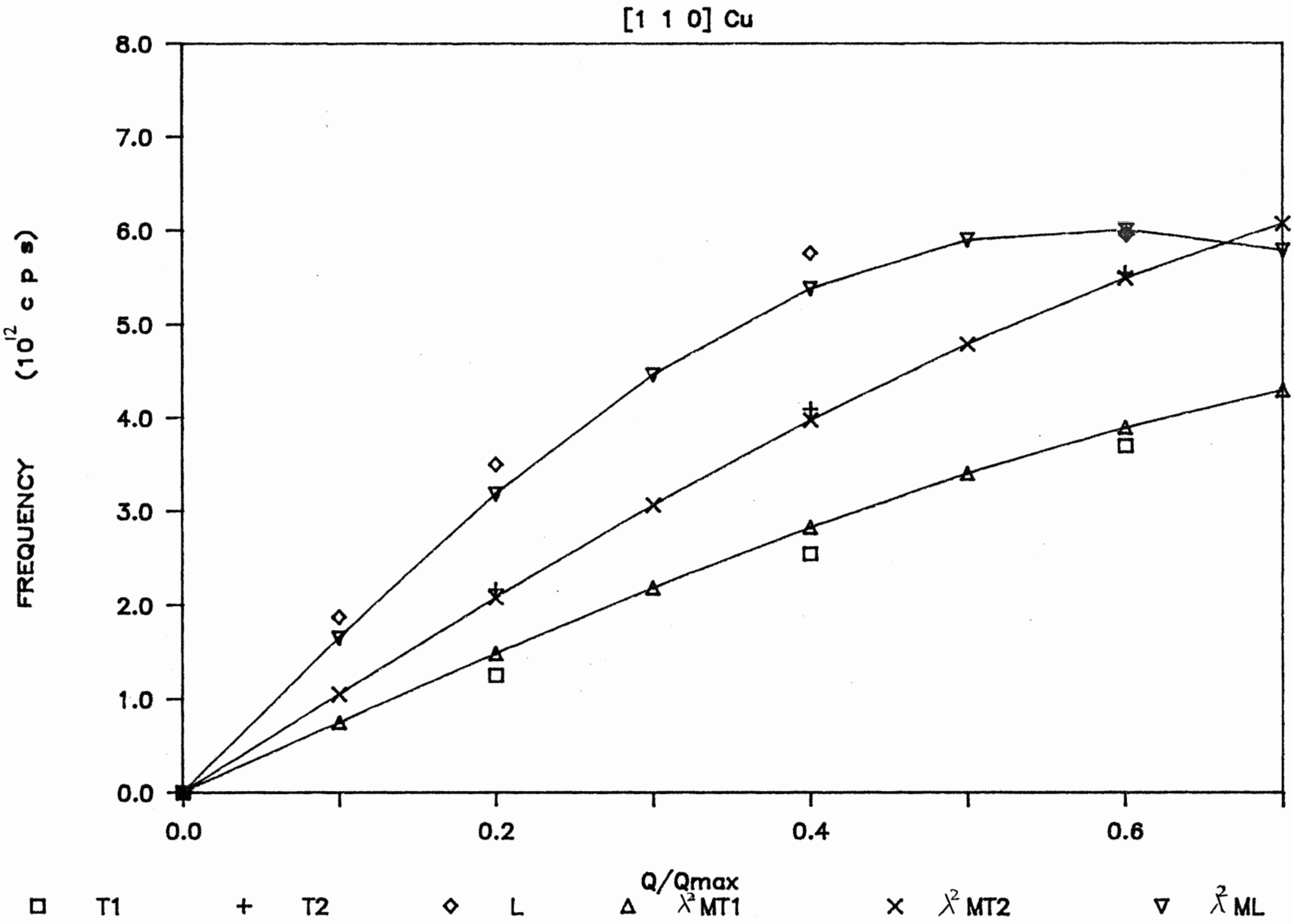
[1 1 0] Cu
8.0
7.0
6.0
5.0
4.0
3.0
2.0
1.0
0.0
FREQUENCY (10^12 c p s)
0.0
0.2
0.4
0.6
Q/Qmax
T1
T2
L
λ² MT1
λ² MT2
λ² ML

Figure 5.12

QH and λ^2 Phonon Dispersion Curves for Cu Along the [1 1 1] Direction With Morse (M) Potential.

T denotes Transverse mode.

L denotes Longitudinal mode.

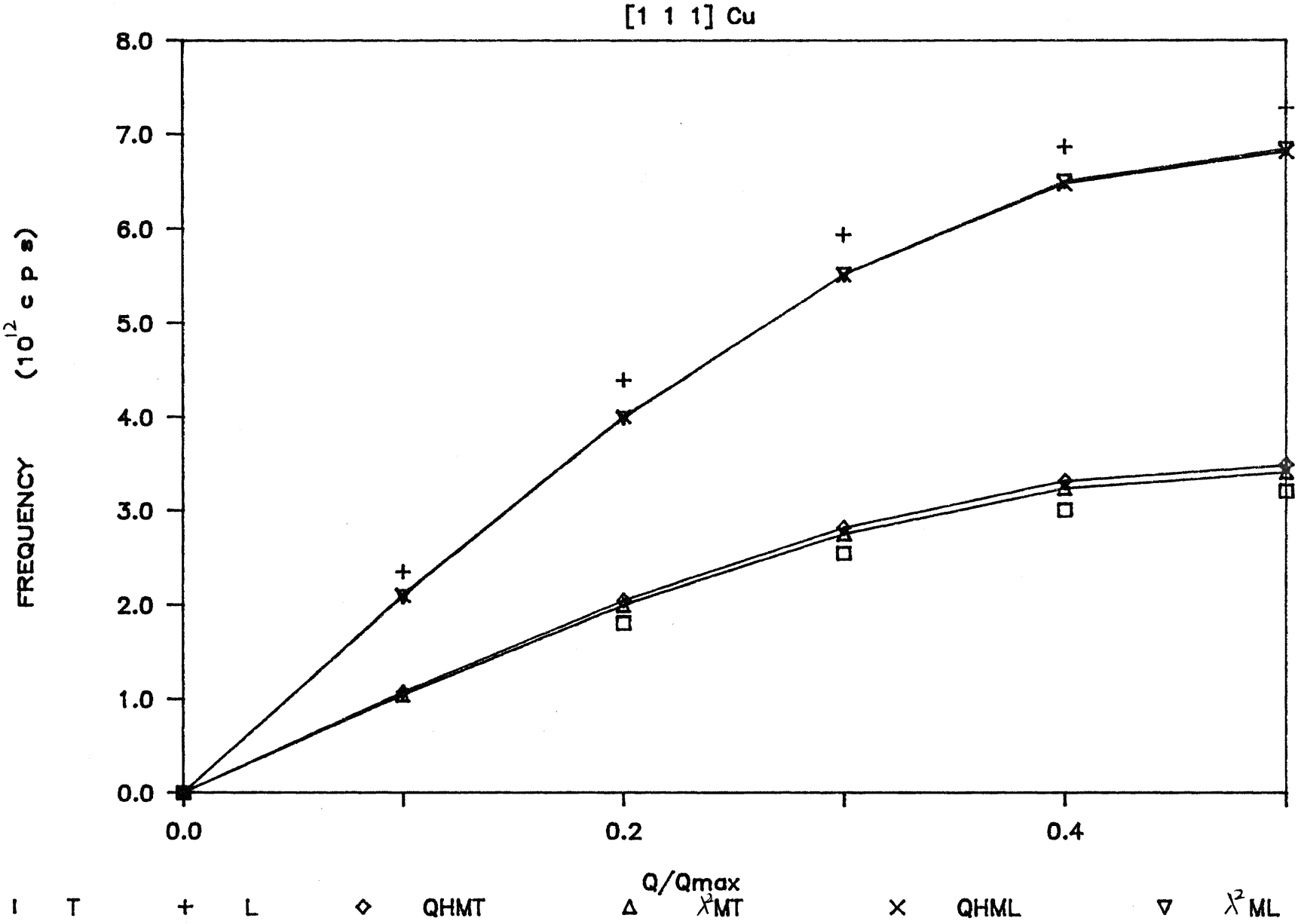
[1 1 1] Cu
8.0
7.0
6.0
5.0
4.0
3.0
2.0
1.0
0.0
FREQUENCY (10^12 c p s)
0.0
0.2
0.4
Q/Qmax
I T + L ◇ QHMT △ λ²MT × QHML ▽ λ²ML

Figure 5.13

QH Phonon Dispersion Curves for Ag Along the [1 0 0] Direction
With Morse (M) and Modified Morse (MM) Potentials.

T denotes Transverse mode.
L denotes Longitudinal mode.

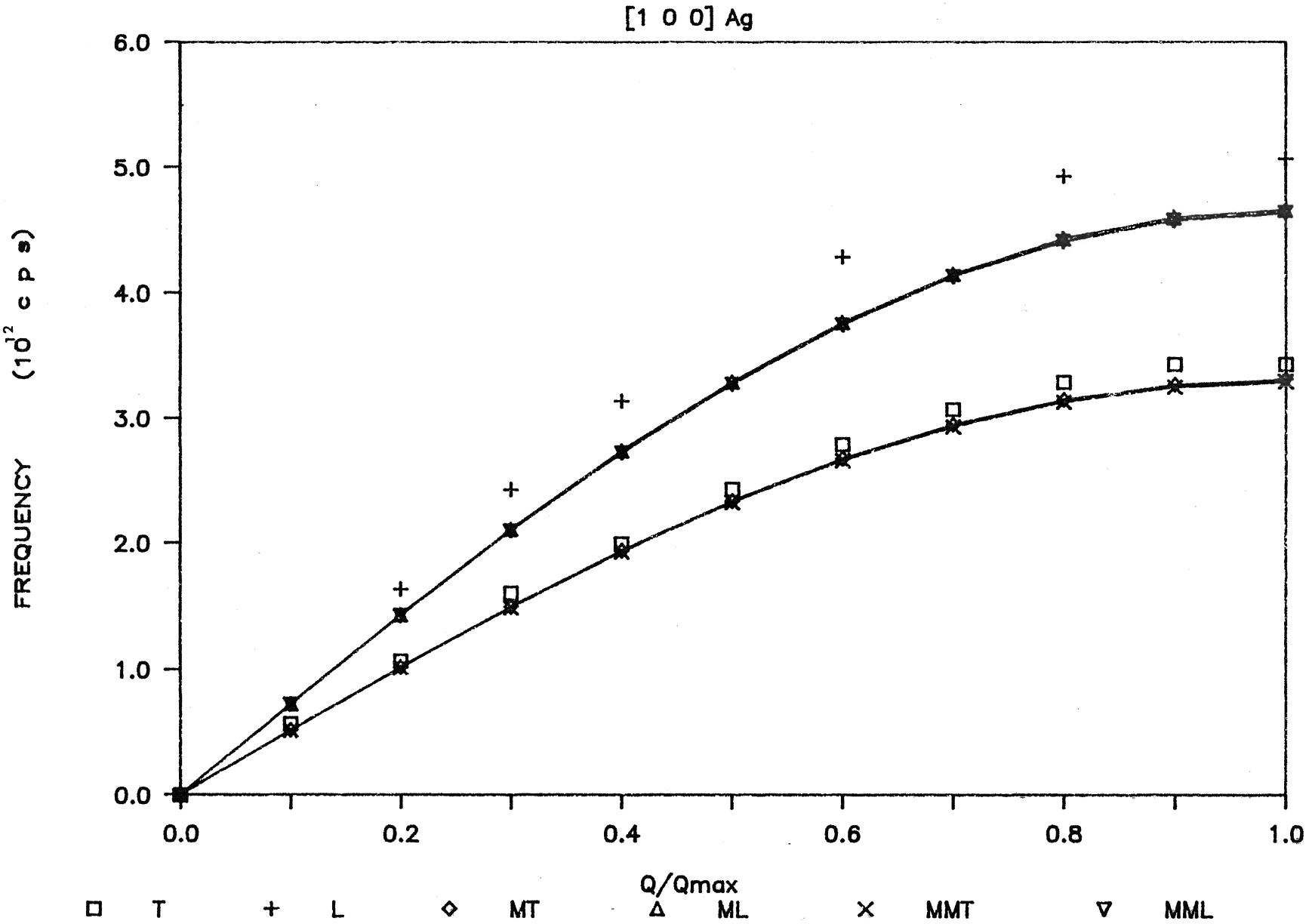
[1 0 0] Ag
FREQUENCY (10^2 c p s)
6.0
5.0
4.0
3.0
2.0
1.0
0.0
0.0
0.2
0.4
0.6
0.8
1.0
Q/Qmax
T
L
MT
ML
MMT
MML

Figure 5.14

QH Phonon Dispersion Curves for Ag Along the [1 1 0] Direction With Morse (M) Potential.

T denotes Transverse mode.

L denotes Longitudinal mode.

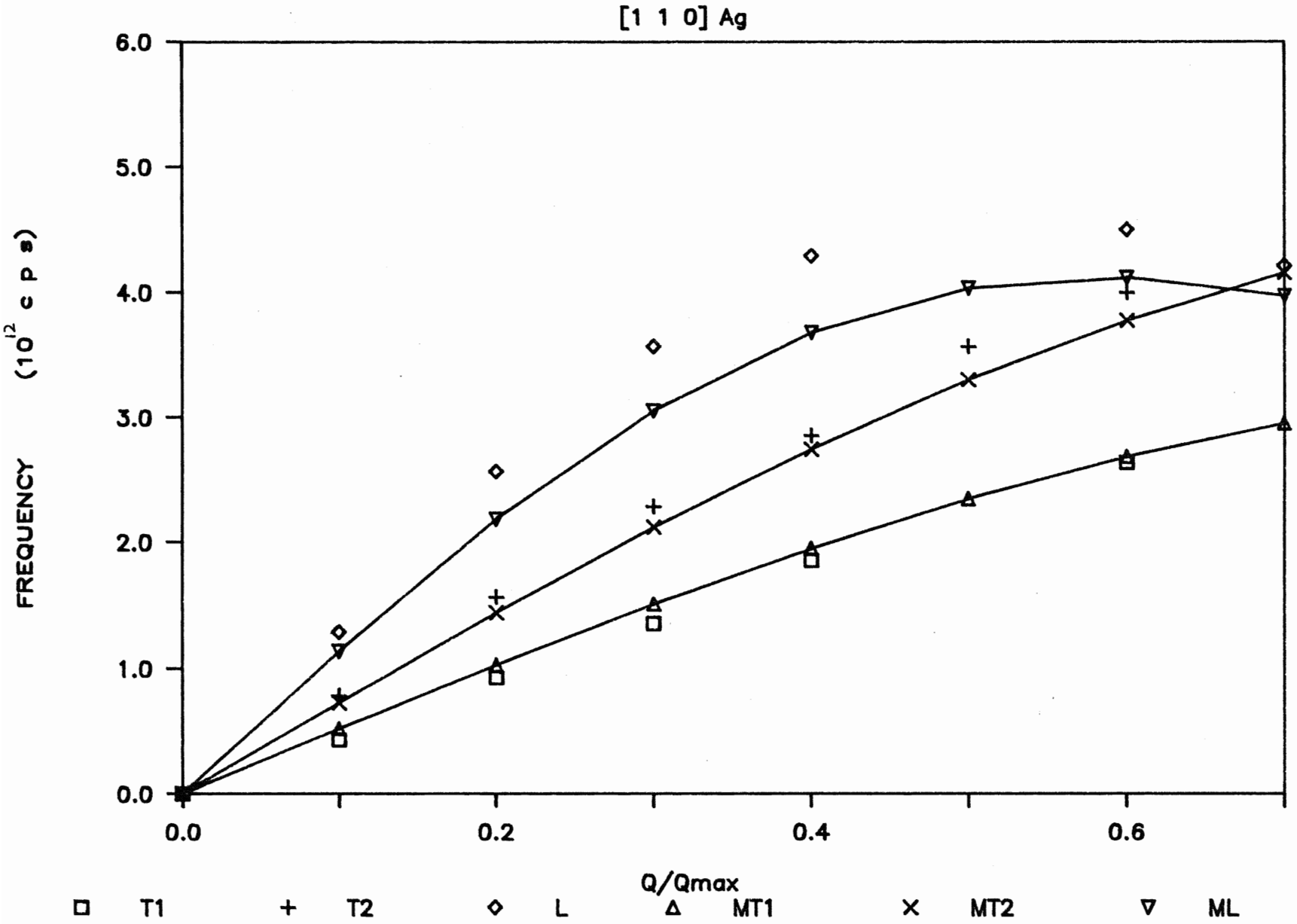
[1 1 0] Ag
FREQUENCY (10^12 c p s)
6.0
5.0
4.0
3.0
2.0
1.0
0.0
0.0
0.2
0.4
0.6
Q/Qmax
T1
T2
L
MT1
MT2
ML

Figure 5.15

QH Phonon Dispersion Curves for Ag Along the [1 1 0] Direction
With Modified Morse (MM) Potential.

T denotes Transverse mode.

L denotes Longitudinal mode.

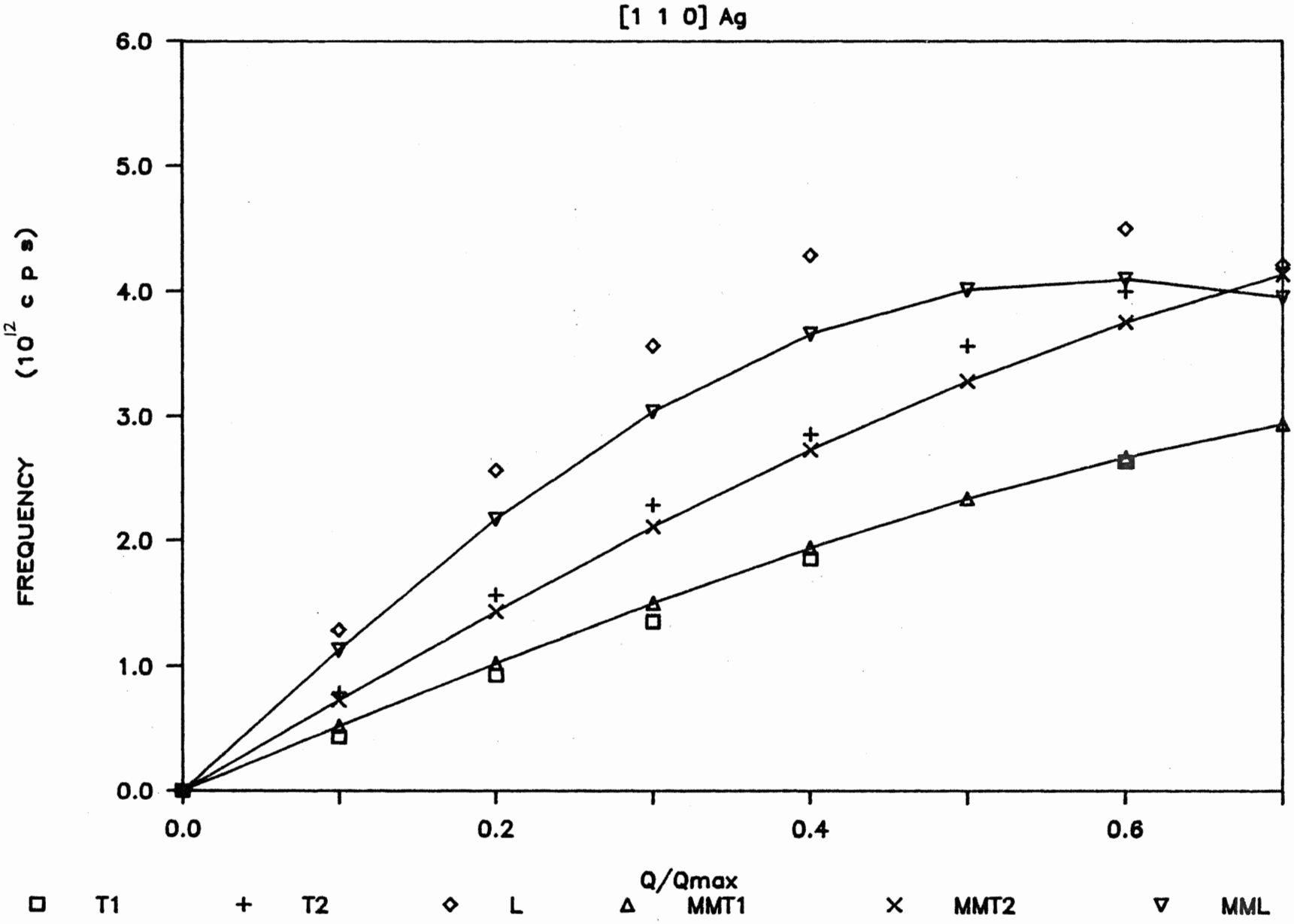
[1 1 0] Ag
6.0
5.0
4.0
3.0
2.0
1.0
0.0
FREQUENCY (10^12 c p s)
0.0
0.2
0.4
0.6
Q/Qmax
T1
T2
L
MMT1
MMT2
MML

Figure 5.16

QH Phonon Dispersion Curves for Ag Along the [1 1 1] Direction
With Morse (M) and Modified Morse (MM) Potentials.

T denotes Transverse mode.
L denotes Longitudinal mode.

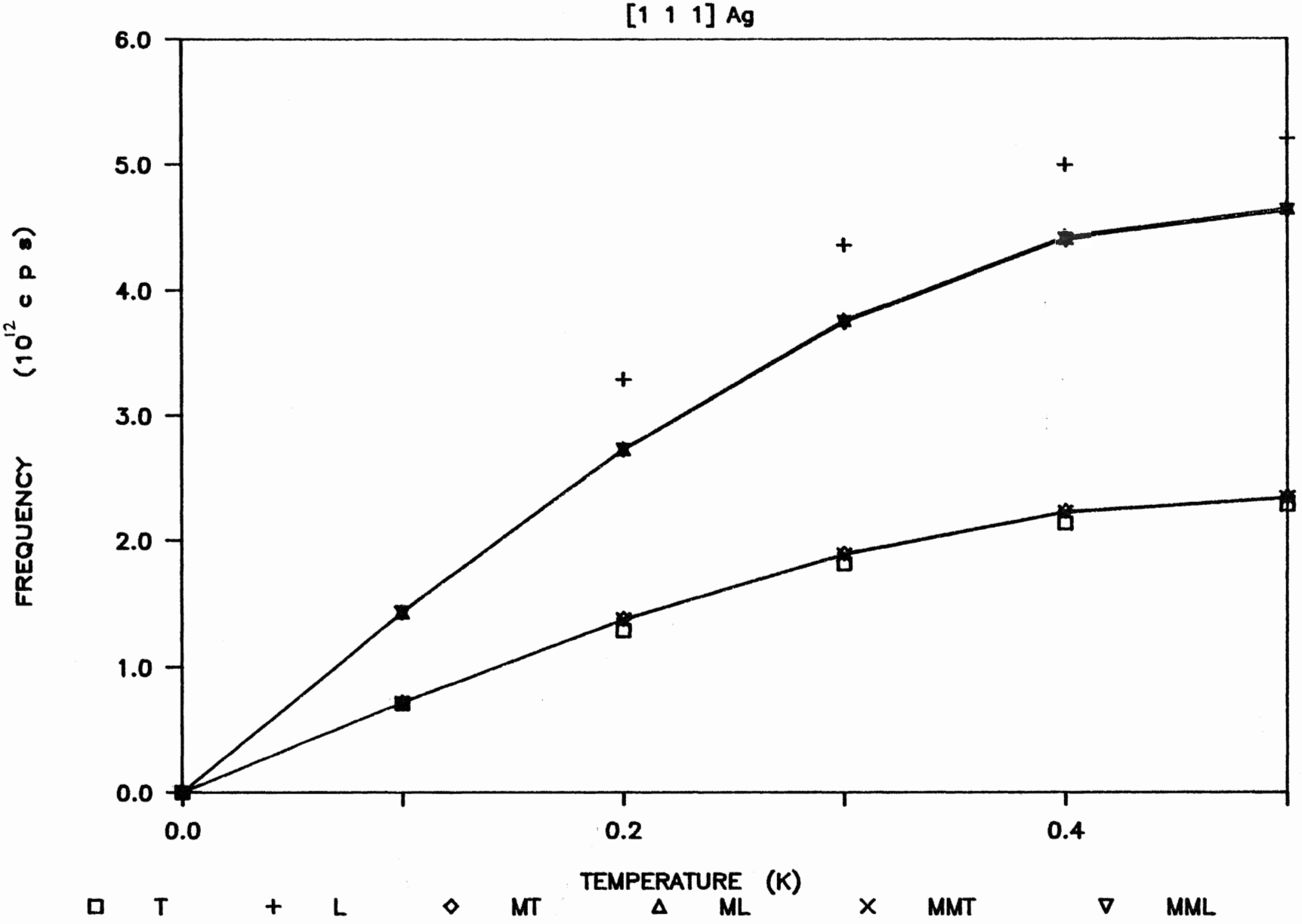
[1 1 1] Ag
6.0
5.0
4.0
3.0
2.0
1.0
0.0
FREQUENCY (10^12 c p s)
0.0
0.2
0.4
TEMPERATURE (K)
T
L
MT
ML
MMT
MML

Figure 5.17

QH Phonon Dispersion Curves for Au Along the [1 0 0] Direction
With Morse (M) and Modified Morse (MM) Potentials.

T denotes Transverse mode.

L denotes Longitudinal mode.

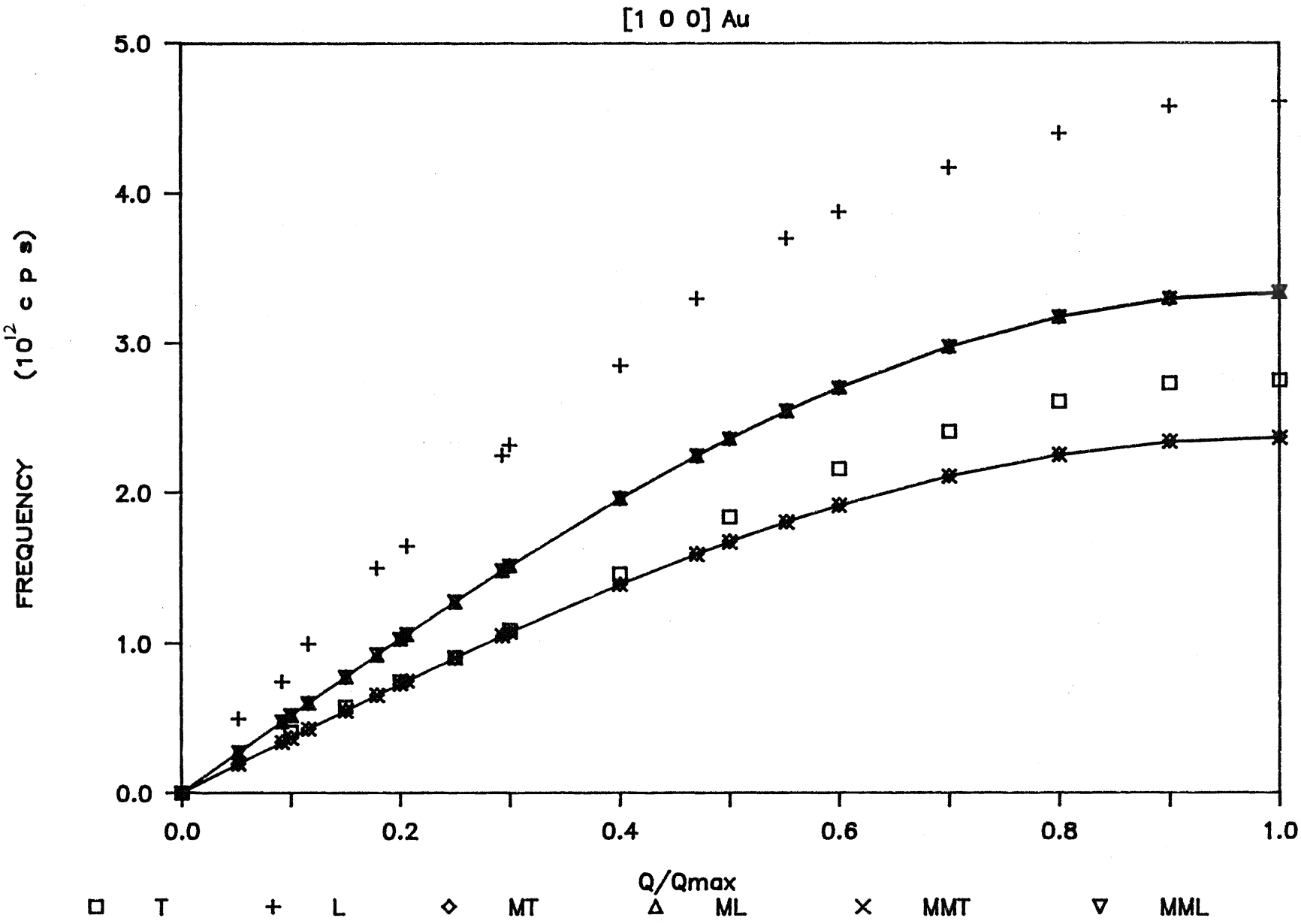
[1 0 0] Au
FREQUENCY (10^12 c p s)
5.0
4.0
3.0
2.0
1.0
0.0
0.0
0.2
0.4
0.6
0.8
1.0
Q/Qmax
T
L
MT
ML
MMT
MML

Figure 5.18

QH Phonon Dispersion Curves for Au Along the [1 1 0] Direction With Morse (M) Potential.

T denotes Transverse mode.

L denotes longitudinal mode.

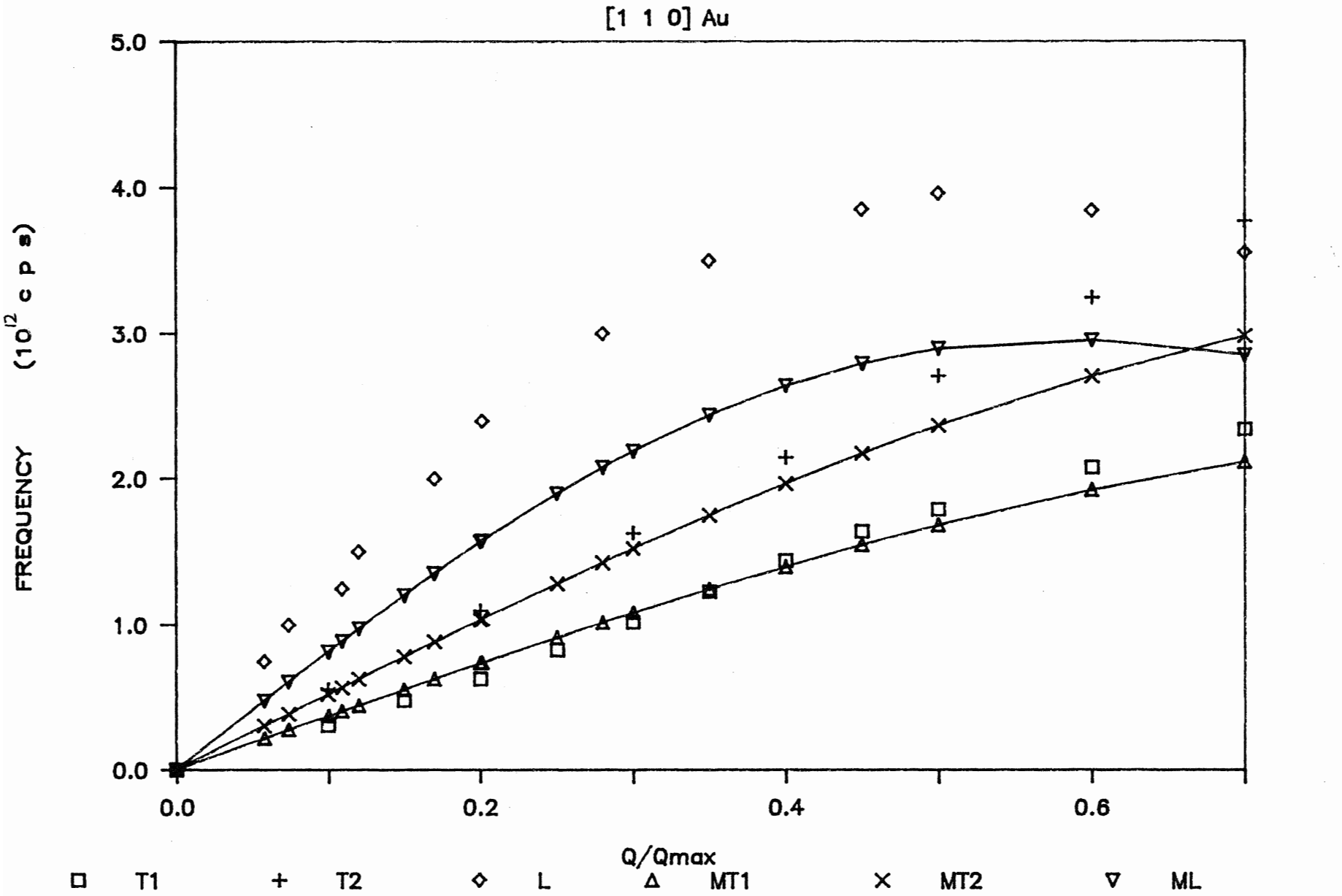
[1 1 0] Au
FREQUENCY (10^12 c p s)
5.0
4.0
3.0
2.0
1.0
0.0
0.0
0.2
0.4
0.6
Q/Qmax
T1
T2
L
MT1
MT2
ML

Figure 5.19

QH Phonon Dispersion Curves for Au Along the [1 1 0] Direction With Modified Morse (MM) Potential.

T denotes Transverse mode.

L denotes longitudinal mode.

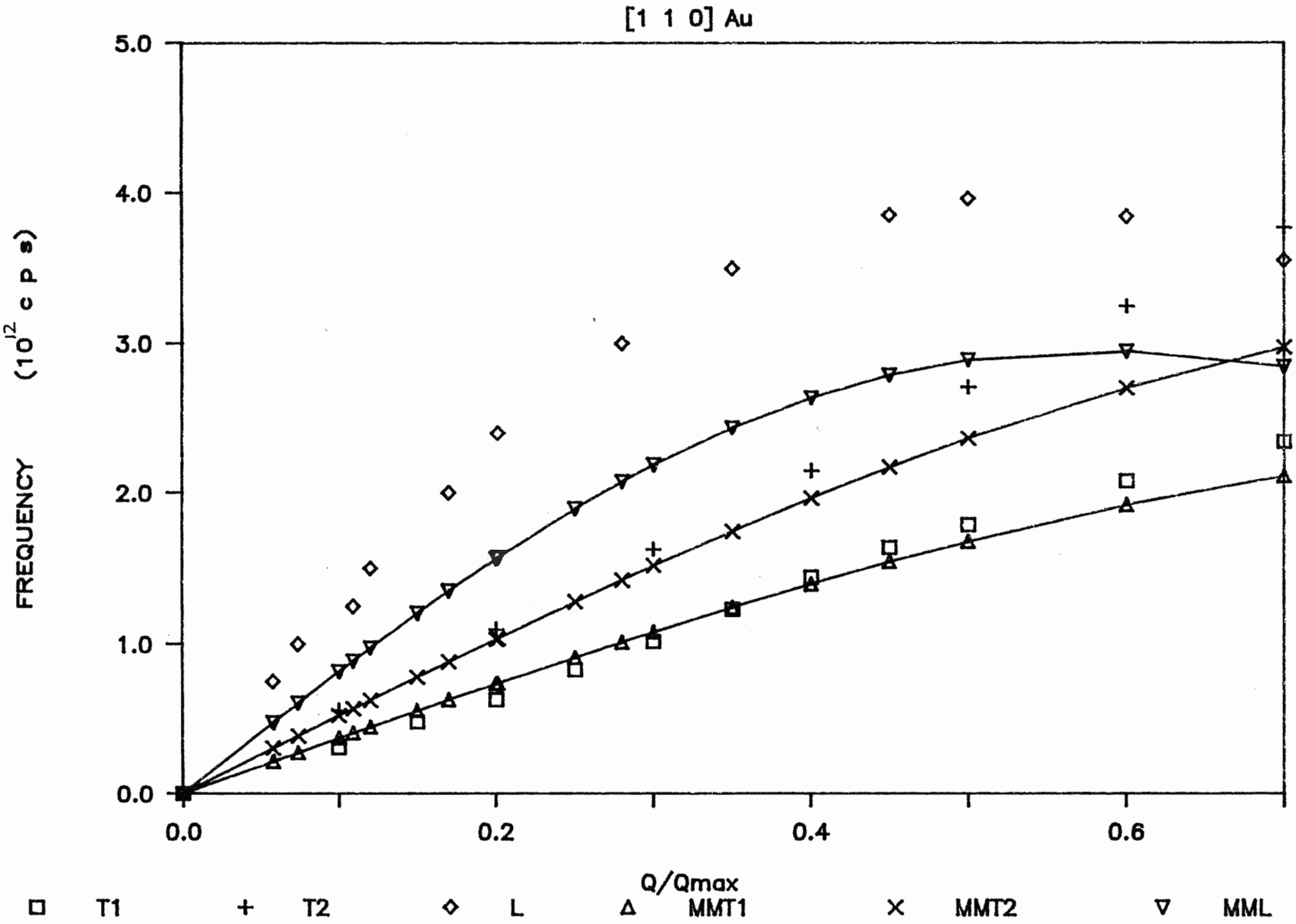
[1 1 0] Au
FREQUENCY (10^12 c p s)
5.0
4.0
3.0
2.0
1.0
0.0
0.0
0.2
0.4
0.6
Q/Qmax
T1
T2
L
MMT1
MMT2
MML

Figure 5.20

QH Phonon Dispersion Curves for Au Along the [1 1 1] Direction With Morse (M) and Modified Morse (MM) Potentials.

T denotes Transverse mode.

L denotes longitudinal mode.

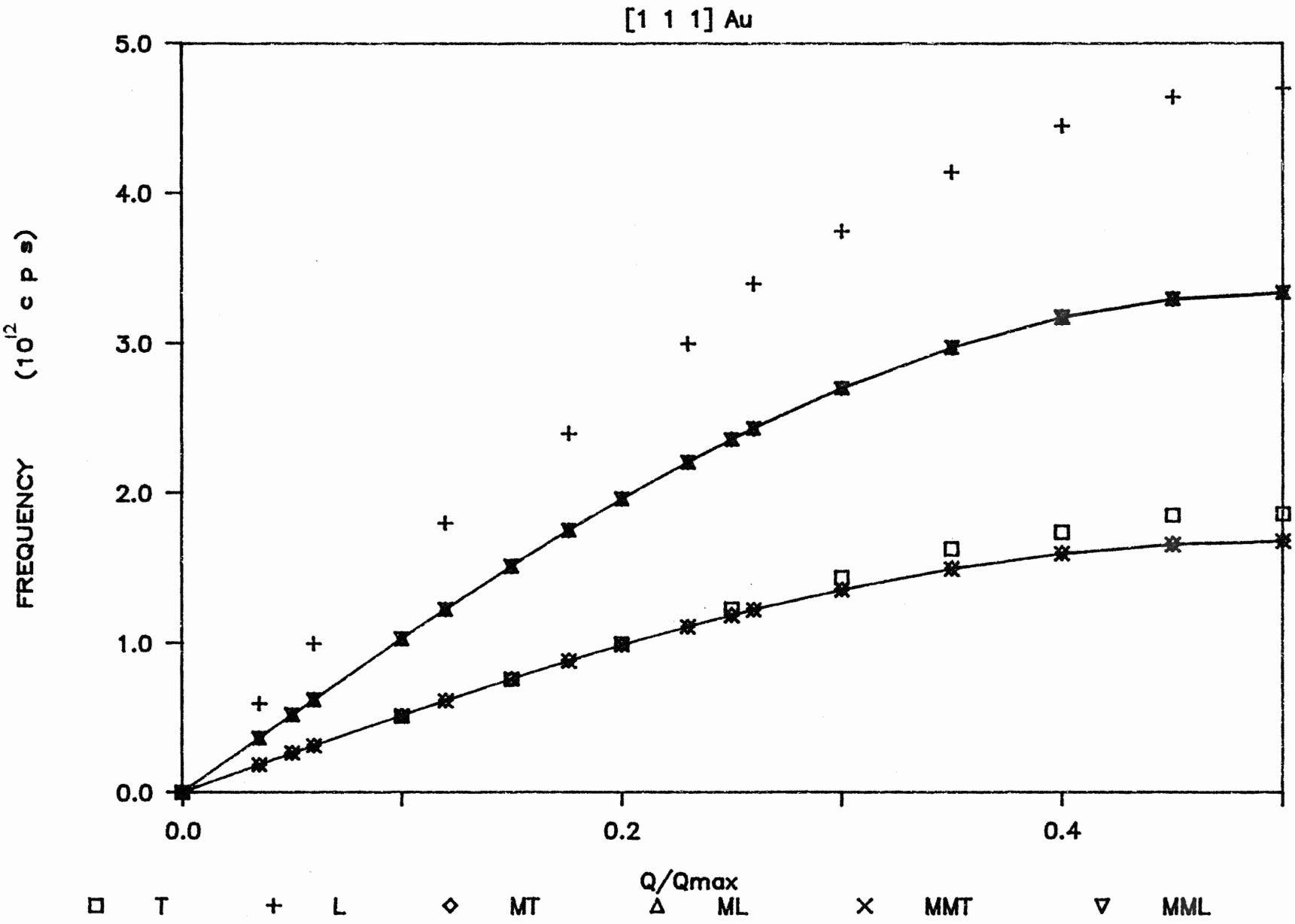
[1 1 1] Au
FREQUENCY (10^12 c p s)
5.0
4.0
3.0
2.0
1.0
0.0
0.0
0.2
0.4
Q/Qmax
T
L
MT
ML
MMT
MML

6. Grüneisen Parameter

6.1. Theory:

In this section we outline the theory which is required for the calculation of the Grüneisen parameter, γ, to the λ^2 order in PT. The parameter γ can be calculated directly from the phonon frequencies ω, where ω is volume dependent. Since anharmonicity can determined for the phonon frequencies, then we should be able to calculate the anharmonic contribution to the Grüneisen parameter. For a mode of $\mathbf{q}j$ the Grüneisen parameter is defined by

$$\gamma(\mathbf{q}j) = -\frac{\partial \ln(\omega(\mathbf{q}j))}{\partial V}$$

$$= -\frac{V}{\omega(\mathbf{q}j)}\frac{\partial \omega(\mathbf{q}j)}{\partial V} \qquad (6.1)$$

Since γ has an anharmonic effect, we shall use in Eq. (6.1) the phonon frequencies that contain both the quasiharmonic and the anharmonic contributions. The expression for this frequency to $O(\lambda^2)$ is presented in Eq. (5.17). To account for anharmonicity, $\gamma(\mathbf{q}j)$ is redefined as:

$$\gamma(\mathbf{q}j) = -\frac{V}{\Omega_{\mathbf{q}j}}\frac{\partial \Omega_{\mathbf{q}j}}{\partial V} \qquad (6.2)$$

where $\Omega_{\mathbf{q}j}$ is the renormalized phonon frequency, and it is given by

$$\Omega_{qj}^2(\omega=0) = \omega_{qj}^2 - \frac{\lambda^2}{2\beta N} \sum_{q_1 j_1} \sum_{q_2 j_2} \Delta(q_1+q_2-q) \times \frac{|\Phi(q_1 j_1, -q_2 j_2, -qj)|^2}{\omega_{q_1 j_1}^2 \omega_{q_2 j_2}^2} +$$

$$+ \frac{\lambda^2}{2\beta N} \sum_{q_1 j_1} \frac{\Phi(q_1 j_1, qj, -q_1 j_1, -qj)}{\omega_{q_1 j_1}^2}$$

$$= \omega_{qj}^2 + \Delta_3(qj) + \Delta_4(qj). \qquad (6.3)$$

$\omega(qj)$ are the quasiharmonic frequncies, and $\Delta_3(qj)$ and $\Delta_4(qj)$ are the cubic and quartic frequency shifts, respectively. Eq. (6.3) can be differentiated with respect to volume and written in the following form:

$$\frac{-V}{\Omega_{qj}} \frac{\partial \Omega_{qj}}{\partial V} = \frac{-V}{2\Omega_{qj}^2} \{ \frac{\partial \omega^2(qj)}{\partial V} + \frac{\partial \Delta_3(qj)}{\partial V} + \frac{\partial \Delta_4(qj)}{\partial V} \} \qquad (6.4)$$

Expanding $1/\Omega_{qj}^2$ in powers of λ and retaining only terms of $O(\lambda^2)$, we obtain:

$$\gamma(qj) = \gamma_{QH}(qj) + \gamma_C(qj) + \gamma_Q(qj) \qquad (6.5)$$

$$\gamma_{QH}(qj) = - \frac{V}{\omega_{qj}} \frac{\partial \omega_{qj}}{\partial V} \qquad (6.6)$$

$$\gamma_C(qj) = \frac{V}{2} \frac{\partial}{\partial V} \{ \frac{\lambda^2}{2\beta N} \sum_{q_1 j_1} \sum_{q_2 j_2} \Delta(q_1+q_2-q) \times \frac{|\Phi(q_1 j_1, -q_2 j_2, -qj)|^2}{\omega_{qj}^2 \omega_{q_1 j_1}^2 \omega_{q_2 j_2}^2} \} \qquad (6.7)$$

$$\gamma_Q(qj) = - \frac{V}{2} \frac{\partial}{\partial V} \{ \frac{\lambda^2}{2\beta N} \sum_{q_1 j_1} \frac{\Phi(q_1 j_1, qj, -q_1 j_1, -qj)}{\omega_{qj}^2 \omega_{q_1 j_1}^2} \} \qquad (6.8)$$

where the quasiharmonic contribution is denoted by $\gamma_{QH}(qj)$, and the cubic and quartic anharmonic contributions by $\gamma_C(qj)$ and $\gamma_Q(qj)$, respectively. Thus, the average of the Grüneisen parameter is given by

$$\gamma_{RE}= \frac{1}{3N}\sum_{qj} \gamma(qj) = \gamma_{QH} + \gamma_C + \gamma_Q \tag{6.9}$$

where γ_{RE} represents the value of γ calculated from the renormalized phonon frequency Ω_{qj}.

The quasiharmonic contribution γ_{QH} can be calculated from the harmonic eigenvalue equation which was introduced in Eqs.(5.1)-(5.2). γ_{QH} is then given by

$$\gamma_{QH} = \frac{1}{36}\sum_{1}{}' \sum_{\alpha\beta} \frac{r_1^3}{B(r_1)} \phi_{\alpha\beta}'(r_1) [S_{\alpha\beta}(0) - S_{\alpha\beta}(1)] \tag{6.10}$$

The cubic and quartic terms are given by

$$\gamma_C = \frac{V}{6N} \frac{\partial}{\partial V} \{ \frac{1}{2\beta N} \sum_{qj} \sum_{q_1 j_1} \sum_{q_2 j_2} \Delta(q_1+q_2-q) \times \frac{| \Phi(q_1 j_1,-q_2 j_2,-qj)|^2}{\omega_{qj}^2 \omega_{q_1 j_1}^2 \omega_{q_2 j_2}^2} \} \tag{6.11}$$

$$\gamma_Q = - \frac{V}{6N} \frac{\partial}{\partial V} \{ \frac{1}{2\beta N} \sum_{qj} \sum_{q_1 j_1} \frac{\Phi(q_1 j_1, qj, -q_1 j_1, -qj)}{\omega_{qj}^2 \omega_{q_1 j_1}^2} \} \tag{6.12}$$

Since the arguments between the parentheses in the above equations are similar to the expressions of F_3 and F_4 given in Eqs. (2.7) and (2.8), we can rewrite γ_C and γ_Q in terms of the first derivatives of F_3 and F_4 with respect to r as follows:

$$\gamma_C = - \frac{r_1 \beta}{3N} \frac{\partial F_3}{\partial r} \tag{6.13}$$

$$\gamma_Q = - \frac{2 r_1 \beta}{9N} \frac{\partial F_4}{\partial r} \tag{6.14}$$

The computational forms of these two derivatives are obtained from Eqs. (3.25) and (3.30)

6.2. Results and Discussion:

The Grüneisen parameter has been calculated for the rare-gas solids: Kr and Xe, and the fcc metals: Cu, Ag, and Au. Tables 6.1 through 6.4 show the results we obtained along with the experimental results. The calculation was carried out for both potentials in the high temperature limit. To investigate the reliability of these results, we compare them with the results obtained from the thermodynamic definition. We should note that γ derived from the renormalized phonon frequency, Ω_{qj}, has been expanded to $O(\lambda^2)$; whereas the thermodynamic expression contains the specific heat in the denominator which is of $O(\lambda^2)$. For comparison we have expanded the thermodynamic definition to $O(\lambda^2)$, and presented the results, $\gamma_{expanded}$, in Tables 6.1 through 6.4 along with those of the full definition. It should be noted that comparison should be made between the results of the full thermodynamic definition γ_{full} and those of the coresponding expression for γ obtained from Ω_{qj}. The latter results can be calculated from Eq. (6.4); however, time did not permit us to carry out these calculation.

The Grüneisen parameter results for Kr and Xe are presented in Tables 6.1 and 6.2. The values of γ_{RE} are higher than the those of the thermodynamic definition. In fact they are closer to the experimental results. However, the experimental value of γ for Xe at 160K drops to 1.94, which is very low comparing to γ_{RE} at that temperature. In general

at low temperature the three calculated results are in fair agreement. As the temperature increases the discrepancy between them worsens.

The results of the Grüneisen parameter for the Cu, Ag, and Au are shown in Tables 6.3 and 6.4. Here we compare γ_{RE} only with the lattice contribution of the thermodynamic definition, because the calculated γ_{RE} does not account for the electronic contribution. In order to account for the electronic contribution, one has to derive a Green's function that contains, along with the phonon-phonon interaction, the phonon-electron and electron-electron interactions. The results that we present here are only those of the phonon-phonon interaction.

Table 6.1: Grüneisen Parameter For Rare-Gas Solids With Morse Potential.

	T(K)	γ_{RE}	γ_{full}	$\gamma_{expanded}$	γ_{EXP}
Kr	70	2.694	2.599	2.570	2.82
	90	2.685	2.524	2.505	2.67
	110	2.661	2.381	2.328	2.76
Xe	60	2.571	2.532	2.508	2.76
	100	2.577	2.492	2.463	2.7
	160	2.546	2.259	2.284	1.94

Table 6.2: Grüneisen Parameter For Rare-Gas Solids With Modified Morse Potential.

	T(K)	γ_{RE}	γ_{full}	$\gamma_{expanded}$	γ_{EXP}
Kr	70	2.584	2.486	2.452	2.82
	90	2.610	2.448	2.421	2.67
	110	2.636	2.378	2.365	2.76
Xe	60	2.431	2.387	2.363	2.76
	100	2.470	2.377	2.3478	2.70
	160	2.528	2.263	2.2559	1.94

Table 6.3: Grüneisen Parameter For fcc Metals With Morse Potential.

	T(K)	γ_{RE}	γ_{full}	$\gamma_{expanded}$
Cu	100	1.082	.982	.984
	700	1.093	1.073	1.070
	1300	1.105	1.065	1.063
Ag	200	1.193	1.178	1.180
	700	1.207	1.182	1.179
	1200	1.220	1.173	1.170
Au	400	0.912	0.901	0.901
	600	0.914	0.900	0.899
	800	0.917	0.896	0.897

Table 6.4: Grüneisen Parameter For fcc Metals With Modified Morse Potential.

	T(K)	γ_{RE}	γ_{full}	$\gamma_{expanded}$
Cu	100	1.418	1.314	1.319
	700	1.401	1.386	1.383
	1300	1.372	1.338	1.341
Ag	200	1.556	1.541	1.544
	700	1.534	1.519	1.514
	1200	1.494	1.439	1.462
Au	400	1.075	1.064	1.064
	600	1.074	1.061	1.059
	800	1.074	1.055	1.054

7. Summary

We have calculated the thermodynamic properties of the rare-gas solids, Kr and Xe, and gold by using the static energy and Helmholtz free energy. The free energy contribution included the quasiharmomic and the two lowest order (cubic and quartic) anharmonic terms. The calculation was carried out in the high temperature limit for a nearest-neighbour centeral-force. The atomic interaction for these materials were represented by Morse potential and modified Morse potential. For Kr and Xe, The λ^2 results of C_V and C_p obtained from the modified Morse potential are quite good. The λ^2 results of the other properties show a breakdown at high temperatures. For gold the λ^2 results calculated with both potentials were similar to those obtained from E(QH) equation of state.

The Mössbauer recoilless fraction was calculated for Kr and Xe, and the result for Kr was in fair agreement with experiment . We have also calculated the Debye-Waller factor for Pb, Al, Cu, Ag, and Au, and compared with experimental results. The results for Pb, Al, and Cu and Ag show a fair agreement for temperatures up to $4/7T_m$. The DWF values for Au were not satisfactory.

In order to test the potentials used in our calculations, we calculated the phonon dispersion curves for the rare-gas solids Kr and Xe, and the metals Cu, Ag, and Au. The calculated curves seem to have the correct shape as compared with the experimental curves, thus indicating

that the first and second derivatives of the potentials are of the correct order of magnitude.

Finally, we determined the Grüneisen parameter from the phonon frequency definition for these materials. Comparing to the thermodynamic calculations, these results are quite good.

References

Y. A. Chang and L. Himmel, J. App. Phys. 37, 3567 (1966).

D. R. Chipman, J. App. Phys. 31, 2012 (1960).

E. R. Cowley and R. C. Shukla, Phys. Rev. B9, 1261 (1974).

R. A. Cowley, Adv. Phys. 12, 421 (1963).

R. A. Cowley, J. Phys. C.: Solid St. Phys. 4, 988 (1971).

G. A. Heiser, R. C. Shukla, and E. R. Cowley, Phys. Rev. B33, 2158 (1986).

R. Hultgren, P. D. Desai, D. T. Hawkins, M. Gleiser, K. K. Kelly, and D. D. Wagman, Selected Values of Thermodynamic Properties of Metals and Alloys (American Society for Metals, Cleveland, 1973).

W. A. Kamitakahara and M. N. Brockhouse, Phys. Lett. 29A, 639 (1969).

M. L. Klein, G. K. Horton, and J. L. Feldman, Phys. Rev. 184, 968 (1969).

B. Kolk, Phys. Lett. 35A, 83 (1971).

D. L. Losee and R. O. Simmons, Phys. Rev. 172, 944 (1968).

W. Ludwig, J. Phys. Chem. Solids 4, 283 (1958).

N. A. Lurie, G. Shirane, and J. Skalyo jr., Phys. Rev. B9, 5300 (1974).

J. W. Lynn, H. G. Smith, and R. M. Nicklow, Phys. Rev. B8, 3493 (1973).

D. L. MacDonald, Acta Crystallogr. 23, 185 (1967).

R. C. MacDonald and W. M. MacDonald, Phys. Rev. B24, 1715 (1981).

R. A. MacDonald and R. C. Shukla, Phys. Rev. B32, 4961 (1985).

R. A. MacDonald, R. C. Shukla, and D. K. Kahaner, Phys. Rev. B29, 6489 (1984).

A. A. Maradudin and P. A. Flinn, Phys. Rev. 129, 2529 (1963).

A. A. Maradudin, P. A. Flinn, and R. A. Coldwell-Horsfall, Ann. Phys. (U.S.A) 15, 337 (1961).

C. J. Martin and D. A. O'Connor, Acta Crystallogr. A34, 500 (1978).

D. L. Martin, Phys. Rev. Lett. 12, 723 (1964).

A. P. Miller and B. N. Brockhouse, Can. J. Phys. 49, 704 (1971).

F. Seitz, Modern Theory of Solids (McGraw-Hill, New York, 1940) p 3.

R. C. Shukla, Int. J. Thermophys. 1, 73 (1980).

R. C. Shukla and G. A. Heiser, Phys. Rev. B33, 2152 (1986).

R. C. Shukla and H. Hübschle, Phys. Rev. B40, 1555 (1989).

R. C. Shukla and R. A. MacDonald, High Temp.-High Pressures 12, 291 (1980).

R. C. Shukla and R. D. Mountain, Phys. Rev. B25, 3649 (1982).

R. C. Shukla and E. R. Muller, Phys. Status Solidi B43, 413 (1971).

R. C. Shukla and C. A. Plint, Phys. Rev. B40, 10337 (1989).

R. C. Shukla and F. Shanes, Phys. Rev. B32, 2513, (1985).

R. C. Shukla and L. Wilk, Phys. Rev. B10, 3660 (1974).

J. C. Slater, Introduction to Chemical Physics (McGraw-Hill, New York, 1939).

M. Simerska, Acta Crystallogr. 14, 1259 (1961).

J. Skalyo jr., Y. Endoh and G. Shirane, Phys. Rev. B9, 1797 (1974).

V. Synecek, H. Chessin, and M. Simerska, Acta Crystallogr. A26, 108 (1970)

Y. S. Touloukian and E. H. Buyco, Specific Heat, Metallic Elements and Alloys, Vol. 4 of Thermophysical Properties of Matter (Plenum Press, New York, 1970).

Y. S. Touloukian, R. K. Kirby, R. E Taylor, and P. D. Desai, Thermal Expansion, Metallic Elements and Alloys, Vol. 12 of Thermophysical Properties of Matter (Plenum Press, New York, 1975).

J. U. Trefny and B. Serin, J. Low Temp. Phys. 1, 231 (1969).

A. O. Urvas, D. L. Losee, and R. O. Simmons, J. Phys. Chem. Solids 28, 2269 (1967).

L. Van Hove, Quantum Theory of Many Particle Systems (Benjamin, New York, 1961).

D. N. Zubarev, Usp. fiz. Nauk. 71, 71 (1960); Soviet Phys.-Uspekhi 3, 320 (1960).